QUANTUM TUNNELING OF ATOMS IN AN OPTICAL POTENTIAL

APPROVED BY
DISSERTATION COMMITTEE:

Supervisor: _____

_____

_____

_____

_____

Copyright
by
Patrick Russell Morrow
1996

This dissertation is dedicated to my loving wife Xiaorong

QUANTUM TUNNELING OF ATOMS IN AN OPTICAL POTENTIAL

by

PATRICK RUSSELL MORROW, B.S.,B.A.

DISSERTATION

Presented to the Faculty of the Graduate School of

The University of Texas at Austin

in Partial Fulfillment

of the Requirements

for the Degree of

DOCTOR OF PHILOSOPHY

THE UNIVERSITY OF TEXAS AT AUSTIN

December 1996

Acknowledgements

I must first thank my advisor Professor Mark Raizen for all of his support, instruction, guidance, correction, and patience over the last five years. It has been a thoroughly enjoyable time working with him.

I would like to thank Fred Moore for much instruction on experimental techniques. I thank Steve Wilkinson who has been a fruitful source of information and useful discussion for this project and also about life. Thanks also go to Bala Sundaram for much theoretical insight with simulations and discussions.

I would like to thank my friends and colleagues in the laboratory. I thank Cyrus Bharucha and Kirk Madison for extensive help with the experiment. I also thank them for their moral support during times of stress. I also thank Bruce 'Skippy' Klappauf for all of his help with other projects in the lab. It is always easy to work hard when you are in the company of a group of fun-loving people such as this crew.

I would also like to thank my friends Craig and Shirley McCluskey, Chad McMillan, Ronald Dass, Daniel Steck, Lynne and Grey Tarkenton, and Martin Fischer for their support. Finally, I thank my wife and friend Xiaorong Wu for her love, patience, understanding, and help in completing this work.

QUANTUM TUNNELING OF ATOMS IN AN OPTICAL POTENTIAL

Publication No. _____

Patrick Russell Morrow, Ph.D.
The University of Texas at Austin, 1996

Supervisor: Mark G. Raizen

We observe quantum tunneling in the center of mass motion of ultracold atoms in an accelerating one-dimensional optical potential. This potential is formed by two counter-propagating laser beams where the frequency of one is offset from the other and ramped in time. We study the tunneling of atoms from the trapped state to the continuum, and observe an exponential decay in the number of atoms that remain trapped as a function of the interaction time, for sufficiently large values of acceleration. Decay rates are compared with Landau-Zener tunneling theory and with numerical simulations. We find that the measured tunneling rates agree well with the quantum numerical simulations given the uncertainty in determination of the well depth. Both the experimental measurement and the quantum simulations are found to oscillate around the Landau-Zener predictions, and these oscillations are due to quantum interference. The results presented here are the first observations of tunneling in atom optics.

Table of Contents

Acknowledgements v

Abstract vi

List of Figures ix

Chapter 1. Introduction 1

Chapter 2. Theoretical Framework 5
2.1 Dipole Force Interaction 5
2.2 Deep Well Limit 10
2.3 Shallow Well Limit 15
2.3.1 Bloch states 15
2.3.2 Bloch oscillations 17
2.3.3 Tunneling 24
2.4 Discussion 26

Chapter 3. Experimental Setup 31
3.1 Overview 31
3.2 Initial Conditions: Trapped and Laser Cooled Sodium Atoms 38
3.3 Interaction Potential 41
3.3.1 Experimental Realization of Accelerated Standing Wave . . . 41
3.3.2 Characterization of the Accelerated Standing Wave 44
3.4 Final Distribution and Detection 51

Chapter 4. Tunneling Experiment 57
4.1 Introduction 57
4.2 Determination of Survival Probabilities and Tunneling Rates 59
4.3 Tunneling Experiment Procedure 78

4.4 Comparison with Theory 83
4.5 Other Factors Leading to Loss Rate from Wells 88
4.6 Tunneling from Higher Bands 92
4.7 Conclusion and Future Work 92
4.7.1 Conclusion 92
4.7.2 Enhanced Resonant Tunneling 94
4.7.3 Non-exponential Decay 95
4.7.4 Atomic Interferometer 97

Appendices

Appendix A. Program to Calculate Heterodyne Frequency 100

Appendix B. Program to Calculate Drag Ratio 111

Bibliography 122

Vita 125

List of Figures

2.1 Atoms in Standing Wave 11
2.2 Tilted Potential 14
2.3 Free Particle Dispersion 18
2.4 Free Particle Dispersion in Reduced Zone 19
2.5 Band Structure for Sinusoidal Potential in Real Space 20
2.6 Band Structure for Sinusoidal Potential in Reciprocal Space . . 21
2.7 Atom in Reciprocal Space under Acceleration 23
2.8 Theoretical Autocorrelation Function 25
2.9 Tunneling of Atom in Tilted Potential Picture 27

3.1 Momentum Transfer Flowchart 33
3.2 Laser Table Overview 35
3.3 Timing Electronics Block Diagram 36
3.4 Term Diagram for Sodium D_2 40
3.5 Timing Control Sequence 42
3.6 Interaction Beam Schematic 45
3.7 Heterodyne Measurement Schematic 52
3.8 Heterodyne Frequency Measurement 53
3.9 Experimental Image of Acceleration Atoms 56

4.1 Two-dimensional Curve Evolution 61
4.2 Evolution of Curves in Time for $V_0/h = 96$ kHz, a_{fast}=6000 m/s^2 63
4.3 Survival Probability for $V_0/h = 96$ kHz, a_{fast}=6000 m/s^2 64
4.4 Evolution of Curves in Time for V_0/h=96 kHz, a_{fast}=7000 m/s^2 65
4.5 Survival Probability for V_0/h=96 kHz, a_{fast}=7000 m/s^2 66
4.6 Evolution of Curves in Time for V_0/h=96 kHz, a_{fast}=8000 m/s^2 67
4.7 Survival Probability for V_0/h=96 kHz, a_{fast}=8000 m/s^2 68
4.8 Evolution of Curves in Time for $V_0/h = 96$ kHz, a_{fast}=9000 m/s^2 69

4.9 Survival Probability for $V_0/h = 96$ kHz, a_{fast}=9000 m/s^2 70
4.10 Evolution of Curves in Time for $V_0/h = 58$ kHz, a_{fast}=3000 m/s^2 71
4.11 Survival Probability for $V_0/h = 58$ kHz, a_{fast}=3000 m/s^2 72
4.12 Evolution of Curves in Time for $V_0/h = 58$ kHz, a_{fast}=5000 m/s^2 73
4.13 Survival Probability for $V_0/h = 58$ kHz, a_{fast}=5000 m/s^2 74
4.14 Evolution of Curves in Time for $V_0/h = 58$ kHz, a_{fast}=7000 m/s^2 75
4.15 Survival Probability for $V_0/h = 58$ kHz, a_{fast}=7000 m/s^2 76
4.16 Survival Probability with Exponential Fit 77
4.17 CCD Image for Accelerated Atoms without Tunneling 80
4.18 CCD Image of Accelerated Atoms with Tunneling 81
4.19 Power Discrimination Effect on Determination of Tunnel Rates . 82
4.20 Decay Rate versus Acceleration for V_0/h=92 kHz 85
4.21 Decay Rate versus Acceleration for V_0/h=72 kHz 86
4.22 Decay Rate versus Acceleration for V_0/h=66 kHz 87
4.23 Heterodyne Showing Non-zero Switching Time 90
4.24 Sinusoidal Potential in Real Space with Multiple Bands Below Wells 93
4.25 Tilted Potential Showing Resonant Tunneling Process 96

Chapter 1

Introduction

Tunneling in center of mass motion of particles is a fundamental process in quantum mechanics and has been investigated both theoretically and experimentally in many contexts. In order for the probability of tunneling to be significant, potential barrier heights and length scales must be small. This condition restricts the classes of systems that may exhibit significant tunneling. Solid state systems are quite often good candidates for tunneling processes because of small length scales and electron mass, and many observations have been made in this area. However, these systems are too complicated to make an absolute comparison with theory and many calculations are highly dependent upon the particular models used. In particular, solid state systems have lattice vibrations, multiparticle interactions, and impurities that can obscure the quantum mechanical tunneling process and make absolute measurements of rates very difficult.

In the past two decades research in laser cooling and trapping of atoms has advanced a new area of physics called atom optics. Since atom optics systems can involve low atomic kinetic energies and short length scales, one might expect that tunneling would be an important process under these conditions. Until now, however, there has not been an observation of tunneling in atom

optics. Tunneling could appear, for example, in a system of atoms confined in a stationary near-detuned optical lattice. The confinement of atoms in the lattice will ultimately be limited by tunneling, and there have been efforts to observe this [1]. Direct observation of tunneling in this system is difficult since loss can also result from spontaneous emission recoil out of the lattice. Additionally, observation of atoms tunneling in these systems requires them to tunnel through many wells to leave the lattice, so the effective tunneling probability is small.

We have been able to observe tunneling in an atom optics system which does not have these complications. Our approach is to launch laser-cooled atoms in a far-detuned, *accelerating* optical lattice and observe atomic tunneling from trapped states to the continuum. This study arose from our efforts to develop a cold atomic beam for interferometry. Our system does not have significant spontaneous emission and only requires atoms to tunnel through a single barrier. Additionally, the high degree of experimental control has enabled a quantitative comparison with theory. The results presented here are the first observations of tunneling in atom optics.

Recently, there have been several experiments involving the interaction of ultra-cold atoms with a standing wave of light (see for example [2, 3, 4, 5, 6, 7]). In these cases, the sources of ultra-cold atoms are typically from magneto-optic traps (MOTs) which can be used to trap and cool relatively large numbers of atoms to very slow velocities [8]. In the current experiment we accelerate the standing wave and measure the transfer of momentum from the light to the atoms. This launching process results in a portion of the atoms accelerated with the standing wave to higher velocities. The number of atoms that are

launched depends on the well depth of the potential, the initial energies of the atoms, and the acceleration. Classically, we can consider the accelerated atoms as point-like particles that are trapped in the wells and move with them. Classical, in this case, means that the well depth is relatively large compared to the atoms' energy. There is a maximum classical acceleration above which the atoms will not be trapped in the wells but will simply ride over them. At accelerations below this classical acceleration it is possible for atoms that were initially trapped in the wells to remain trapped. These atoms will be launched.

Quantum mechanically, though, the atoms can tunnel from the trapped state to the continuum. We find that the acceleration where the atoms begin to tunnel from the wells is much lower than the maximum classical acceleration. This effect will limit the number of atoms that can be launched at high accelerations much more than predicted classically. The number of atoms that can be accelerated is important if the atomic accelerator is to be used as the source for an atomic interferometer. For the experiment described in this work, we measure the loss rate of the atoms from the accelerating wells. We find that the number of atoms in the wells decays exponentially in time and this allows a characterization in terms of a decay constant. This constant depends on the acceleration and the well depth. Qualitatively from theory, we understand that the loss rate from tunneling should increase with lower well depth and higher accelerations. Classically, the loss rate is only dependent on acceleration above the classical value where all the atoms are lost.

The current experiment measures decay rates at low well depths where quantum mechanical tunneling is significant. In this case the quantum dynamics are described best by the band picture used previously in solid state

physics problems. We made careful and detailed measurements of decay constants and compared them with Landau-Zener theory and also with quantum simulations. We found good agreement between the simulations and the experiment. Landau-Zener theory is approximately correct but lacks some important features present in this system.

Future extensions of these measurements are to study the short-time tunneling behavior that has been predicted to deviate from an exponential decay [9, 10, 11], and to use the accelerator for interferometry.

Chapter 2

Theoretical Framework

The tunneling experiments described here rely on an interaction of an electromagnetic field with an atom. In this particular experiment, the atoms interact with an optical standing wave light field created by two counter-propagating traveling waves. This interaction can be analyzed using the dipole force. This analysis involves an approximation which leads to an effective Hamiltonian that has the internal degrees of freedom of the atom integrated out. The dipole force is the standard technique of analysis for many atom optic problems and here we restrict our attention to the case of the accelerated standing wave. The effective Hamiltonian that results describes only the center of mass motion of the atom and has two limiting regimes, deep wells and shallow wells.

2.1 Dipole Force Interaction

The electric field created by two counter-propagating traveling waves with one offset in frequency relative to the other is given by (in one dimension)

$$\begin{aligned} \vec{E}(x,t) &= \hat{y}E_0\cos(\omega_L t + k_L x) + \hat{y}E_1\cos((\omega_L - \Delta\omega)t - k_L x) \\ &= \hat{y}\frac{1}{2}[E_0 e^{i(\omega_L t + k_L x)} + E_1 e^{i((\omega_L - \Delta\omega)t - k_L x)} + c.c.]. \end{aligned} \tag{2.1}$$

The standing wave is along the x-axis and is linearly polarized along the y-axis. k_L and $-k_L$ are the wave vectors of the beams and $\Delta\omega$ is the frequency offset between the two beams. We consider a two-level atom interacting with an external electric field [13, 14, 15].

$$\hat{H}(x,t) = H_{cm} + H_{internal} + H_{interaction} \tag{2.2}$$

Where

$$H_{cm} = \frac{\hat{p}^2}{2M} \tag{2.3}$$

is the center of mass kinetic energy, p is the center-of-mass momentum of the atom of mass M,

$$H_{internal} = \hbar\omega_0 |e\rangle\langle e| \tag{2.4}$$

is the internal energy Hamiltonian of a two-level atom, and the interaction potential between the atom's dipole $\vec{d}$ and the field in the dipole approximation is

$$\begin{aligned} H_{interaction} &= \vec{d}\cdot\ \vec{E} \\ &= -d_{eg}(|e\rangle\langle g|e^{i\omega_0 t} + |g\rangle\langle e|e^{-i\omega_0 t})|E| \\ &= -\frac{d_{eg}}{2}[E_0\sigma^+ e^{-ik_L x}e^{i(\omega_0-\omega_L)t} + E_1\sigma^+ e^{+ik_L x}e^{i(\omega_0-\omega_L+\Delta\omega)t} \\ &\quad + E_0\sigma^- e^{ik_L x}e^{i(\omega_L-\omega_0)t} + E_1\sigma^- e^{-ik_L x}e^{i(\omega_L-\omega_0-\Delta\omega)}] \end{aligned} \tag{2.5}$$

after discarding terms with $e^{\pm i(\omega_L+\omega_0)t}$ in the rotating wave approximation. Here $\sigma^\pm$ are Pauli spin-raising and spin-lowering operators. d_{eg} is the resulting dipole constant from the ground to the excited state. These parts yield the Hamiltonian

$$\begin{aligned}\hat{H}(x,t) &= \frac{\hat{p}^2}{2M} + \hbar\omega_0|e\rangle\langle e| \\ &- \frac{d_{eg}}{2}[E_0\sigma^+ e^{-ik_Lx}e^{i(\omega_0-\omega_L)t} + E_1\sigma^+ e^{ik_Lx}e^{i(\omega_0-\omega_L+\Delta\omega)t} \\ &+ E_0\sigma^- e^{ik_Lx}e^{i(\omega_L-\omega_0)t} + E_1\sigma^- e^{-ik_Lx}e^{i(\omega_L-\omega_0-\Delta\omega)}]. \qquad (2.6)\end{aligned}$$

The center of mass wave function is separable so we consider only its motion along the x-axis. We can represent the atomic state as

$$\Psi(x,t) = \Psi_g(x,t)|g\rangle + \Psi_e(x,t)e^{-i\omega_L t}|e\rangle. \qquad (2.7)$$

Applying Schrödinger's equation

$$i\hbar\frac{\partial}{\partial t}\Psi = \hat{H}\Psi \qquad (2.8)$$

yields the following equation of motion

$$\begin{aligned}i\hbar(\frac{\partial\Psi_g}{\partial t}|g\rangle &+ \frac{\partial\Psi_e}{\partial t}e^{-i\omega_L t}|e\rangle - i\omega_L\Psi_e e^{-i\omega_L t}|e\rangle) = \\ &- \frac{\hbar^2}{2M}\frac{\partial^2\Psi_g}{\partial x^2}|g\rangle - \frac{\hbar^2}{2M}\frac{\partial^2\Psi_e}{\partial x^2}e^{-i\omega_L t}|e\rangle \\ &+ \hbar\omega_0\Psi_e e^{-i\omega_L t}|e\rangle \\ &- \frac{d_{eg}}{2}[E_0 e^{-ik_Lx}e^{i(\omega_0-\omega_L)t} + E_1 e^{ik_Lx}e^{i(\omega_0-\omega_L+\Delta\omega)t}]|e\rangle\Psi_g \\ &- \frac{d_{eg}}{2}[E_0 e^{ik_Lx}e^{-i\omega_0 t} + E_1 e^{-ik_Lx}e^{-i(\omega_0-\Delta\omega)}]|g\rangle\Psi_e. \qquad (2.9)\end{aligned}$$

We define the detuning from resonance as $\delta_L = \omega_0 - \omega_L$. Operating on Equation 2.9 with $\langle g|$ from the left results in

$$i\hbar\frac{\partial\Psi_g}{\partial t} = -\frac{\hbar^2}{2M}\frac{\partial^2\Psi_g}{\partial x^2} - \frac{d_{eg}}{2}[E_0 e^{i(k_Lx-\omega_0 t)} + E_1 e^{-i(k_Lx+\omega_0 t+\Delta\omega t)}]\Psi_e. \qquad (2.10)$$

Similarly we operate on Equation 2.9 with $\langle e|$ from the left and get

$$i\hbar\frac{\partial\Psi_e}{\partial t} = -\frac{\hbar^2}{2M}\frac{\partial^2\Psi_e}{\partial x^2} - \frac{d_{eg}}{2}[E_0 e^{i(\omega_0 t-k_Lx)} + E_1 e^{i(k_Lx+\omega_0 t+\Delta\omega t)}]\Psi_g + \hbar\delta_L\Psi_e. \qquad (2.11)$$

Sufficiently large detuning δ_L allows us to neglect spontaneous emission and to simplify these equations by adiabatic elimination of the excited state amplitude. By setting $\frac{\partial \Psi_e}{\partial t} = 0$ and $\frac{\partial^2 \Psi_e}{\partial x^2} = 0$, Equation 2.11 becomes

$$\Psi_e = \frac{d_{eg}}{2\hbar\delta}[E_0 e^{i(\omega_0 t - k_L x)} + E_1 e^{i(k_L x + \omega_0 t + \Delta\omega t)}]\Psi_g. \tag{2.12}$$

If we substitute Equation 2.12 into Equation 2.10 we obtain

$$i\hbar\frac{\partial \Psi_g}{\partial t} = -\frac{\hbar^2}{2M}\frac{\partial^2 \Psi_g}{\partial x^2} - \frac{d_{eg}^2}{4\hbar\delta}[E_0^2 + E_1^2 + 2E_0 E_1 \cos(2k_L x - \Delta\omega t)] \tag{2.13}$$

resulting in the Hamiltonian

$$\hat{H} = \frac{\hat{p}^2}{2M} - \frac{d_{eg}^2}{4\hbar\delta}[E_0^2 + E_1^2 + 2E_0 E_1 \cos(2k_L x - \Delta\omega t)]. \tag{2.14}$$

Or equivalently, ignoring a constant potential offset we obtain

$$\hat{H} = \frac{\hat{p}^2}{2M} - \frac{d_{eg}^2}{2\hbar\delta}[E_0 E_1 \cos(2k_L x - \Delta\omega t)]. \tag{2.15}$$

The end result is that the effective interaction Hamiltonian is a sinusoidal potential moving at a velocity $v = \Delta\omega/2k_L$ and we identify the well depth V_0 as

$$V_0 = \frac{E_0 E_1 d_{eg}^2}{2\hbar\delta}. \tag{2.16}$$

We have derived in detail the interaction of an atom with the light field using the dipole force approximation to remove the internal degrees of freedom of the atom. Qualitatively we may note that the main result of the dipole force approximation is that the center of mass of the atom experiences a potential proportional to the gradient in the intensity of the light [13]. From this we can complete a simple analysis of the interaction as follows.

Consider again two counter-propagating traveling electromagnetic waves added together each with wave vector $k_L = 2\pi/\lambda$ where λ is the laser wavelength and offset in frequency $\Delta\omega$.

$$\vec{E} = \vec{E_0} e^{i(\omega t - \vec{k_L}\cdot\vec{x})} + \vec{E_1} e^{i((\omega-\Delta\omega)t - \vec{k_L}\cdot\vec{x})} \tag{2.17}$$

This leads to the intensity of

$$\begin{aligned} |I| &= \vec{E}^* \vec{E} \\ &= E_0^2 + E_1^2 + 2E_0 E_1 \cos(\Delta\omega t - 2k_L x). \end{aligned} \tag{2.18}$$

The velocity of the resulting standing wave is given according to $v = \Delta\omega/(2k_L)$. In the frame moving at v compared to the laboratory, the nodes of this standing wave appear stationary. The force that the center of mass of the atom experiences is proportional to the spatial gradient of the intensity of the light field given by

$$F \propto \frac{dI}{dx} \propto \cos[2k_L(vt - x)]. \tag{2.19}$$

This is a sinusoidal potential where the nodes are traveling at a velocity v. If the velocity of this standing wave is changed in time, the nodes experience an acceleration proportional to the time derivative of the velocity. The simplest example is a linear ramp in frequency giving a constant acceleration of the wells. Under this accelerating potential, a trapped point-like atom will be accelerated along with the wells. For sodium (λ=589 nm) a frequency offset of 100 kHz gives a velocity of 3 cm/s which is one photon recoil. If we apply a linear ramp on the frequency of 10 kHz/μsec for example we obtain an acceleration of 3000 m/s^2. The maximum acceleration applied to the atoms is not limited by the equipment switching time but is limited by the physics of the interaction. In

general, the physics can be categorized into two limiting regimes, deep wells and shallow wells. The deep well limit has negligible loss due to quantum mechanical tunneling. However, loss can occur from classical mechanics at high accelerations even in deep wells. Weaker wells involve loss due to quantum mechanical tunneling that becomes significant at much lower accelerations than the deep well case.

2.2 Deep Well Limit

As was shown in Section 2.1 using the dipole force approximation we have an effective Hamiltonian in the form of a standing wave with nodes moving at a velocity given by $\Delta\omega/2k_L$. We now impose a linear ramp on the frequency difference to give a constant acceleration to the nodes of the standing wave.

$$\hat{H} = \frac{\hat{p}^2}{2M} - V_0 \cos(2k_L(x - \frac{a}{2}t^2)). \tag{2.20}$$

Where $a = \frac{1}{2k_L}\frac{d(\Delta\omega)}{dt}$. We first transform Equation 2.20 to a new form. We can rewrite the potential in the frame of reference of the atom using generating functions. We rewrite

$$H(x, p, t) = \frac{p^2}{2M} + V(x - v(t), t) \tag{2.21}$$

in new coordinates

$$\bar{H}(\bar{x}, \bar{p}, t) = H(x, p, t) + \frac{\partial F_2(x, \bar{p}, t)}{\partial t} \tag{2.22}$$

where

$$\begin{aligned} \bar{x} &= \frac{\partial F_2(x, \bar{p}, t)}{\partial \bar{p}} \\ p &= \frac{\partial F_2(x, \bar{p}, t)}{\partial x} \end{aligned} \tag{2.23}$$

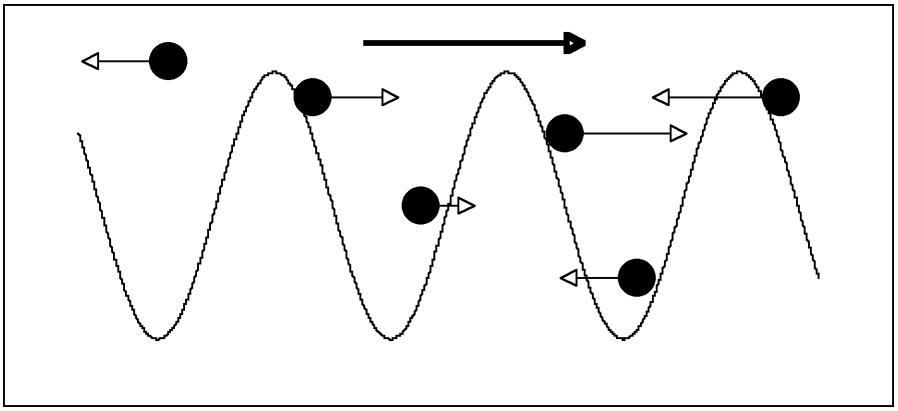

Figure 2.1: In the limit of deep wells, some of the atoms are trapped in the wells and are accelerated with the standing wave. Initially, the atoms in the MOT are spatially spread over many nodes and spread with a Gaussian velocity distribution. Some atoms have total energy less than the well depth and can be trapped and accelerated.

defining the transformations as

$$\bar{x} = x - f(t) \tag{2.24}$$

$$\bar{p} = M\dot{\bar{x}} \tag{2.25}$$

giving

$$\begin{aligned} \bar{p} &= p - Mf'(t) \\ \frac{\partial F_2}{\partial \bar{p}} &= x - f(t) \\ \frac{\partial F_2}{\partial x} &= \bar{p} + Mf'(t) \\ F_2 &= \bar{p}x - \bar{p}f(t) + Mxf'(t) \end{aligned} \tag{2.26}$$

$$\bar{H}(\bar{x}, \bar{p}, t) = \frac{p^2}{2M} + V(\bar{x}, t) + M(\bar{x})f''(t) + Mf(t)f''(t) + \frac{M}{2}[f'(t)]^2. \tag{2.27}$$

Now we set f(t)=$\frac{1}{2}at^2$ and $V = V_0 \cos(2k_L(x - f(t)))$

$$\bar{H}(\bar{x}, \bar{p}, t) = \frac{\bar{p^2}}{2M} + V_0 \cos(2k_L\bar{x}) + Ma^2t^2 + Ma\bar{x} \tag{2.28}$$

So in the frame of reference of the atom, the potential can be rewritten by subtracting the term Ma^2t^2, which does not effect the dynamics. The resulting potential is given by

$$V_0 \cos(2k_L x) + Max. \tag{2.29}$$

Although the Schrödinger equation could be solved for all cases, in the limit of deep wells, one can understand the interaction of the atoms with the light more simply. This limit pertains to a situation where the atoms can be pictured as structureless particles interacting with an impenetrable sinusoidal potential that is accelerating, with no quantum mechanical tunneling between

wells or resonant effects (see Figure 2.1). When the interaction beam is turned on, some of the atoms in the cold MOT find themselves trapped in the nodes of the standing wave. Classically, if the initial total energy of an atom is less than the classical barrier depth V_{bc}, it can be trapped in the well. To calculate the barrier depth we consider the potential in the tilted form in Figure 2.2. The maximum classical acceleration is calculated by finding when the force from acceleration is greater than the force from the periodic trapping potential.

$$F_{atom} = Ma - V_0 2k_L \sin(2k_L x) \tag{2.30}$$

From this, we see that when a is greater than $a_{cl} = \frac{V_0 2k_L}{M}$ there are no longer any minima of the potential. Figure 2.2 shows the tilted potential with the barrier height. The extrema of this potential are given by

$$\begin{aligned} \sin(2k_L x) &= \frac{Ma}{V_0 2k_L} \\ &= \frac{a}{a_{cl}} \end{aligned} \tag{2.31}$$

The minima occur twice in one period and satisfy the criteria

$$\sin(\frac{\pi}{2} \pm \alpha) = \frac{a}{a_{cl}}. \tag{2.32}$$

The potential difference between the minimum and maximum gives the barrier height.

$$\begin{aligned} V_{cb} &= V_{max} - V_{min} \\ &= V_0[\cos(\frac{\pi}{2} - \alpha) - \cos(\frac{\pi}{2} + \alpha)] + Ma[\frac{\pi}{2} - \alpha - (\frac{\pi}{2} + \alpha)] \end{aligned} \tag{2.33}$$

Replacing $\alpha = \frac{\pi}{2} + \sin^{-1}(\frac{a}{a_{cl}}) = \cos^{-1}(\frac{a}{a_{cl}})$ we obtain

$$V_{cb} = 2V_0[[1 - (\frac{a}{a_{cl}})^2]^{\frac{1}{2}} - \frac{a}{a_{cl}} \cos^{-1}(\frac{a}{a_{cl}})]. \tag{2.34}$$

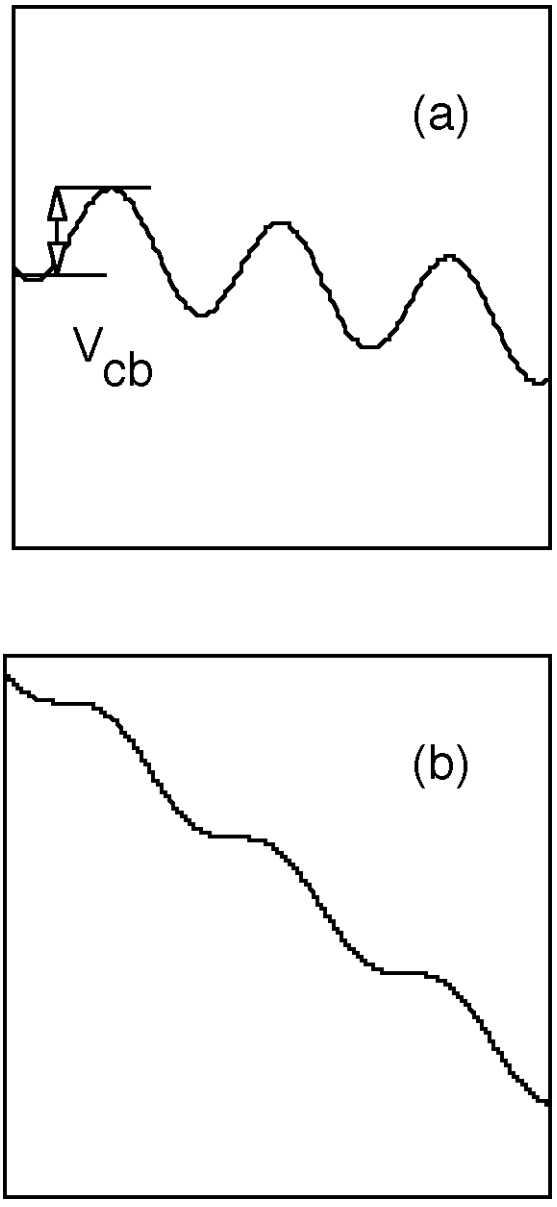

Figure 2.2: Frame (a) shows potential where the acceleration is less than a_{cl} and the classical barrier well depth V_{cb}. Frame (b) shows the case where the acceleration is beyond a_{cl} and there are no wells remaining.

The maximum classical acceleration where the atoms can remain trapped is also the condition that the barrier depth in the tilted frame becomes zero. In the laboratory frame, the atom simply rides over the wells as they pass by. We will now see that quantum mechanical tunneling leads to a loss from the wells at a much lower acceleration.

2.3 Shallow Well Limit

As the well depth is lowered, quantum mechanical effects must be included in the description of the physics. As is well known from solid state physics, in a perfectly periodic lattice, one can use Bloch's theorem to solve Schrödinger's equation [16]. Band gaps in dispersion relations exist for non-zero periodic potentials, whether it be from a delta-function potential (Kronig-Penny model) or from a sinusoidal potential as in our experiments. The Bloch states are a complete set of states and are completely spatially delocalized. However, when the acceleration is added, the Bloch states are not exact eigenfunctions so the spatial spread of the solutions becomes localized in a superposition of Bloch states. It is physically reasonable that the initial spatial spread of the atoms is only over a distance comparable to a few periods of the standing wave. This means that the initial atomic wave packet will be projected into a superposition of several Bloch states upon application of the periodic potential.

2.3.1 Bloch states

We first review the properties of Bloch states and band structure. In the quantum system, we wish to solve the Schrödinger equation. A free particle

Hamiltonian's eigenstates are given by.

$$\hat{H}\Psi = -\frac{\hbar^2}{2m}\frac{d^2\Psi}{dx^2} = E\Psi \tag{2.35}$$

and has an energy dispersion relation given by

$$E(k) = \frac{\hbar^2 k^2}{2m}. \tag{2.36}$$

When plotted, this relation gives a parabola (see Figure 2.3), but in this case we can also plot it in the so-called reduced zone picture. This is shown in Figure 2.4. In this picture we fold back the curve to the first zone when the wave vector magnitude exceeds $\pm k_B/2$ where $k_B = \pi/a_x$ and a_x is the lattice spacing. In the optical system the reciprocal lattice vector $k_B = 2k_L$ since $a_x = \lambda/2$. Consequently from the reduced zone, rather than state the particle having an absolute value of k-vector and energy, we describe it with a k-vector confined to the first Brillouin zone (less than k_L) and a band number.

The application of a potential U(x) with the same periodicity as the lattice spacing a_x results in a Hamiltonian

$$\hat{H}\Psi = -\frac{\hbar^2}{2m}\frac{d^2\Psi}{dx^2} + U(x)\Psi = E\Psi \tag{2.37}$$

and will be solved by the Bloch states given by

$$\Psi_k(x) = \mu_k(x)exp(ikx) \tag{2.38}$$

where $\mu_k(x)$ is some function that has the same periodicity of the lattice. In terms of the dispersion relationship, the non-zero periodic potential opens up band gaps at the edges of the Brillouin zone. For the particular case of a sinusoidal potential from the standing wave, the Schrödinger equation is solved by Mathieu functions [17].

The band structure for this sinusoidal potential with V_0/h of 68 kHz and an acceleration of zero is shown in Figure 2.6. The first three bands are shown in this particular figure. The band gaps represent regions of energy and wavenumber where the atom's wave function cannot exist. The x-space picture of the bands is also informative and is shown in Figure 2.5. In this figure the potential from the standing wave is also shown for comparison to the energy of the bands and the gaps. For this well depth, there is only one band within the wells so only atoms in this band would be considered as trapped in the wells. As the well depth is increased, the gaps get larger and the bands get smaller. This reflects the fact that inter-band tunneling decreases as the wells get deeper. In the case of very deep wells, the bound states should be identical to that for a single well since the wells are very weakly coupled.

We now include a time dependent velocity term to the sinusoidal part of the potential. Here we consider only a linear acceleration a which gives

$$V_0 \cos(2k_L(x - \frac{a}{2}t^2)). \tag{2.39}$$

Although the Bloch functions are not strictly solutions to this Hamiltonian when a is not zero, they still provide a useful basis in which to describe the physics.

2.3.2 Bloch oscillations

Consider an atom that is initially prepared in the lowest band near the center of the Brillouin zone, e.g. an atom with near-zero wavenumber (k). When the acceleration is imposed on the lattice, the wavenumber k changes in time. As k approaches the edge of the Brillouin zone (k_L), the atom can do one of two

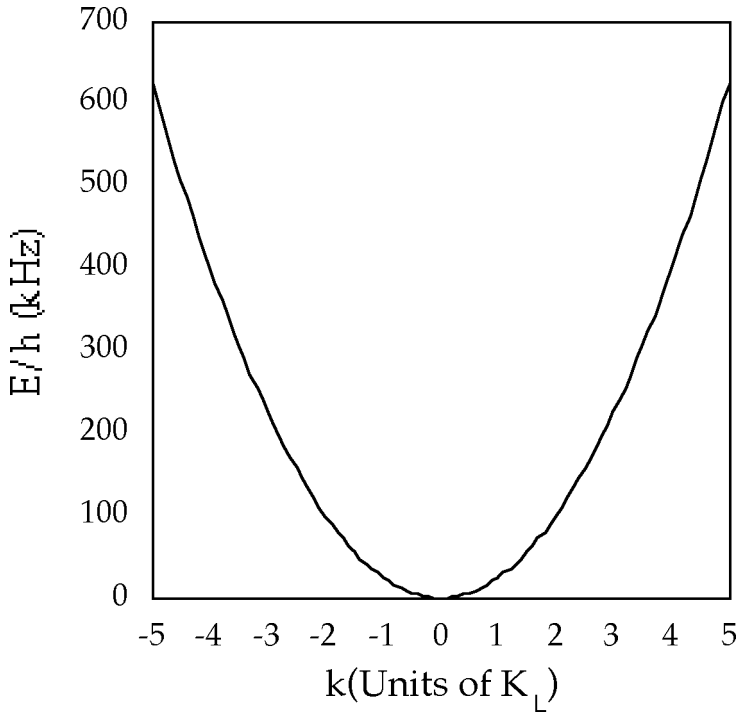

Figure 2.3: The dispersion relations for a free sodium atom in units of k_L.

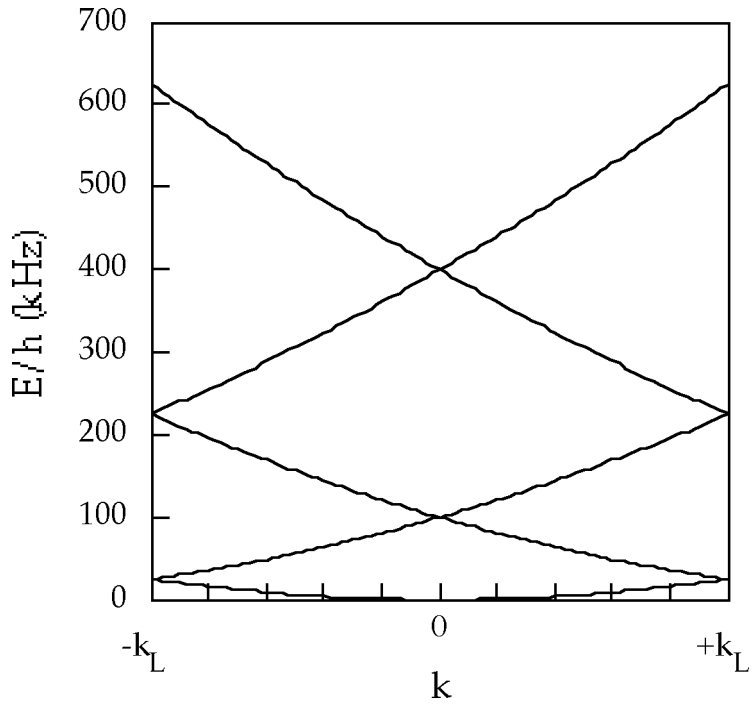

Figure 2.4: The dispersion relations for a free sodium atom shown in the reduced band picture. Values of energy for momentum above k_L are folded back from higher zones to the first zone.

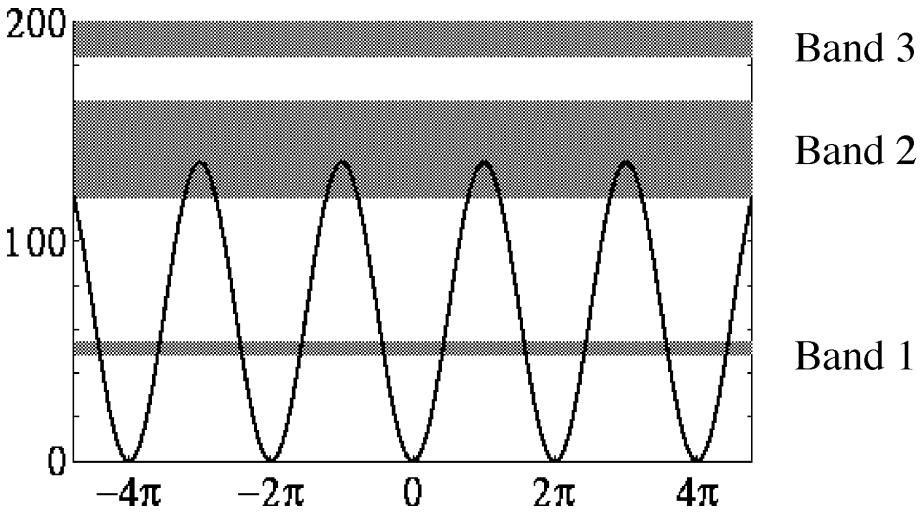

Figure 2.5: Band structure of an optical lattice, with V_0/h=68 kHz. The curved line is the periodic potential plotted as a function of position, x. the allowed energy bands are the shaded regions, identified as 1,2,3 while the energy gaps are blank.

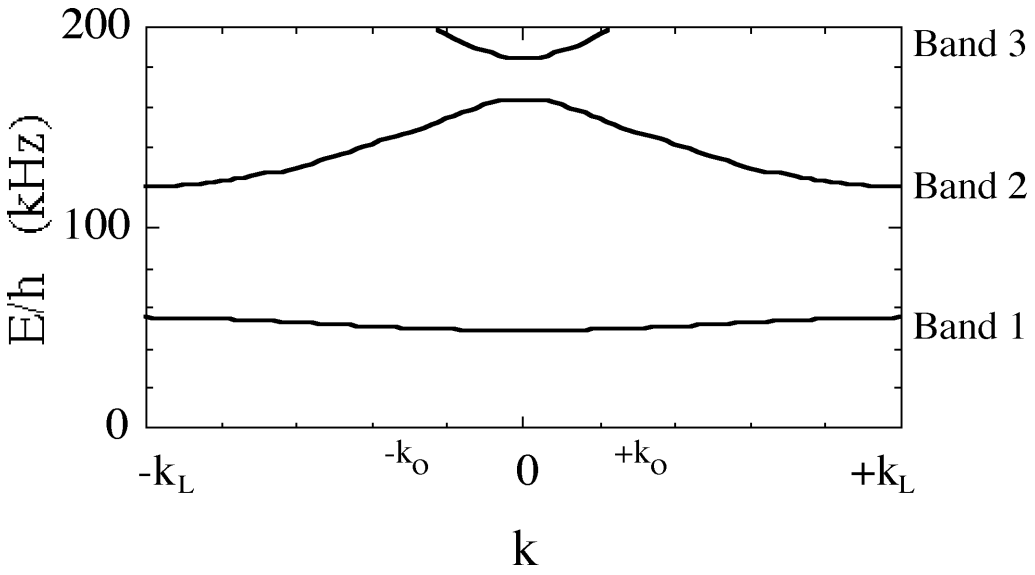

Figure 2.6: The dispersion relations for the sinusoidal potential with $V_0/\mathrm{h} = 68$ kHz. The three lowest bands are identified.

things. The atom can either Bragg reflect to the other edge of the Brillouin zone and remain in the first band or it can undergo a Landau-Zener transition to the second band. These processes are shown schematically in Figure 2.7. If the atom stays in the lower band, the velocity of the atom will spontaneously change directions when it Bragg reflects. The atom will continue to accelerate in the positive k direction until it reaches the edge of the Brillouin zone again. This process of acceleration and Bragg reflection is known as a Bloch oscillation and causes an oscillation in momentum. The rate of change of momentum is given by

$$\frac{dk}{dt} = Ma. \tag{2.40}$$

The amount of time it takes to cross $2\hbar k_L$ in momentum gives a Bloch period of

$$T_B = \frac{2\hbar k_L}{Ma}. \tag{2.41}$$

These oscillations in momentum have been observed recently in an atom optics system with cesium [7]. They are also related to the Wannier Stark Ladders that have been observed in solid state superlattices [18] and very recently in our atom optics system using sodium [2]. Figure 2.8 shows that the Bloch oscillations are also observed in the theoretical autocorrelation function, which is calculated by evaluating the overlap integral of the evolved state with the initial state of a wave function confined to the lowest band in the wells at zero acceleration. The acceleration in this case is 4500 m/s^2 and the well depth is 55 kHz. This gives a Bloch oscillation of 13.3 μs which agrees with the simulation.

These Bloch oscillations should also be seen in x-space as the particle undulates back and forth at the Bloch period. Although the particle moves

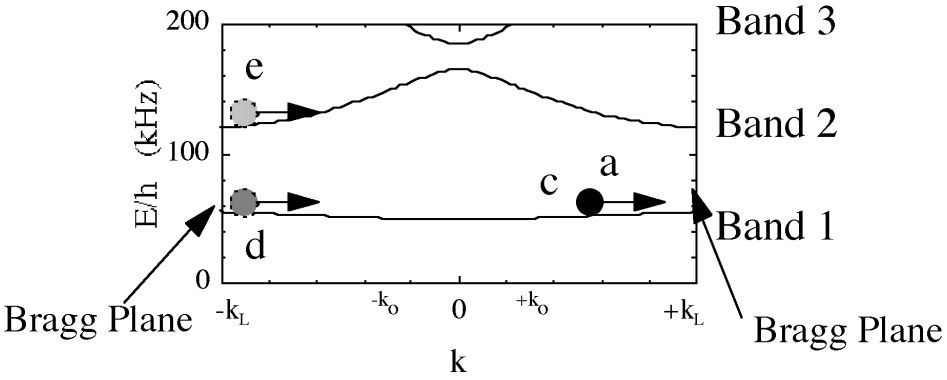

Figure 2.7: Figure shows reciprocal space where an atom is prepared with momentum of zero and is accelerated to the edge of the Brillouin zone (c). At this point the atom can either stay in the lowest band (d) or make a transition to the upper band (e).

back and forth locally, its overall global motion will continue to drift in the direction of the acceleration.

2.3.3 Tunneling

The process we are most interested in is when the atom makes a Landau-Zener tunneling transition from the trapped state to the continuum. The probability of making the transition to the upper band can be described by Landau-Zener theory for an avoided crossing [19]. The transition probability will obviously increase as the acceleration is increased. This can be described in simple terms relating to the Heisenberg uncertainty principle. This process is similar in many avoided-crossing problems. The transition probability between levels becomes significant when the time that the atom spends near the band gap becomes comparable to the the inverse energy gap,i.e.

$$\Delta E \cong \frac{\hbar}{\Delta t} \tag{2.42}$$

In the theoretical calculation we can see tunneling from the lowest band by the reduction in the magnitude of the autocorrelation function (see Figure 2.8). We fit an exponential to the maximums of the peaks to determine the decay rate, starting from the third peak to avoid any possible short-time non-exponential effects. The experiments as well as the simulations show that the survival probability follows an exponential in time.

Landau-Zener theory can estimate the tunneling rate with the following functional form in laboratory units [17]

$$\Gamma_{LZ} = \frac{a}{2v_r} exp(-\frac{a_c}{a}). \tag{2.43}$$

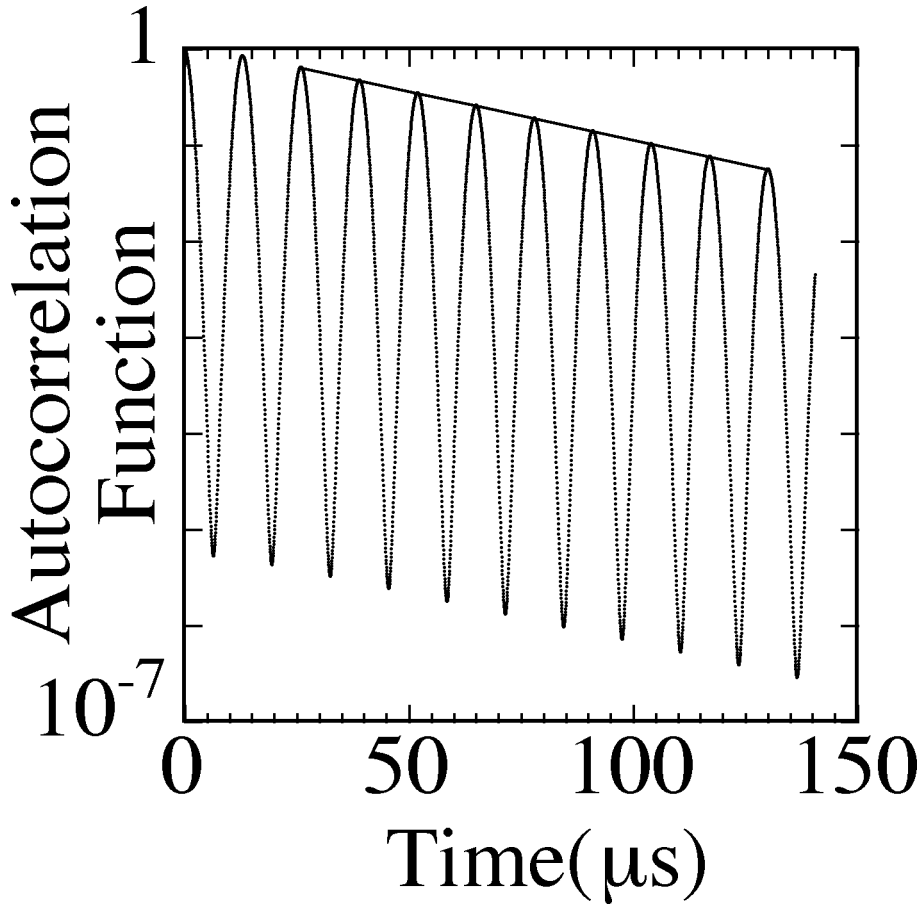

Figure 2.8: Theoretical autocorrelation function starting the lowest state in a well for the case a=4500 m/s^2 and V_0/h = 55 kHz. The solid line is an exponential fit to the peaks of the oscillations, starting from the third peak to avoid short-time, non-exponential effects.

The critical acceleration a_c (not to be confused with the classical acceleration a_{cl}) is related to the band gap of the system by $a_c = 2\pi(E_{gap}/2)^2/2\hbar^2 k_L$ where E_{gap} is the energy between the gap. v_r is the recoil velocity of 3 cm/s. This functional form will be compared to experimental measurements in Section 4.4.

A complementary model of the tunneling process uses the x-space picture with the tilted potential. In this picture, loss from the wells occurs from the atoms tunneling from bound states in the wells to the continuum. This is shown schematically in Figure 2.9

2.4 Discussion

Many properties of tunneling can be deduced by considering a single-barrier potential [12]. To obtain the classical limit of no tunneling or reflection, the wells essentially must be decoupled from each other and this requires either of two conditions. The first condition is that the well depth must not be comparable to the energy of the atom. The potential will not support tunneling or reflection behavior if the atom's energy is either much larger than the well depth or much smaller than the well depth. The second condition is that the width of the barrier must not be comparable to the spatial spread of the wave packet for the particle. For an atom in a bound state, these two conditions are equivalent to stating that the wave function must not be able to penetrate the barriers. We can extend these arguments to the case of multiple wells as in the standing wave but care must be taken since coherent effects from the periodicity can radically change the behavior (e.g. Bragg reflections). Since the standing wave's periodicity is fixed at 295 nm, the tunneling probability for this experiment is determined primarily by the well depth, although it is

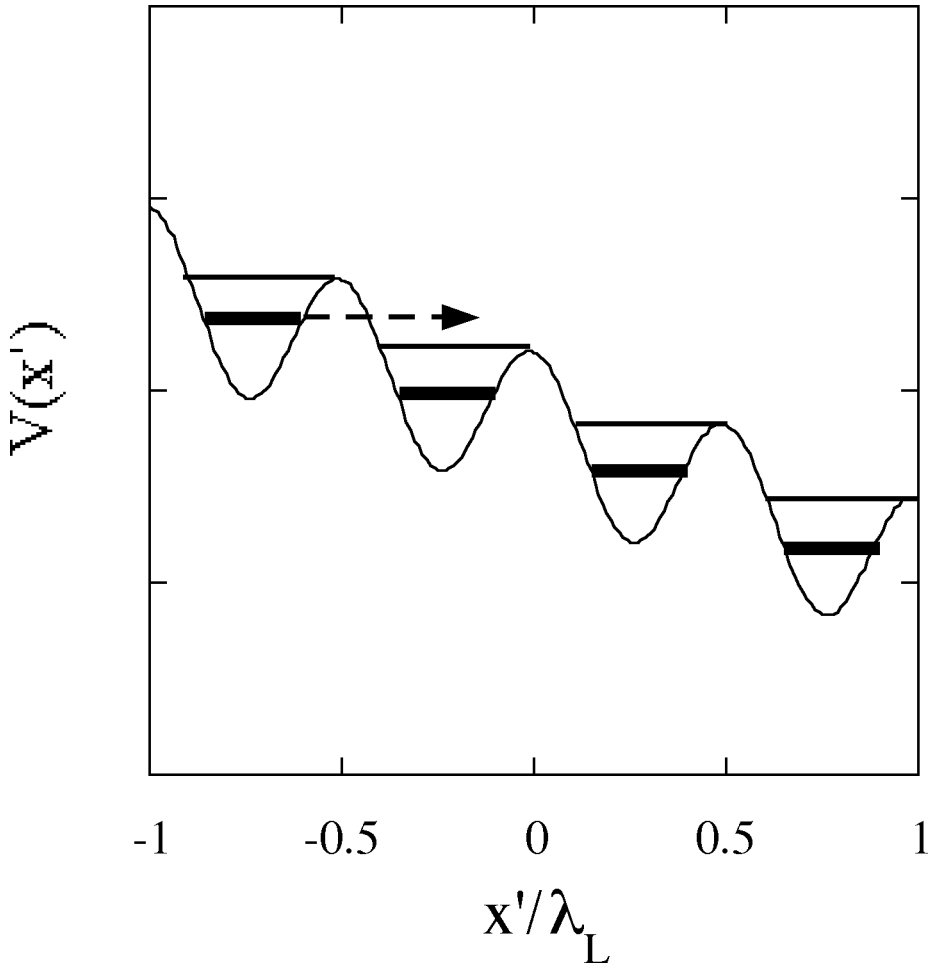

Figure 2.9: Schematic diagram of atom tunneling from bound state in well to the continuum.

possible to increase the periodicity of the standing wave by changing the angle between the two traveling beams.

If the well depth is comparable to the the center of mass energy of the atom, quantum mechanical effects such as reflection and tunneling occur. In this limit, the atom's wave function can be delocalized over many periods of the standing wave. In this case, the band picture used in many condensed matter problems is useful. This is the most interesting regime because here we can study many interesting effects of quantum transport in optical lattices such as Bloch oscillations and Landau-Zener tunneling. These are the experimental conditions where we study tunneling rates.

Many of the phenomena that we have discussed in the optical lattice context are also closely related to solid state physics problems. This is because the optical potential (Equation 2.29) is the same form as potentials arising in solid state systems. For example, consider an electron in a one-dimensional sinusoidal potential created perhaps from a lattice of ionic sites or a superlattice created by alternating layers of material with different band gaps. This potential is

$$V = V_0 \sin(\frac{2\pi x}{a_x}) \tag{2.44}$$

where a_x is either the lattice spacing or the superlattice layer width. V_0 is an effective well depth. When an additional static electric field is applied in the x-direction, the potential for the electron becomes

$$V = V_0 \sin(\frac{2\pi x}{a_x}) + eE_0 x. \tag{2.45}$$

Here we see that Equation 2.45 has the same form as Equation 2.29 if we replace eE_0 with Ma and a_x by $\lambda/2$. Examples of solid state devices that utilize tun-

neling are the tunnel diode which has been produced and used in applications for many years and, more recently, the resonant tunnel diode and the resonant tunnel transistor which are used in ultra-high frequency applications [20]. In the tunnel diode the tunneling is inter-band as the electron goes from the valence band on the p-side of the junction to the conduction band on the n-side. In the resonant tunnel diode the tunneling occurs inter-band as the electron tunnels across a barrier created by stacked materials with different band gaps. Our experiment is also a measurement of intra-band tunneling rates of atoms that tunnel from the lowest trapped band to the continuum of higher bands.

In our analysis of periodic potentials, we considered the potential as having perfect periodicity, however, we need to determine the conditions that will make this assumption valid. In solid state systems at non-zero temperature lattice vibrations (phonons) cause the ions to move and temporally break the periodicity. Other issues with a solid state system include impurities in the crystal that can also break the periodicity, collisions, and other multiparticle interactions between electrons that can become significant because the carrier density is high. The complications arising from phonons diminish at lower temperatures and consequently many solid state experiments are performed at cryogenic conditions, but the other complications are still significant even at low temperatures. In the atomic system, however, these problems with the lattice are negligible over the time scale of the experiment. The optical lattice potential has no vibrations if there are no spontaneous emission events and the phase of the laser light does not randomly shift over the duration of the experiment. Furthermore, the sample of sodium atoms is dilute enough to neglect multiparticle interactions. Consequently, we can consider the potential

as perfectly periodic.

There are two other differences between the atom system and the electron system. First, the electron is an indivisible particle with no internal structure, while the atom is comprised of several electrons orbiting a nucleus in many different shells resulting in a very complicated internal structure. We saw earlier that the internal structure of the atom can be neglected if the interaction with the laser is far-detuned from resonance using the dipole force approximation. Thus, we consider only center of mass motion in the interaction. Second, the atom that we will consider is sodium which is a boson, while the electron is a fermion. In the atomic sample from the MOT, the density is not large enough for Bose statistics to be important, however in the electron system Fermi statistics are usually very important. In the future it might be interesting to study the atomic system at higher densities for bosonic atoms and to compare it with a system of fermionic atoms such as ^6Li, but this would require starting with samples much colder and denser than the MOT.

Chapter 3

Experimental Setup

3.1 Overview

The study of the interaction of atoms with a one-dimensional accelerating optical lattice requires the measurement of momentum transfer from light to atoms. This is accomplished by preparing the atoms in a suitable initial condition with known momentum and position distribution, applying the interaction potential, and measuring the resulting final momentum distribution of atoms. The experiment is a four step process carried out by a system of computer controlled acousto-optic modulators, electro-optic modulators, and magnetic field coils. The measurement flow chart is shown schematically in Figure 3.1.

The initial conditions are ultra-cold sodium atoms trapped in a standard magneto optic trap (MOT) [8]. The MOT is created by three pairs of counter-propagating circularly polarized laser beams and a magnetic field gradient provided by a pair of anti-Helmholtz coils. The magnetic field from the anti-Helmholtz coils is approximately zero at the center of the trap and has a gradient that is cylindrically symmetric and an additional gradient in the axial direction. The magnetic field gradients (with the lasers) provide a restoring force to the center of the trap. This restoring force arises because the laser beams are detuned to the red of resonance so that as the atoms move from the

center of the trap the magnetic field increases and consequently Zeeman shifts the atoms closer into resonance with one of the beams. This creates an imbalance in the radiation pressure that pushes the atoms to the point of lowest magnetic field.

Next, all the trapping potentials are turned off and the interaction potential is applied for some period of time, usually less than 1.5 ms. During this period the standing wave accelerates and the momentum distribution changes. The next step is to turn off the interaction and allow the atoms to free drift in the dark, usually less than 3 ms.

The final step occurs when the trapping laser beams are turned back on in the absence of the magnetic fields. In this configuration, the laser beams provide a viscous force (optical molasses) on the atoms, and for the duration of the exposure freezes them in place. The fluorescence from the atoms is then imaged on a CCD camera. Since we know the drift time, the initial position and momentum distribution of the atoms, and the final position distribution, we can calculate the final momentum distribution of the atoms. The CCD image is a representation of the final velocity distribution of the atoms if the time in which the atoms are interacting with the optical potential is short enough. If this time is too long, the atoms will move so that the final spatial distribution can not be deconvolved to an exact final velocity distribution. Using this technique in the tunneling experiment we can accurately determine which atoms tracked the velocity of the standing wave.

The laser table overview is shown in Figure 3.2. The 'workhorse' of the system is the Coherent Innova 200 Argon Ion laser that pumps two single mode dye lasers, one a commercial Coherent 899 ring laser and the other a home built

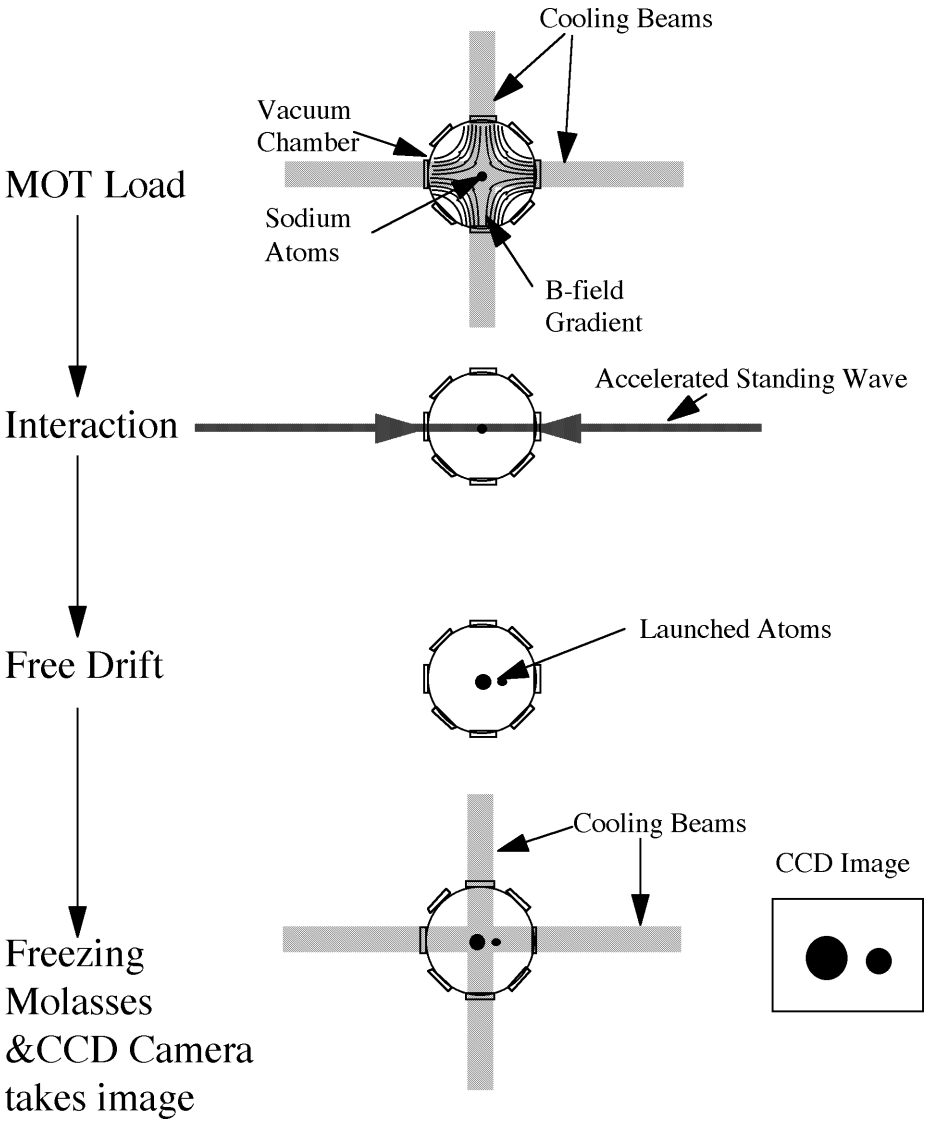

Figure 3.1: The time sequence for a momentum transfer measurement from a time-dependent interaction. The four steps include: MOT load (6 seconds) during which a CCD exposure can be taken, interaction with the standing wave (1.5 ms), free drift (3 ms), and freezing molasses and CCD exposure (10 ms).

dye laser [21]. The frequency of the light from the Coherent dye laser is locked about 80 MHz to the red side of the saturated absorption line obtained from a separate sodium cell. The error signal for locking is obtained from a double lock-in using FM spectroscopy [22]. The Coherent laser's light is used for the MOT and molasses laser beams to cool and trap the sodium atoms and also for the final detection. AOM1 (Acousto-optic modulator at 80 MHz) is used to stabilize the MOT/molasses laser power and to turn off the light during the interaction process. The frequency of the light in the MOT/Molasses beams is 20 MHz to the red of the sodium resonance. EOM1 (Electro-optic modulator) is used to put sidebands on the cooling/trapping beams for the repumping out of the F=1 state (see Figure 3.4). The light from the home built laser is used for the interaction/acceleration beams described later.

The timing in these experiments was controlled by a 486-33 MHz PC with three National Instruments I/O boards: an AT-MIO-16F-5 board with A/D and D/A converters and TTL ports, a PC-DIO-24 board with TTL I/O, and a GPIB-PCIIA board for higher level control, especially useful for programming arbitrary waveform generators. In general, the timing accuracy of the computer is limited to 20 μs, and the jitter is about 10 μs. This makes it impossible for important timing to be controlled by the PC; therefore it was necessary to use triggered Fluke-Phillips PM 5712/5715 pulse generators for all the crucial timing. The computer served two purposes: to program the arbitrary waveform generators and to trigger the pulse generators which controlled all the important timing. The programming of the computer was accomplished from National Instruments Lab Windows-DOS using Microsoft C 6.0 for the stand-alone executable files. The timing electronics diagram for the tunnel-

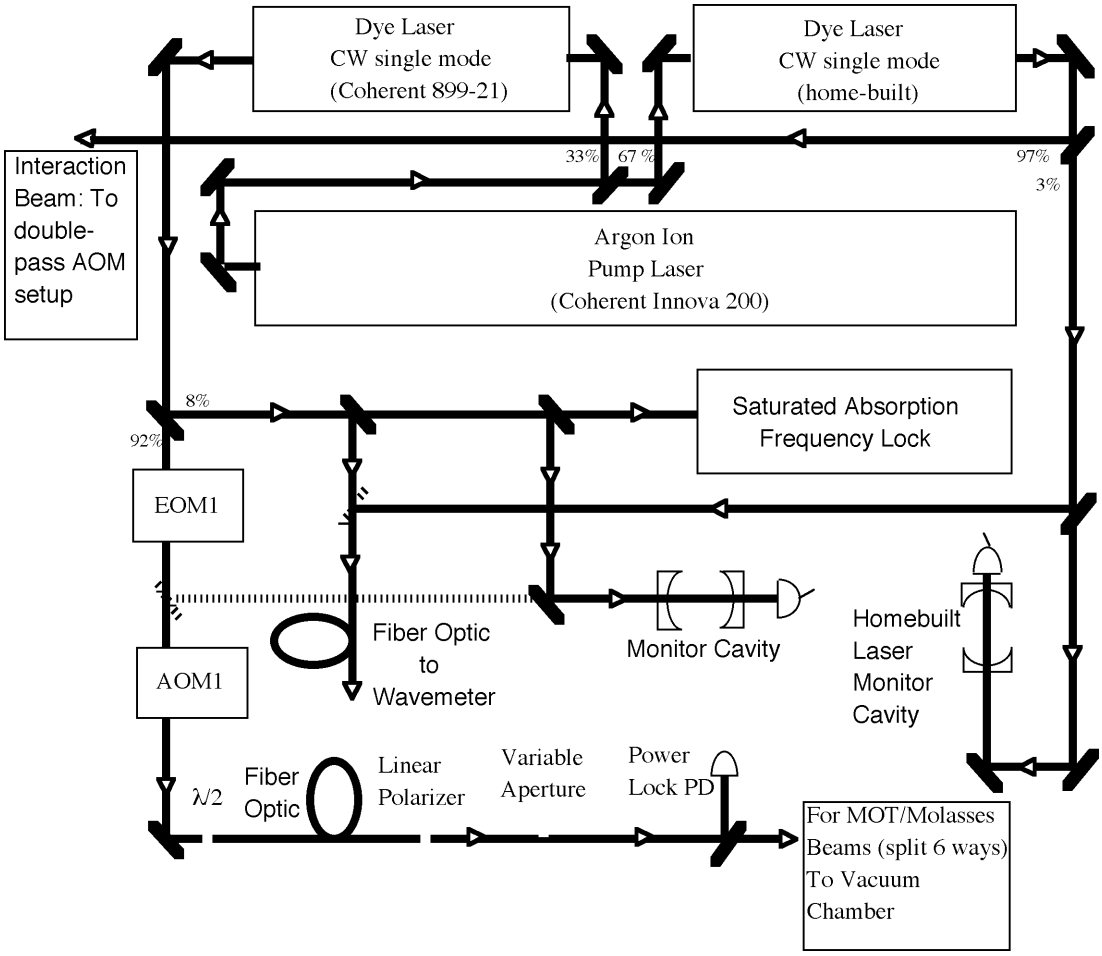

Figure 3.2: The block diagram of the laser table. Related figures are the block diagram for timing electronics (Figure 3.3) and the interaction beam/double pass diagram (Figure 3.6).

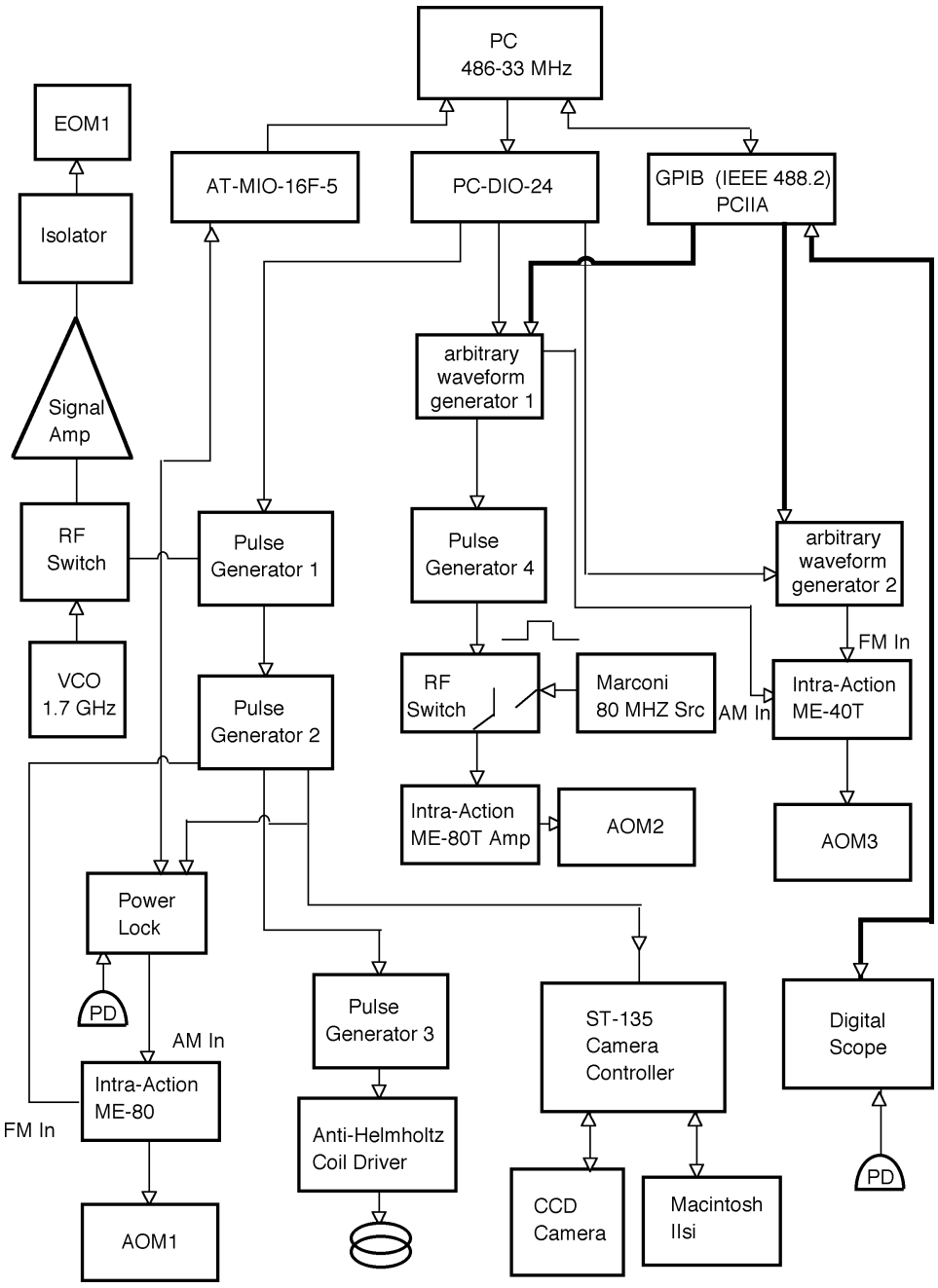

Figure 3.3: The block diagram of the electronics. The timing is controlled by pulse generators and arbitrary waveform generators with trigger provided by the 486 PC.

ing experiments is shown in Figure 3.3 and the timing diagram is shown in Figure 3.5.

The experiment is started by a trigger from the PC-DIO-24 panel which does two things: It triggers pulse generator 1 which controls the MOT/molasses light level and it triggers the arbitrary waveform generators 1 and 2 which trigger the AOMs for the interaction beam. Pulse generator 1 subsequently sends a trigger for the EOM to switch on the 1.7 GHz sidebands and also sends a trigger to pulse generator 2. For the tunneling experiment, the sidebands were left on continuously. Pulse generator 2 then triggers the AOM to turn off the MOT/Molasses beams, sends a delayed trigger to pulse generator 3 which turns off the trap's magnetic field, and sends a delayed trigger to the camera controller to take an image after the allotted drift time. The trigger to the amplitude port of the AOM1 driver is also sent to the frequency modulation port. The light from an acousto-optic modulator has an angle dependency which is proportional to the frequency of the acoustic wave. Since this light from AOM1 goes into an optical fiber, the fiber is misaligned when the frequency changes. It was originally noticed that even though the signal to the amplitude port was zero, a small amount of RF was present sending some resonant light through. This current configuration of shifting the beam off the fiber ensured that no resonant MOT/molasses light was present during the interaction portion of the experiment. Arbitrary waveform generator 1 (Tektronix AWG5105) is programmed via GPIB to provide square pulses of arbitrary length. AOM2 and AOM3 are used for the interaction beam described in Section 3.3. Channel 1 of this waveform generator is sent to the amplitude modulation port of the frequency-shifted Intra-Action ME-40T AOM driver (double-passed) to control

the light level in AOM3. Channel 2 is sent to pulse generator 4 operating in T/2 mode so that the output pulse follows the input signal. Pulse generator 4 controls an RF switch (Mini-Circuits 2FSWHA-1-20) which lets an 80 MHz source from a Marconi model 2022D digital frequency synthesizer (stable to 1 Hz) connect to the amplifier portion of an Intra-Action ME-80T and finally drive AOM2. The VCO portion of the Intra-Action ME-80T was bypassed since it does not have the frequency stability of the Marconi synthesizer. We did use a VCO for the double-passed AOM but using the Marconi for the 80 MHz beam insured a higher stability than if we used VCOs for both drivers. The PC-DIO-24 also provides the trigger for arbitrary waveform generator 2 (Stanford Research Systems DS345). This arbitrary waveform generator provides the signal to the FM port of the AOM3 driver giving the frequency sweep and is also programmed by GPIB. Finally, the GPIB interface also communicates with the digital scope (Tektronix 524A) which obtains waveforms from two photodiodes (Thorlabs PDA150) to characterize the power in the two interaction beams.

3.2 Initial Conditions: Trapped and Laser Cooled Sodium Atoms

The initial condition for the experiments is approximately 10^5 sodium atoms trapped in a standard magneto-optic cell trap with six $\sigma^+\sigma^-$ laser beams. The atoms are confined in an approximately Gaussian distribution in space (σ =.15 mm) and momentum ($\sigma = 6\hbar k_L$ centered at p=0). The trap envelope is a quartz sphere with nine 1-inch fused silica windows fritted onto the main sphere. The chamber is connected to a vacuum-distilled sodium ampule that was opened after the bakeout and a Varian Star-Cell 20 l/s ion pump. The

final background pressure of the system is 5×10^{-10} Torr with a approximate sodium vapor pressure of 5×10^{-11} Torr. The windows are not anti-reflection coated for the experiments presented here, but a new trap envelope consisting of a stainless steel manifold with 16 anti-reflection coated windows is being constructed for future experiments.

The light for the MOT and optical molasses comes from a Coherent 899-21 single-mode dye laser tuned to the sodium D_2 line at 589 nm. This dye laser is pumped by approximately 9 Watts (33%) of multi-line power from the Coherent Innova 200 argon-ion laser (see Figure 3.2). About 92% of the Coherent dye laser power goes through an electro-optic modulator to produce sidebands at 1.7 GHz. The sidebands are used as the repumper from the F=1 dark state (see Figure 3.4). The electro-optic modulator is a $LiTaO_3$ crystal surrounded by an RF resonating structure and generates sideband amplitudes that are typically 15% of the carrier power. The other 8% of the power is split and used for two things. A small fraction (about 1-2 mW) is sent through an optical fiber (OZ Optics) to another table that has a scanning Michelson interferometer wavemeter (NIST LM-11) that has an accuracy of 1 part in 10^7. The rest of this power is used for saturation absorption spectroscopy of a sodium cell which is used to lock the laser frequency to about 20 MHz below resonance on the sodium D_2 line (see Figure 3.4). Of the 92% which went through the electro optic modulator, a small fraction (1-2 mW) of this is used in a scanning Fabry-Perot cavity used for laser diagnostics and sideband characterization. The rest goes through an acousto-optic modulator (AOM1) which is used to lock the power level of the beam to within 1% and finally through an optical fiber to be split six ways to form the MOT beams. The

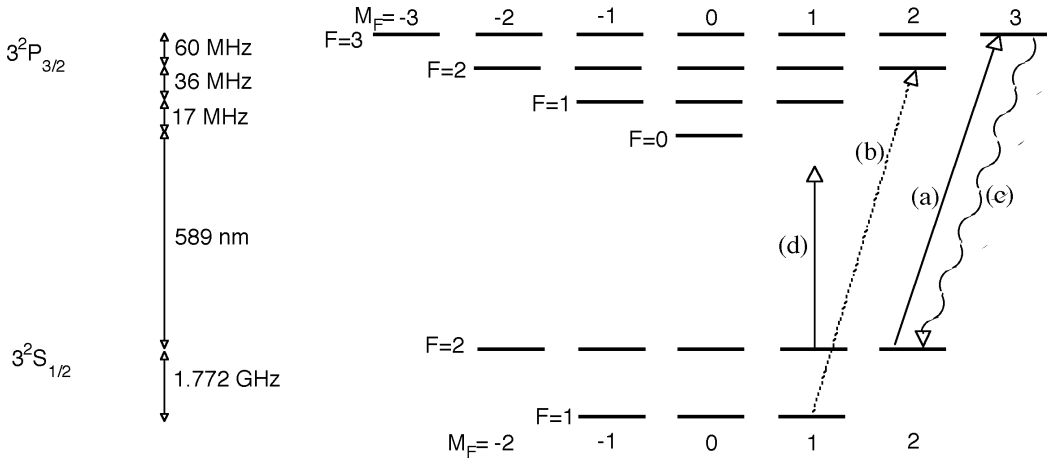

Figure 3.4: Term Diagram for the Sodium D_2 line. For the $3S_{1/2}$ state I = 3/2 and J = 1/2, and since F = J + I, F = 1,2. For the $3P_{3/2}$ state J = 3/2 so F = 0, 1, 2, 3. The magnetic sublevels are $-F \leq m_F \leq F$. Representative examples of (a) the cooling and trapping beams, (b) the optical pumping sideband, (c) spontaneous decay, and (d) the interaction Hamiltonian are shown.

power lock circuit driving AOM1 is also fast enough (switching time 40 μs) to be used to switch on and off the MOT resonant beams. AOM1's switching time by itself is much faster than this however. Also, as described earlier, the frequency offset on AOM1 was shifted to intentionally misalign the fiber to ensure that no resonant light was on during the interaction portion of the experiment (see Figure 3.5).

The magnetic field coils are constructed from roughly 100 turns each of 24 gauge wire with a radius of 4 cm. The coils are configured in the anti-Helmholtz configuration, where the separation is equal to the radius and the current in each coil runs in the opposite direction of the other one. This configuration creates zero magnetic field at the center with a gradient of 10 G/cm at the center with an approximate current of 1 Ampere. Because the coils must be

switched off quickly, a feedback loop consisting of a Burr Brown OPA541BM high current operational amplifier was used to lock the current to a level which could be switched quickly ($< 150\mu$s). The details of this feedback circuit are in [22]. In addition to these coils there are three sets of Helmholtz coils which were used to null residual magnetic fields. They are adjusted to optimize the spread in the atomic cloud (see Section 4.1).

3.3 Interaction Potential

3.3.1 Experimental Realization of Accelerated Standing Wave

In the previous chapter we described the dipole force potential using a two-level model for the atom. In sodium, the $3S_{1/2}$ ground state manifold has two hyperfine levels (F=1,2) and the $3P_{3/2}$ excited state manifold has four hyperfine levels (F=0,1,2,3). Each of these states has 2F+1 magnetic sublevels (see Figure 3.4). It can be shown that for linearly polarized light that is detuned far from resonance and large compared to the $3P_{3/2}$ splitting, the ac Stark shift (the potential) is independent of magnetic sublevel [22, 23]. Furthermore, we have shown experimentally that the laser cooling process leaves the atomic population in the F=2 ground state when the trapping optical fields are turned off. Thus at the beginning of the interaction time, the atoms are in one of magnetic sublevels of the F=2 ground state. If there is negligible probability of spontaneous emission, the atom will remain in the same state that it started in. Therefore, the resulting force on each atom will be the same.

In the tunneling experiments, the accelerated standing wave was created from the homebuilt single mode dye laser far-detuned to the blue of the sodium resonance. We also performed the experiment with the laser far-detuned to the

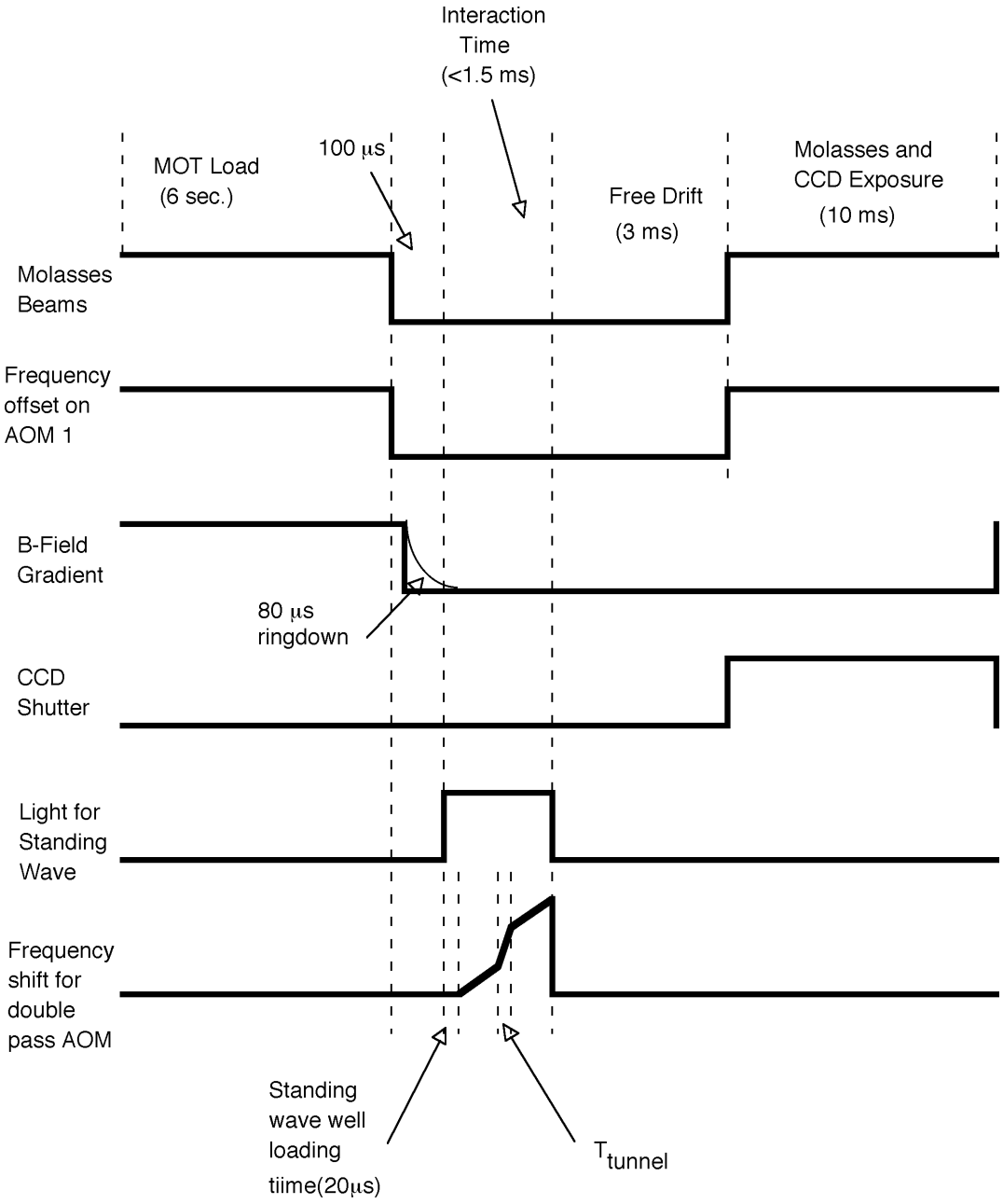

Figure 3.5: The pulse timing shows how the four step measurement process is controlled electronically.

red of resonance and found the results to be independent. The only difference would be that potential nodes in the red detuned case appear as antinodes in the blue detuned case. The full laser power (1.1 W) was split into two beams which were shifted in frequency from each other and aligned over the atomic sample in a counter-propagating configuration. The realization of the accelerated standing wave is centered on the frequency offset between two counter-propagating laser beams. In the experiment, this was accomplished by shifting both laser beams in frequency using AOMs and changing the offset of one of them in time. It is necessary to use the time-varying AOM in the double pass configuration because in single pass, the angle of the deflected beam from the AOM changes with acoustic driving frequency. If properly aligned, after retro-reflection in double pass the second deflected beam will be aligned with the original input beam (see Figure 3.6). The quarter wave plate and polarizing beamsplitting cube combination allow the separation of the input beam and the double passed beam. A lens is placed in the retro-reflected beam to re-collimate the light for good deflection efficiency in the double pass. The fixed AOM (AOM2) is set at 80 MHz and the double pass AOM (AOM3) is shifted a few MHz around a center frequency of 40 MHz. Thus, both beams are shifted up approximately 80 MHz but one varies over a few MHz. The double pass AOM was aligned by maximizing the deflected beam intensity first in single pass (usually about 90%) and then adjusting the reflecting mirror to maximize the double passed spot (final power about 170 mW). The spot is finally passed through a spatial filter consisting of two fast lenses and a 50 μm pinhole, and then re-collimated. Since standard stainless pinholes are easily destroyed, diamond aperture wire dies from Indiana Wire Die were used in-

stead. After the pinhole, a variable iris blocks all but the center lobe. When the double pass AOM is correctly aligned, the spot should not move spatially when the frequency is sweeped. This is one criteria for a good alignment of the double pass. The spot from the fixed AOM is also spatially filtered in a similar manner. The frequency sweep is accomplished by input to the ST-335 controller input. The input sequence is a three step process accomplished by GPIB programming of the arbitrary waveform generator as described in Section 4.1. To monitor the power of the beams in situ, anti-reflective coated 3/8" thick windows were inserted into each of the interaction beams to split off a very small amount of power to two fast photodiodes with amplifiers (Thorlabs PDA150) which have a frequency response of 50 MHz. The voltage from both photodiodes was monitored on a digitizing scope (Tektronix 524A). The voltages from the photodiodes were calibrated to the laser power in CW mode (see Section 3.3.2). Because of the spatial filter, any spot movement from the AOM will manifest itself in power reduction. By capturing the power waveform in the photodiode, a final optimization of the double pass AOM was done to eliminate beam walk with the sweep. Power fluctuations through the pinhole spatial filter were reduced to $\pm 1\%$ through the tunneling portion of the frequency sweep and $\pm 7\%$ over the entire sweep of almost 10 MHz (5 MHz before the double-pass).

3.3.2 Characterization of the Accelerated Standing Wave

The important parameters of the standing wave are those which determine the well depth (Equation 2.16) and the velocity of the nodes. The well depth can be determined from the power in the laser beams, spot size, and detuning. The

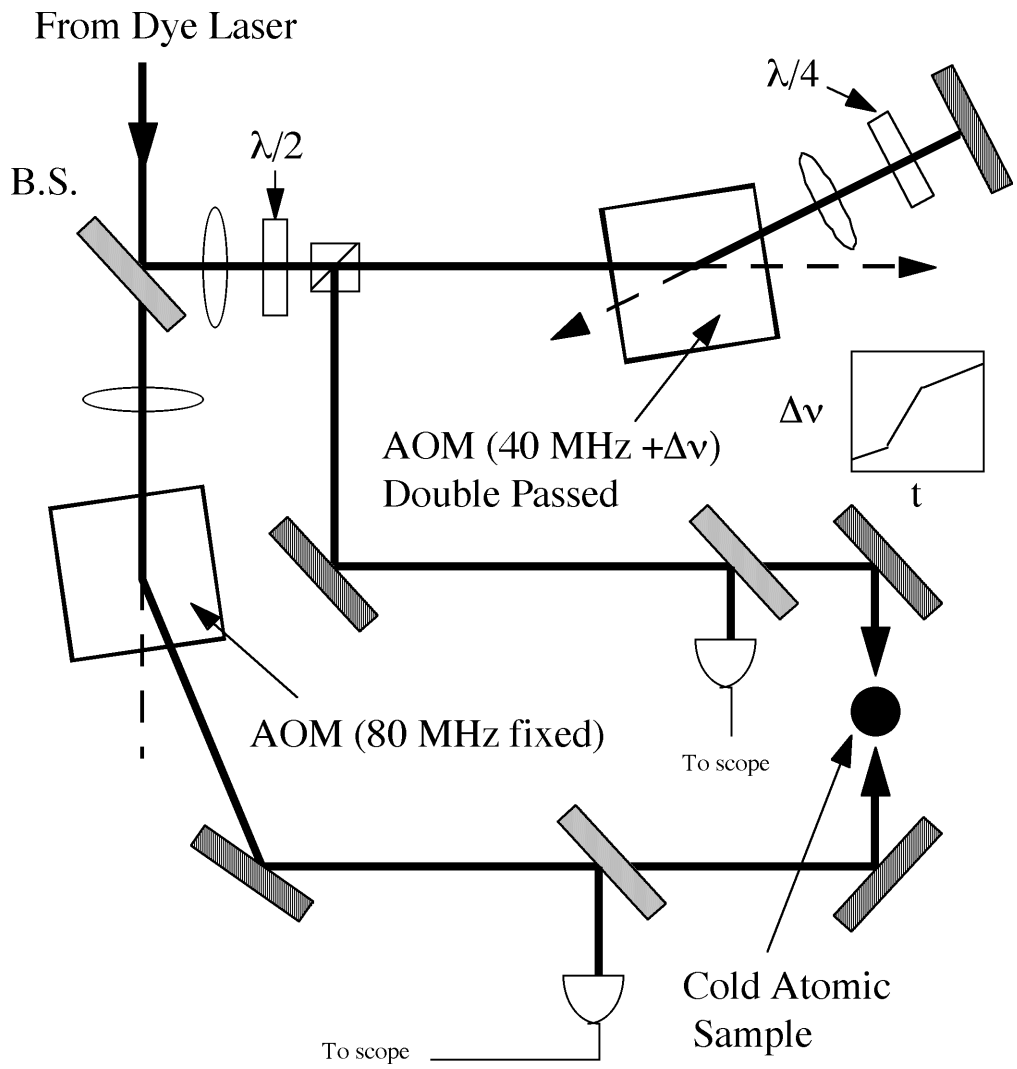

Figure 3.6: Figure shows the setup for the accelerated standing wave interaction beam. The signals from the photodiodes are recorded on a digitizing oscilloscope and stored on computer for later analysis.

beam power was measured on a Coherent Fieldmaster power meter which was calibrated with respect to a NIST traceable Newport model 1825-C power meter with model 818-UV head that has an absolute accuracy of ±5%. The width of the beam was measured by moving a knife-edge across the profile in front of a detector. From this, the distance between the 70% and 30% power points is measured. If the focus at the spatial filter is small compared to the aperture, then the output is Gaussian. A normalized Gaussian intensity distribution, characterized by a spot size w_o ($1/e^2$ intensity radius) is:

$$I(x,y) = \frac{2}{\pi \mathrm{w}_o^2} e^{-\frac{2(x^2+y^2)}{\mathrm{w}_o^2}}. \tag{3.1}$$

Integrating from the $x_{70\%} - x_{30\%} = d$ power points with an knife edge

$$0.70 - 0.30 = \int_{-d/2}^{d/2} dx \int_{-\infty}^{\infty} dy I(x,y) \tag{3.2}$$

results in

$$\frac{2}{5} = \mathrm{erf}(\frac{d}{\sqrt{2}\mathrm{w}_o}), \tag{3.3}$$

where erf is the error function. By solving numerically, the measured value d is related to the spot size w_o by $\mathrm{w}_o = 1.91\ d$. A Gaussian profile was assumed for the tunneling experiments reported here. Since the field strength E_0 must be determined to connect to Equation 2.16 a better way in the future may be to use a commercial beam profiler. For now E_0 is experimentally characterized by the total power ($\langle P \rangle$) and the $x_{70\%} - x_{30\%} = d$ power points. Using this technique we determined the spot size of the beam from the 80 MHz fixed AOM to be 1.91 mm and the spot size from the 40 MHz shifted AOM to be 1.95 mm. A 'flat,' linearly polarized traveling Gaussian beam has the form

$$\vec{E}_{Gauss} = \hat{y} E_0 e^{-(\frac{\sqrt{x^2+y^2}}{\mathrm{w}_0})^2} \cos(\omega_L t + k_L x). \tag{3.4}$$

The time-averaged intensity has the form

$$\langle I \rangle = \frac{1}{2} c \epsilon_o E_o^2. \tag{3.5}$$

The integrated power can then be calculated

$$\langle P \rangle = \int \langle I \rangle dA \ = \pi \mathrm{w}_o c \epsilon_o E_o^2 \int_0^\infty dr e^{-2\frac{r}{\mathrm{w}_0^2}} \ = \frac{\pi c \epsilon_o \mathrm{w}_o^2 E_o^2}{4} \ , \tag{3.6}$$

where $r = \sqrt{x^2 + y^2}$, which gives

$$E_o = \sqrt{\frac{4\langle P \rangle}{c \epsilon_o \pi \mathrm{w}_o^2}}. \tag{3.7}$$

This gives the expression for field strength used in Equation 2.16 in terms of experimentally measured quantities. As was stated earlier, the power of the beams can be monitored by capturing the voltage waveform from two fast photodiodes (Thorlabs PDA150) onto the digitizing oscilloscope (Tektronix 524A). The photodiodes were calibrated by measuring the power before the chamber on the Coherent Fieldmaster and comparing with the voltage from the photodiodes. This measurement was repeated for many different powers. To obtain the power at the atoms, the measured power was corrected by the reflection from the two surfaces on the front window (4% each). The power was then plotted versus voltage and curved fit with a line, which showed excellent linearity for the power range used. During the short time during the experiment when the interaction beam was on, the digitizing scope collected the waveforms from the photodiodes and transferred them through GPIB interface to the 486 PC where the minimum, maximum, and average of each laser power was stored on disk for later evaluation and discrimination. The laser power level could be then well known except that there are other uncertainties in the standing wave field strength at the atoms including most significantly interference fringes

caused by the windows, wave vector mismatch and misalignment between the two counter-propagating beams. It is also possible that these fringes could move shot to shot, causing a time-varying change in the well depth. Another problem with the Gaussian beam is that since the cloud of atoms is spread partially over a portion of the interaction beam, not all the atoms experience the same well depth. The interaction beam spot size is 2 mm and the radius of the MOT is .075 mm. The resulting well depth for atoms at the edge of the MOT is 99.7% of the well depth for atoms at the center of the MOT, so it is a small effect. In the Wannier-Stark work [2], this was also an issue and was addressed by binning up a small area on the CCD chip for final analysis (see Section 3.4). Ideally one should have an *in situ* measurement of the power on the atoms by analyzing the effect on the atoms, such as the Mollow triplet. However, this measurement is difficult to implement. Absolute power calibration is therefore the largest experimental uncertainty.

The procedure for alignment of the interaction beams was to first to tune the laser near the sodium resonance and align one beam onto the atoms in the trap. When the beam frequency is near resonance, it will push the atoms along its direction. It was aligned for maximum pushing effect on the atoms. The second beam was then aligned onto the first beam until they were collinear, and the laser was detuned from resonance for the experiment. Finally, the simple single acceleration experiment was run several times between which small alignments could be made to optimize the number of atoms accelerated.

To obtain the detuning of the standing wave beams, a small portion of the interaction beam was sent through a single mode OZ fiber optic to a scanning Michelson interferometer (NIST LM-11). The wavemeter is a scanning

interferometer formed by corner cube reflectors that are translated via an air-bearing cart-track arrangement. The light of unknown frequency traverses essentially the same path as that of a laser of known frequency. As the corner cubes move, the interference pattern is scanned through successive fringes and the ratio of the fringes counted simultaneously for each laser yields the ratio of the laser wavelengths in air. The ratio of the wavelengths in vacuum can be determined if the small correction for the dispersion in air between the reference wavelength and that of the unknown laser is taken into account. Specifically, the frequency of the known laser comes from a stabilized HeNe:

$$\nu_{HeNe} = 473\ 612\ 192 \text{ MHz } (\pm 30\text{MHz}) \tag{3.8}$$

Since the wavelength of the sodium D_2 line in air is

$$\lambda^{air}_{NaD_2} = 588.9950 \text{ nm}, \tag{3.9}$$

the wavelength ratio in air is

$$\frac{\lambda^{air}_{HeNe}}{\lambda^{air}_{NaD_2}} = 1.0743992 \tag{3.10}$$

In practice, the detuning was chosen after the electric fields were measured to give the desired well depth V_0. Since spontaneous emission becomes less of an issue for further detuning, it is favorable to obtain a particular well depth with the highest power possible and furthest detuning. Consequently, the beam powers were optimized to their maximum and the detuning was chosen to provide the desired well depth. To set the detuning, the laser was tuned until the wavelength meter ratio read

$$ratio = 1.0743992 \pm \frac{\delta(GHz)}{.0474} \tag{3.11}$$

where the second term gives the calibration for the detuning δ which could be either detuned blue or red. The detuning was continuously monitored throughout the experiments to ensure that the interaction laser did not drift or hop modes since it was not actively locked to any error signal.

All these measurements described here could determine the well depth. A typical set of parameters is 1.9 mm for spot size, a detuning of 20 GHz, and beam powers between 30 and 45 mW, which gives well depths between $V_0/\mathrm{h}=$ 66 kHz to 100 kHz.

The velocity of the standing wave was characterized by heterodyne of the two interaction beams. A 50% beamsplitter was inserted into the path of the two beams and one path was retro-reflected back to the beamsplitter (see Figure 3.7). The other path was attenuated and focused onto another Thorlabs photodiode which was also captured onto the Tektronix TDS 524A digitizing scope. The waveform was stored on PC disk through the GPIB interface and evaluated with a C+ program on a UNIX machine. Since the beat frequency on the photodiode is exactly the frequency separation between the two beams, a measurement of this frequency gives the velocity of the standing wave ($v = \Delta\omega/2k_L$). Since the offset ($\Delta\omega$) is changing in time, one way to determine the instantaneous frequency is to measure the time between subsequent zero crossings. The C+ program which calculated the heterodyne frequency in this way is shown in Appendix A. Figure 3.8 shows a sample measured heterodyne frequency versus time plot where the target values of accelerations and velocities are confirmed. By curve fitting each section of the plot, we determined the slope (acceleration) of the each section and its uncertainty. In this figure the acceleration was determined to be 6041 $\pm$ 10 m/s^2 and the tar-

get value was 6000 m/s^2. Other heterodynes produced similar results so we determined that the error bar on acceleration is $\pm$ 50 m/s^2. The frequency jitter on the heterodyne was confirmed to give a bandwidth less than 10 kHz by measuring the photodiode signal on a spectrum analyzer over a period of a minute. Consequently, on the time scale of the experiment (less than 1.5 ms), the bandwidth should be less than this.

3.4 Final Distribution and Detection

After the interaction time, the measurement of the atoms' momentum is accomplished by a time of flight measurement. This process consists of two parts: a free drift in the dark and a detection of the final position distribution. The free drift time occurs usually for about 3 ms during which all the light and magnetic fields are switched off (see Figure 3.5). After the drift, the resonant lasers are switched on again without the magnetic fields. This provides the optical molasses which stops the atoms and also scatters light from them which is imaged on the CCD camera. To detect the atoms' positions accurately after the free drift requires the atoms to be practically at rest while the camera takes an image. The viscous force from the optical molasses causes the velocities of the atoms to damp out in roughly 10 μs. This technique can produce very accurate measurements of momentum if the interaction time is not too long. If the freeze-in time is less than 10 ms the atoms do not move during the image and we obtain an accurate determination of position [22]. The detection system consists of a Princeton instruments Charge Coupled Device (CCD) camera system and controller. The controller is connected to a Macintosh IIsi computer via a GPIB NuBus interface. The CCD camera with a Sigma f/2.8 lens

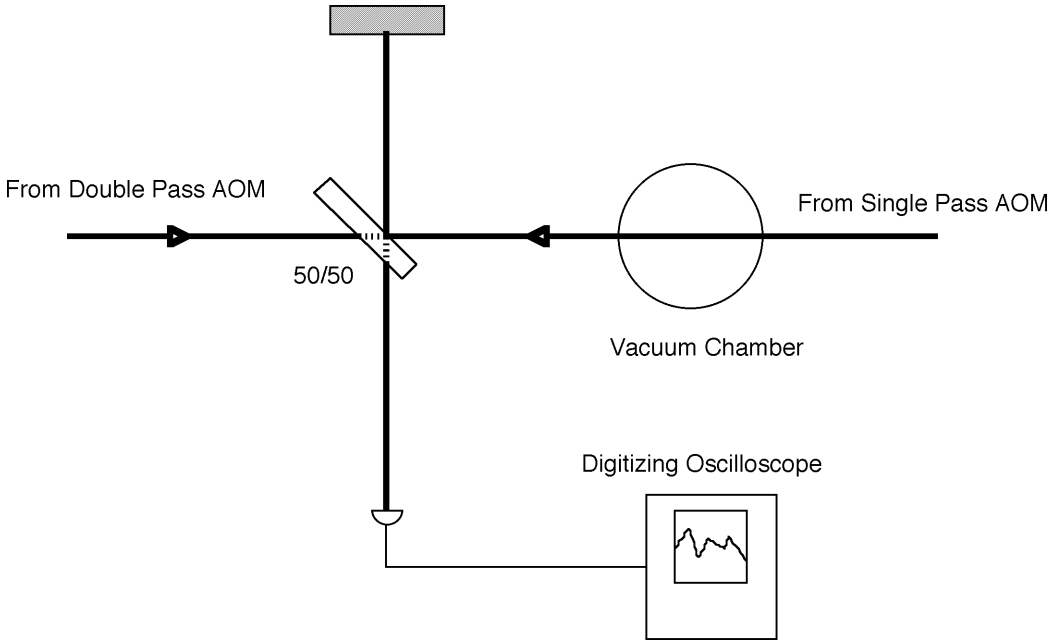

Figure 3.7: A 50/50 beamsplitter is inserted into the path of the interaction beams. One reflection is sent to a mirror and the other one is sent to a photodiode. The signal on the scope oscillates at the difference frequency of the two laser beams.

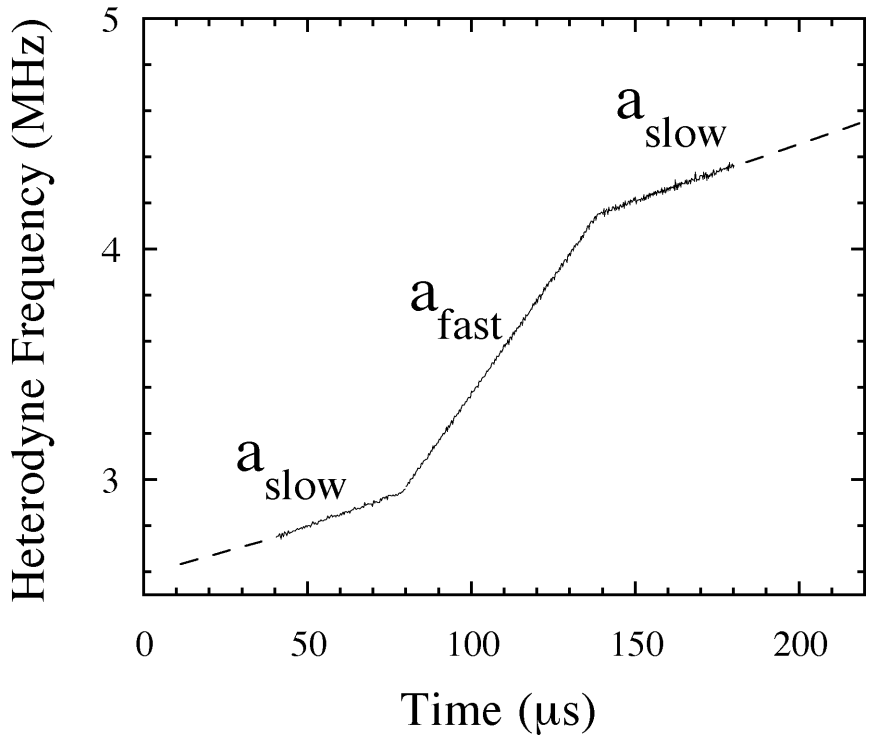

Figure 3.8: Measured heterodyne beat frequency as measured on the photodiode. The three step acceleration process is shown. For this particular run, the target values a_{slow}=1500 m/s^2 and a_{fast}=6000 m/s^2. The dotted lines are to represent that the signal continues to earlier and later times for an actual run. By curve fitting each section of the curve it is determined a_{slow1}=1521 $\pm$ 20 m/s^2, a_{fast}=6041 $\pm$ 10 m/s^2, a_{slow2}=1522 $\pm$ 15 m/s^2. The error bar from the target range is the $\pm$ 50 m/s^2

was suspended about 15 inches from the vacuum chamber and could focus on the atoms which were trapped and accelerated. One problem with the accelerated system which was not a problem with the quantum chaos work involved the spatial extent of the freezing beams. The large final velocities which the atoms can be accelerated to become large spatial profiles after the time of flight measurement, in some cases comparable to the spatial extent of the freezing beams. The Gaussian profile of the freezing beams causes the fluorescence rate to decrease when the final distance was more than about 7 mm ($1/e^2$ point). This for example corresponds to a velocity of 80 recoils with a free drift time of 3 ms. Consequently, the final distribution was kept below this limit. The binning window was chosen to be 10 pixels wide by 240 pixels long (16 pixels represent 1 mm at the atoms), which limits the measurements to a set of atoms that are colder than the initial conditions for the one transverse direction which is integrated out (10 pixels). This essentially limits the detection of transverse atoms to those which see the same effective well depth V_0 within $\pm 5\%$, and excludes those atoms which moved down the Gaussian beam profile of the interaction beams during the duration of the experiment. The CCD camera detection software is KestrelSpec which integrated the two-dimensional images onto one-dimensional curves for analysis. The power in the molasses beams is controlled by feedback to an AOM (AOM1) from a photodiode and is stabilized to 1% [22]. This allowed good background subtraction since it eliminated power fluctuations in the molasses beams from shot to shot. Figure 3.9 shows a CCD picture after a typical acceleration experiment with deep wells. The peak on the left are from atoms which have been accelerated to a velocity near 80 photon recoils (2.4 m/s) and the large central peak on the right is from atoms

which were not trapped in the wells and remained at their initial velocities. The upper frame shows an integration of the two dimensional picture binned appropriately. Although the well depth for this run was significantly deeper than in subsequent work, the results also exhibit quantum mechanical tunneling, which can be seen in the region between the two peaks. This quantum tunneling is identified to be from higher bands as described later in section 4.6.

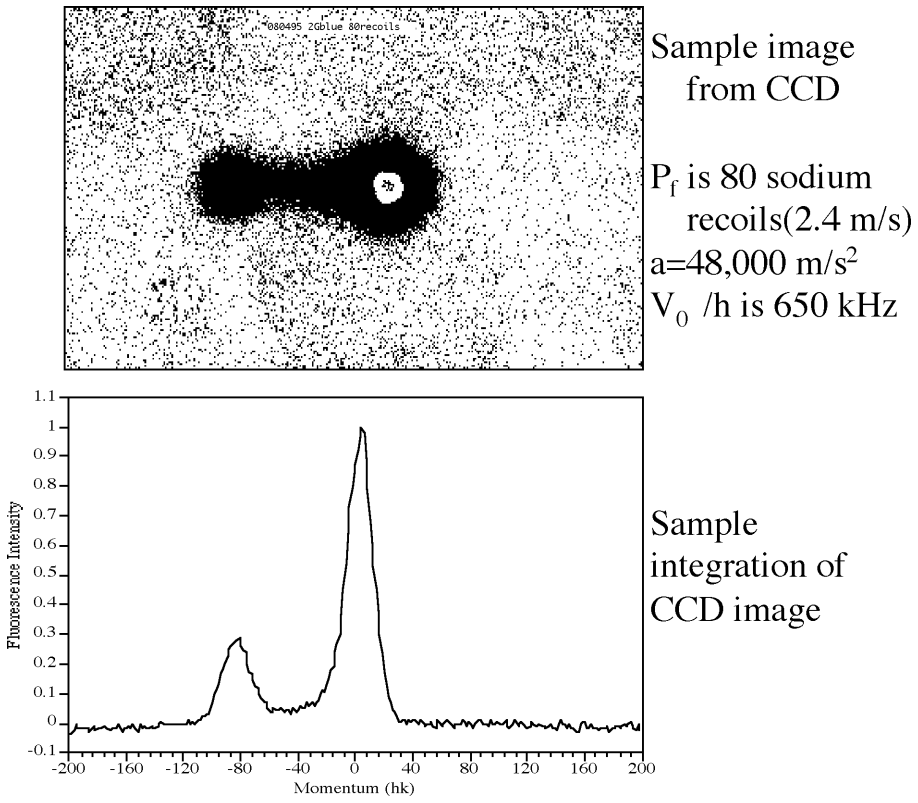

Figure 3.9: Upper frame shows a sample CCD picture of the spatial distribution of the fluorescence from atoms after acceleration. The well depth is deep compared to the initial energies of the atoms. The lower frame shows the conversion of the spatial information into a momentum distribution.

Chapter 4

Tunneling Experiment

4.1 Introduction

The ultimate goal of the experiment is to measure the tunneling rate from bound states to the continuum. For all of the data presented here, the well depth was chosen such that only one energy band was within the wells (see Figure 2.5). We will be considering only tunneling between this lowest band to the second band during an acceleration. In this case, it is possible to tell whether an atom has made the transition out of the lowest band. Since the band gaps between the higher bands above the second one are small, the atoms are practically free particles as tunneling can readily occur between these bands. Consequently, only atoms which remain in the lowest band will be accelerated with the standing wave and atoms in the higher band are considered to be in the continuum. This makes it simple to tell whether an atom has made the transition from the lowest band by monitoring whether the atomic velocity tracks with accelerating wells.

During the interaction process, atoms initially trapped in the MOT can be (1) trapped and accelerated by the standing wave for the full duration of the experiment, (2) trapped for some time before tunneling out of the wells, or (3) not trapped at all by the standing wave. To distinguish atoms which

have tunneled from the wells from atoms which remain trapped in the wells, a three step acceleration process was implemented. The three step process is designed to (1) prepare an initial state where the atoms are in the lowest band, (2) interact with a potential in which tunneling can occur, (3) measure the final percentage of atoms which survive after the tunneling potential.

As shown in Figure 3.8 the three step process involves two accelerations slow enough not to induce loss from tunneling and a faster acceleration in which tunneling rates are to be measured. This plot is an experimental heterodyne beat frequency (as described in Section 3.3.2) which can be calibrated to a velocity curve. After initial trapping and cooling of atoms in the MOT, the interaction standing wave is turned on for 20 μs with no acceleration (see Figure 3.5). During this time, a portion of the cold atomic sample is trapped in the lowest band. These atoms are the ones with initial wave functions that significantly overlap with the eigenstates of the lowest band of the standing wave. The first slow acceleration separates in momentum those atoms which are trapped in the wells from the rest of the distribution. Typically, the slow acceleration rate (a_{slow}) is 1500 m/s^2 and we confirmed that negligible tunneling occurs from it (see Figure 4.1 panel a) by doing a single step acceleration. Typically the velocity reaches 1.05 m/s when the acceleration is then switched to a higher value in the range 4500-10000 m/s^2, changing the tilt of the wells and increasing the probability of tunneling between the bound state and the continuum. This point of middle velocity must be such that atoms in the lowest band which were trapped and accelerated are far enough out in velocity so as not to be confused with atoms which are in higher bands. The reason this is important is because we want to measure only tunneling rates from the lowest

band to the higher band, but if there are atoms in higher bands decelerating and moving down in band index, there is an equal probability that these atoms will finally tunnel to the lower band. If we spatially separate the two classes, there will be no ambiguities from atoms which might have tunneled into the lowest band from higher bands.

After a controlled period of time, T_{loss}, the acceleration is switched back to a_{slow} and continues until the standing wave reaches a final velocity v_f typically 2.4 m/s. Like the first slow acceleration, this again separates in momentum the atoms still in the wells from those which have tunneled. Now the ratio of the number of atoms tunneled to atoms to atoms still trapped can be measured.

4.2 Determination of Survival Probabilities and Tunneling Rates

A typical final distribution of atoms is shown in Figure 4.1 (b). The large peak centered around x=0 mm corresponds to atoms that were not trapped by the standing wave. The small peak centered at x=7 mm corresponds to atoms that remained trapped and were accelerated to v_f and the area under the peak is proportional to the number of these atoms. The asymmetric peak between the large and small peak represents atoms that tunneled out to the continuum during the fast acceleration. Intuitively, the number of tunneled atoms should be peaked at lower velocities since the tunneling rate is assumed constant in time, more atoms are available to tunnel out at earlier times (lower standing wave velocities). In fact, the shape has an exponential tail on the right side from which we could in principle extract the decay constant, but this would

be very difficult. An easier way is to consider only the ratio of the number of atoms that have survived to the number of atoms were initially launched. We can obtain this by merely comparing the areas under the two peaks. This means we do not need to extract the actual numbers of atoms which each peak represents.

To measure the tunneling rate, the experiment is repeated many times with varying T_{loss}. Figure 4.2 through 4.15 show integrated curves as the fast acceleration time or loss time (time which tunneling can occur) is adjusted alternating with plots of the survival probability versus decay time. Note that all the curves on each figure have the same acceleration, and only the loss time is adjusted. To get a survival percentage we integrate to get the area under the small peak and divide it by the area under both the small curve and the middle curve. By normalizing this way we eliminate sensitivity to variations in the number of atoms which were initially accelerated. Initially, we normalized the number of atoms surviving to the total area under all three curves, but the present method gave better results, especially at low accelerations where the number of tunneled atoms was small. These variations in number of atoms initially accelerated could be due to dynamics of the MOT, fluctuating MOT temperature, or fringes moving from shot to shot. The program which was used to calculate the survival probability is presented in Appendix B.

The data in these figures conclude that the decay trends are exponential with the time constant dependent upon well depth and acceleration. Figure 4.2 shows an example of a large number of points which we took to completely confirm the decay was exponential. In these figures we see that the decay rate follows approximately the trends predicted by Landau-Zener theory (see

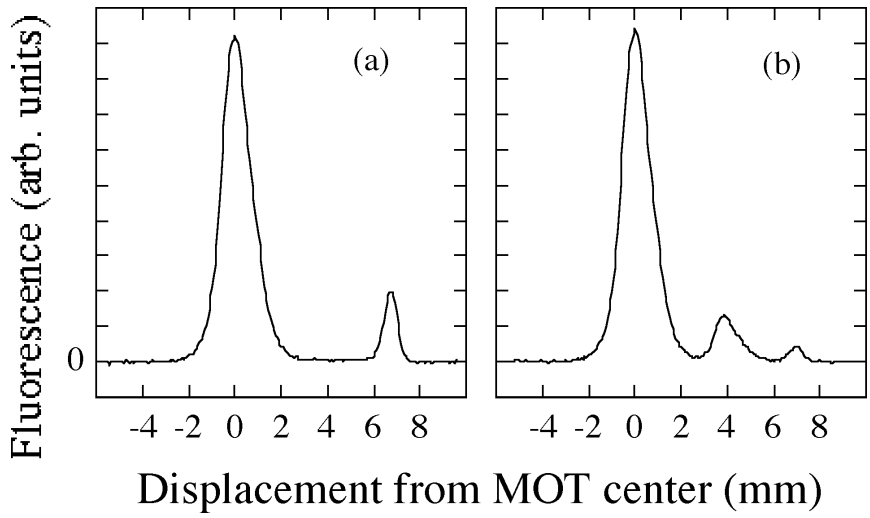

Figure 4.1: Distribution of atoms after exposure to an accelerating standing wave. The displacement is the distance from the atoms' initial location in the magneto-optic trap. The fluorescence is proportional to the number of atoms at a given displacement. In (a) a fraction of the atoms was trapped by the standing wave and accelerated for 1500 μs to a final velocity of 2.2 m/s. The atoms then drifted ballistically for 3 ms, allowing them to separate spatially from the main distribution. Here $V_0/\mathrm{h} = 86$ kHz. In (b) A fast acceleration of 10,000 m/s^2 was turned on for a duration of 47 μs leading to substantial tunneling.

Equation 2.43). Namely, the decay rate increases with higher accelerations and lower well depths. Originally, our first results with different accelerations gave almost the same decay rate. This was confusing initially until we compared the results to the quantum simulations and understood that the points were on a resonance (see Section 4.4) which is not predicted by Landau-Zener theory.

Once the curves were collected, we analyzed the data from the photodiode signals. If the average power over the time of the experiment spiked more than ±3% outside the target power, the curve was eliminated from the analysis. All the previous plots contain many data points to map out the exponential, but once we established that the trends were definitely exponential, we took data only at four different times for each acceleration. A sample plot with the curve fit for the four points is shown in Figure 4.19. Typically these points were at T_{loss}=0%, 20%, 40%, 60% of $(V_{final} - V_{offset})/a_{fast}$ where V_{final} is the final velocity and V_{offset} is the velocity at which the fast acceleration portion begins as shown in the figure. This figure also shows the points for the discriminated and undiscriminated points. Notice that there is a small change in the determined slope for the decay depending whether we discriminated or not. In general, the curve fits for the discriminated data provided better fits to an exponential. This is also shown in this figure by noting that the R for the fit is higher for the discriminated set. Because of this we finally discriminated all the data to get the best results. These plots were created on KaleidaGraph for the Power MacIntosh which includes curve fitting routines. The curves are fitted with an exponential without any offset (y=exp(-ax)) giving a slope equal to Γ (the inverse of the lifetime). The error bar in slope gives the sigma for the Γ. In all cases this error bar is less than ±4% (typically ±2%). This error

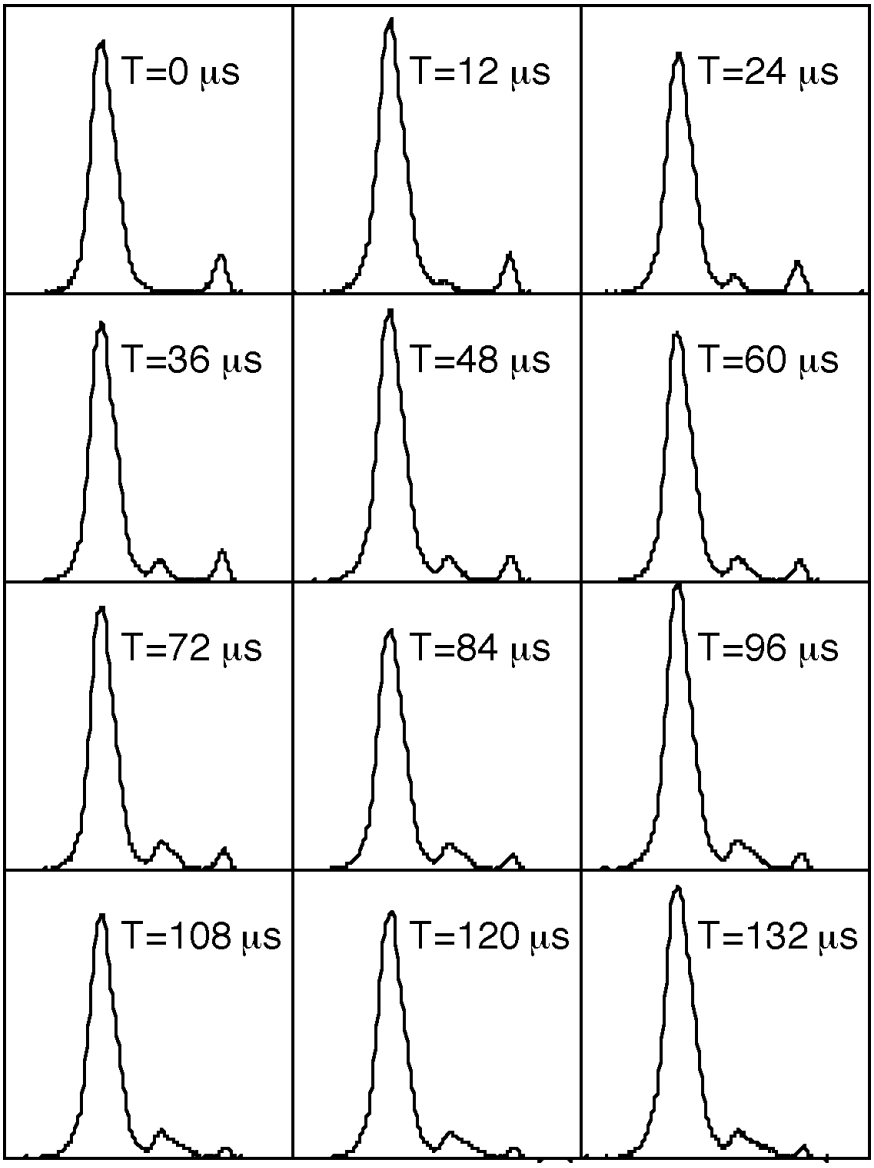

Figure 4.2: The panel shows the evolution of the curves as the loss time is varied. The parameters for this case are $V_0/h = 96 \pm 25\%$ kHz, a_{fast}=6000 m/s^2, a_{slow}=1500 m/s^2.

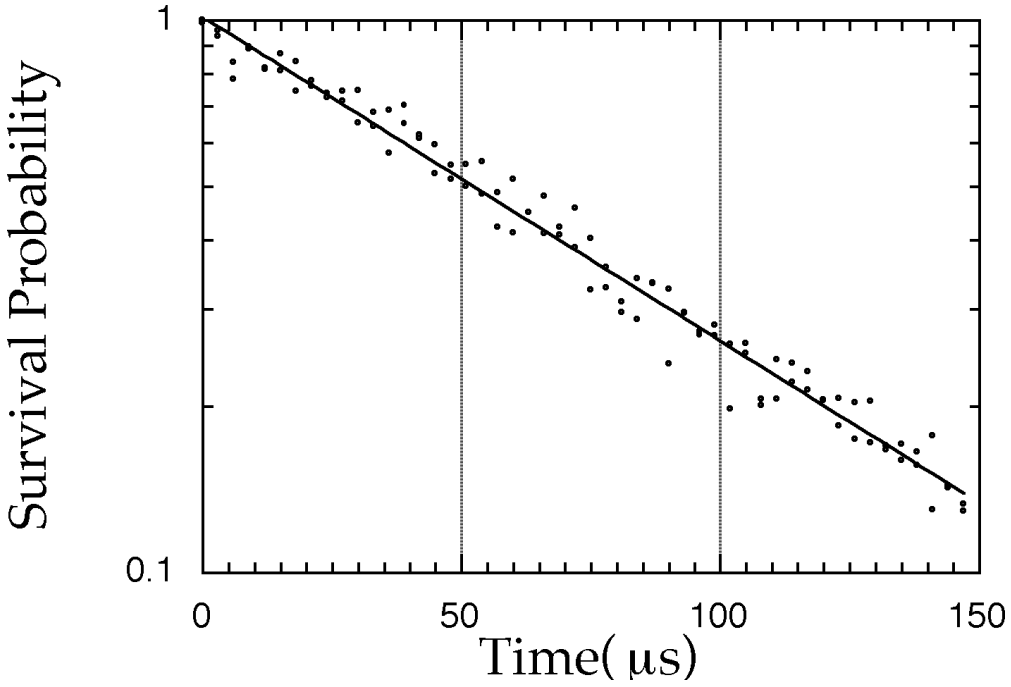

Figure 4.3: The survival probability for the previous page ($V_0/h = 96 \pm 25\%$ kHz, a_{fast}=6000 m/s^2, a_{slow}=1500 m/s^2). The solid line is fit to an exponential and for this case gives 74 μs.

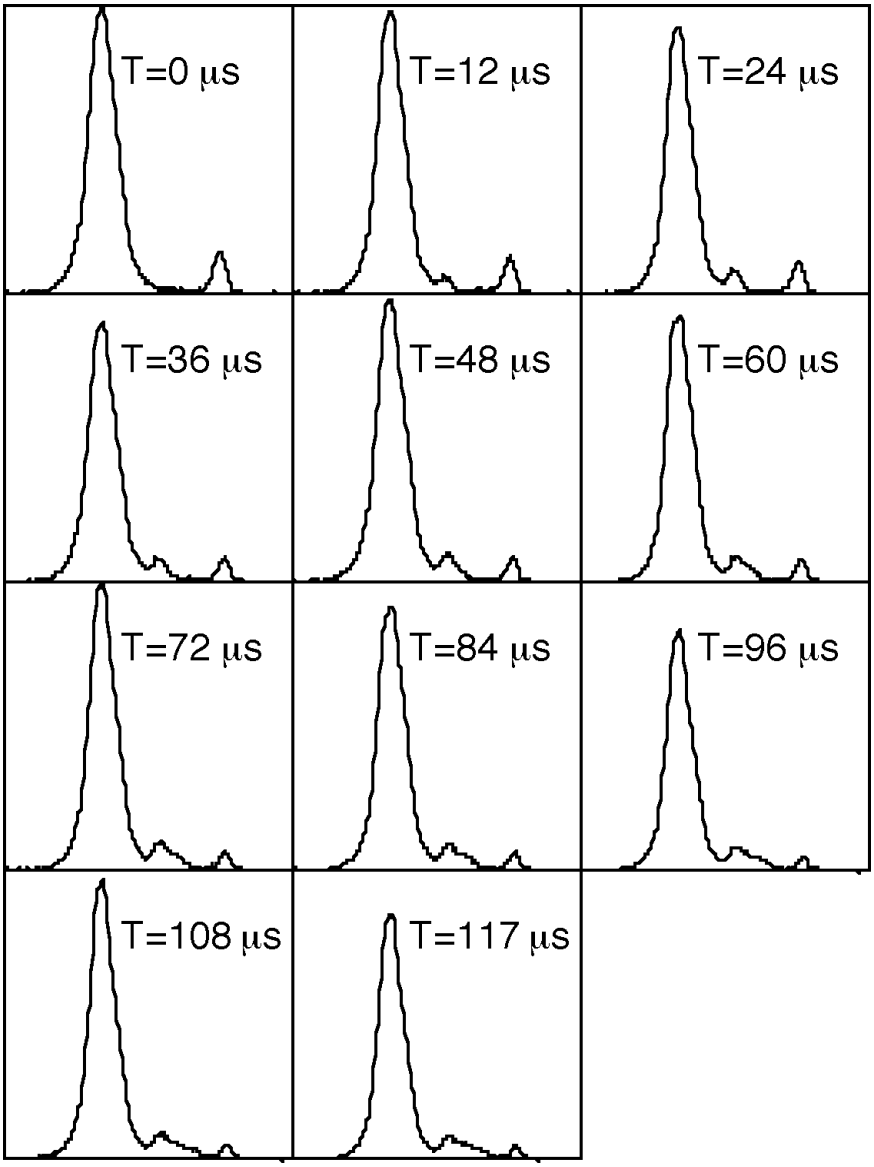

Figure 4.4: The panel shows the evolution of the curves as the loss time is varied. The parameters for this case are $V_0/h = 96 \pm 25\%$ kHz, a_{fast}=7000 m/s^2, a_{slow}=1500 m/s^2.

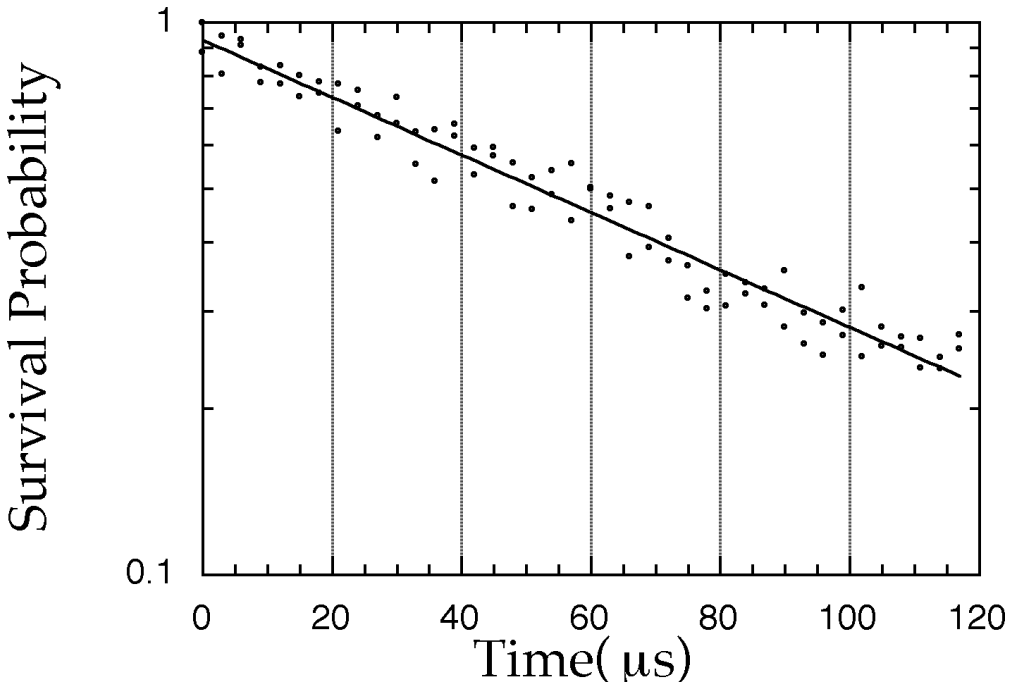

Figure 4.5: The survival probability for the previous page ($V_0/h = 96 \pm 25\%$ kHz, a_{fast}=7000 m/s^2, a_{slow}=1500 m/s^2). The solid line is fit to an exponential and for this case gives 83.5 μs.

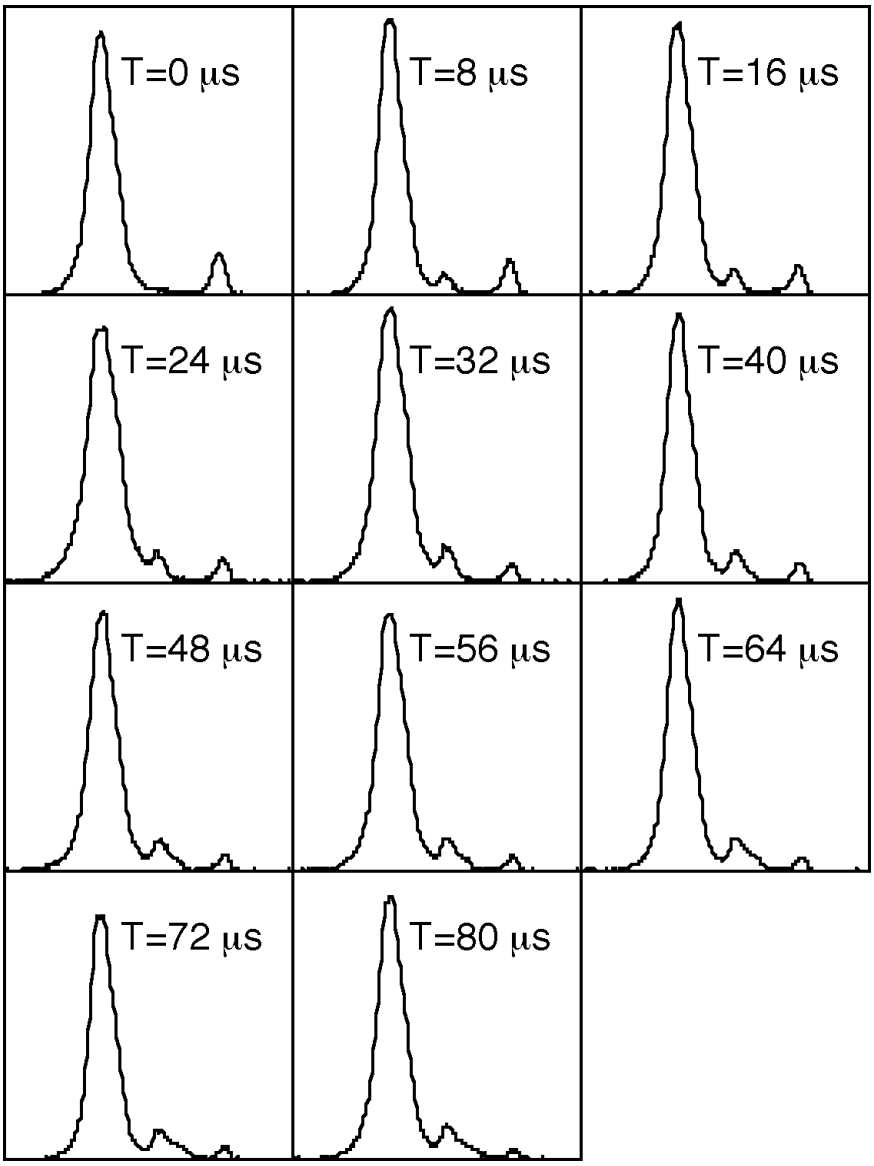

Figure 4.6: The panel shows the evolution of the curves as the loss time is varied. The parameters for this case are $V_0/h = 96 \pm 25\%$ kHz, a_{fast}=8000 m/s^2, a_{slow}=1500 m/s^2.

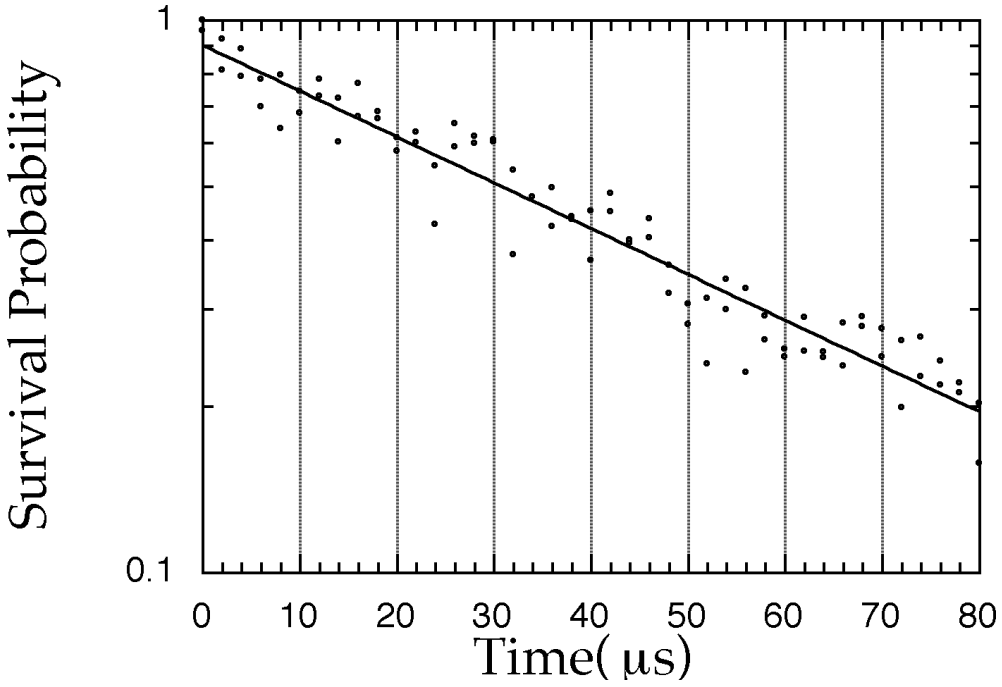

Figure 4.7: The survival probability for the previous page ($V_0/h = 96 \pm 25\%$ kHz, a_{fast}=8000 m/s^2, a_{slow}=1500 m/s^2). The solid line is fit to an exponential and for this case gives 52.3 μs.

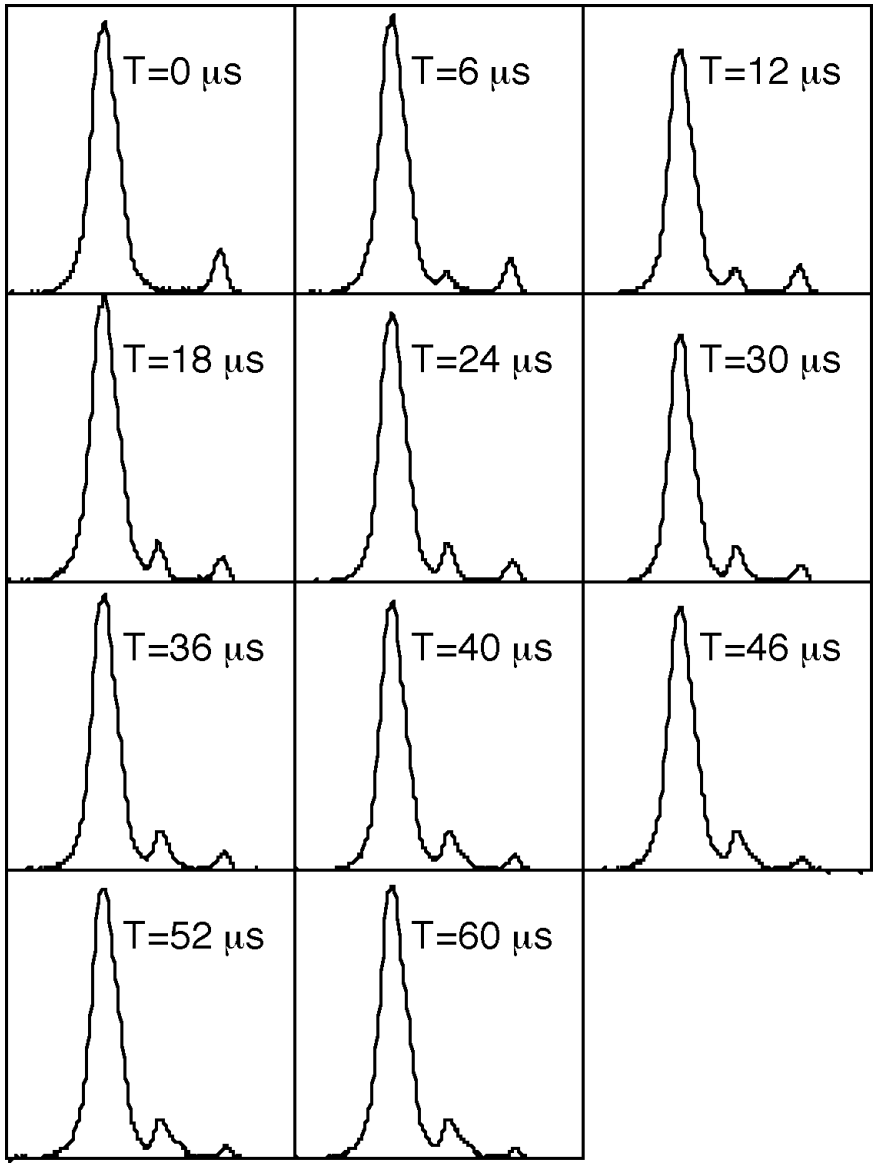

Figure 4.8: The panel shows the evolution of the curves as the loss time is varied. The parameters for this case are $V_0/h = 96 \pm 25\%$ kHz, a_{fast}=9000 m/s^2, a_{slow}=1500 m/s^2.

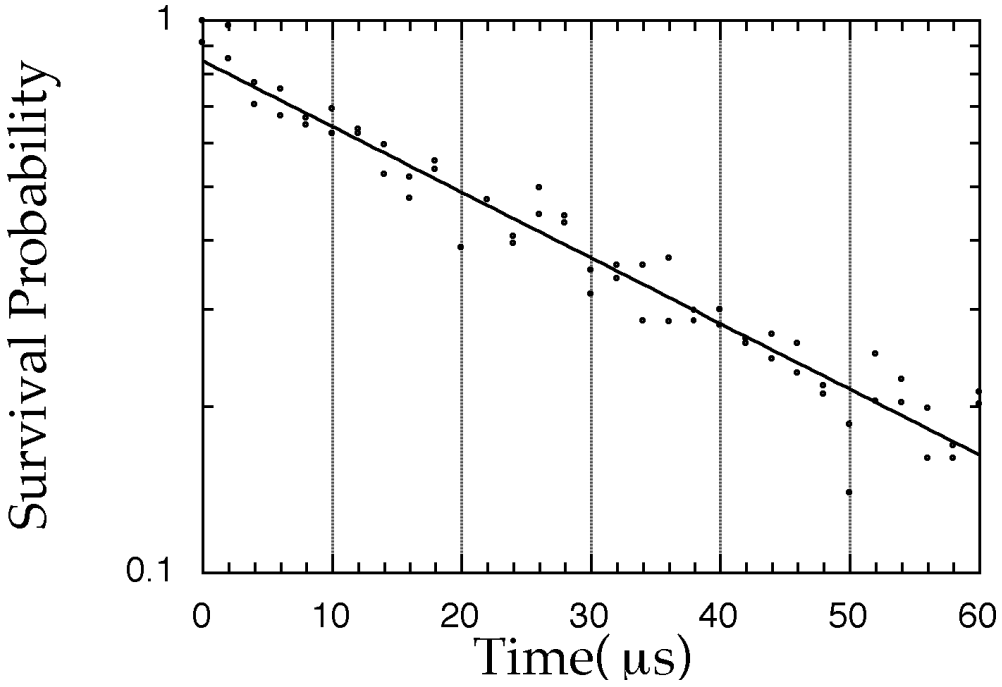

Figure 4.9: The survival probability for the previous page ($V_0/h = 96 \pm 25\%$ kHz, a_{fast}=9000 m/s^2, a_{slow}=1500 m/s^2). The solid line is fit to an exponential and for this case gives 36.5 μs.

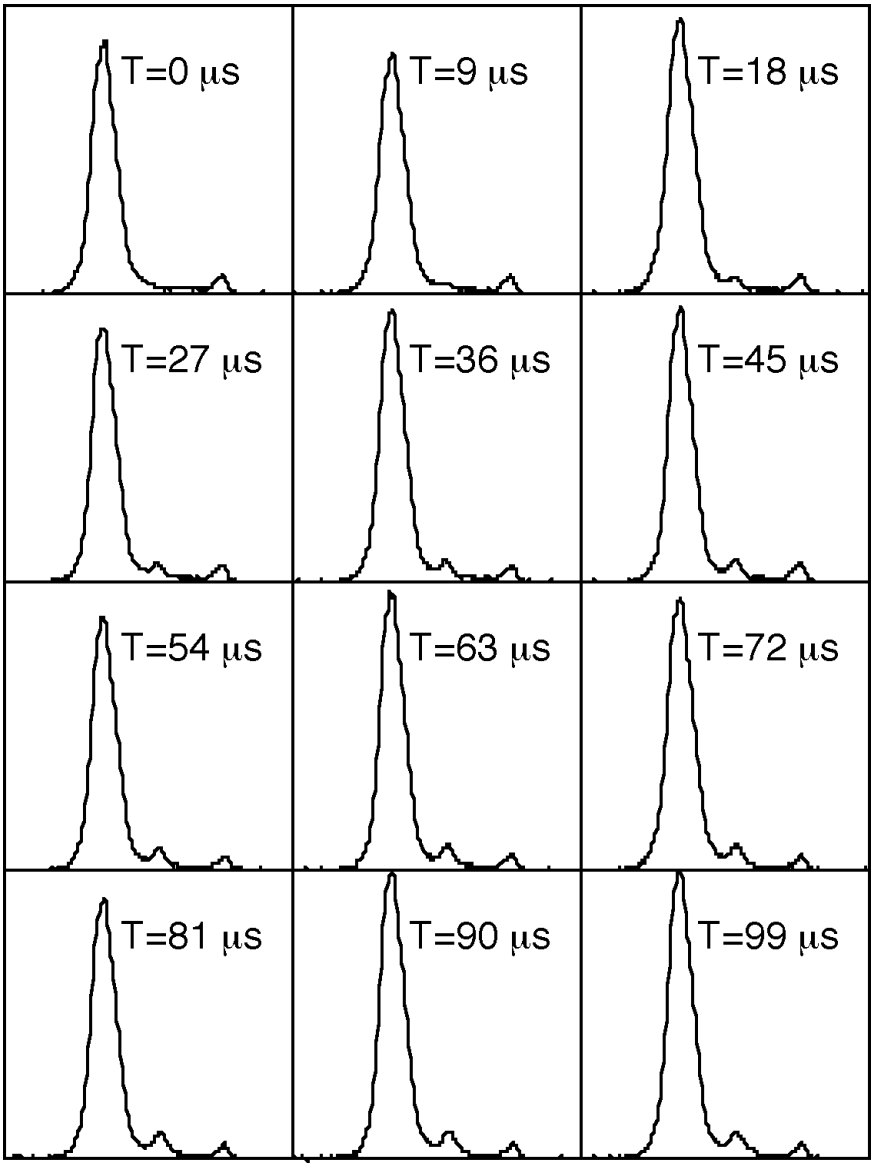

Figure 4.10: The panel shows the evolution of the curves as the loss time is varied. The parameters for this case are $V_0/h = 58 \pm 25\%$ kHz, a_{fast}=3000 m/s^2, a_{slow}=1500 m/s^2.

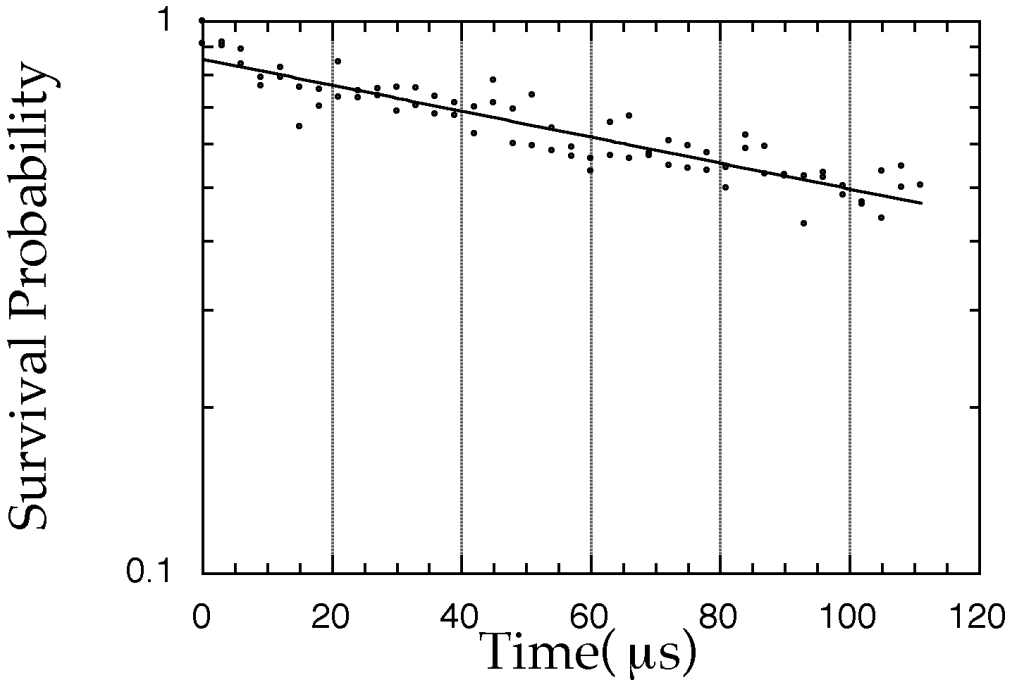

Figure 4.11: The survival probability for the previous page ($V_0/h = 58 \pm 25\%$ kHz, a_{fast}=3000 m/s^2, a_{slow}=1500 m/s^2). The solid line is fit to an exponential and for this case gives 184 μs.

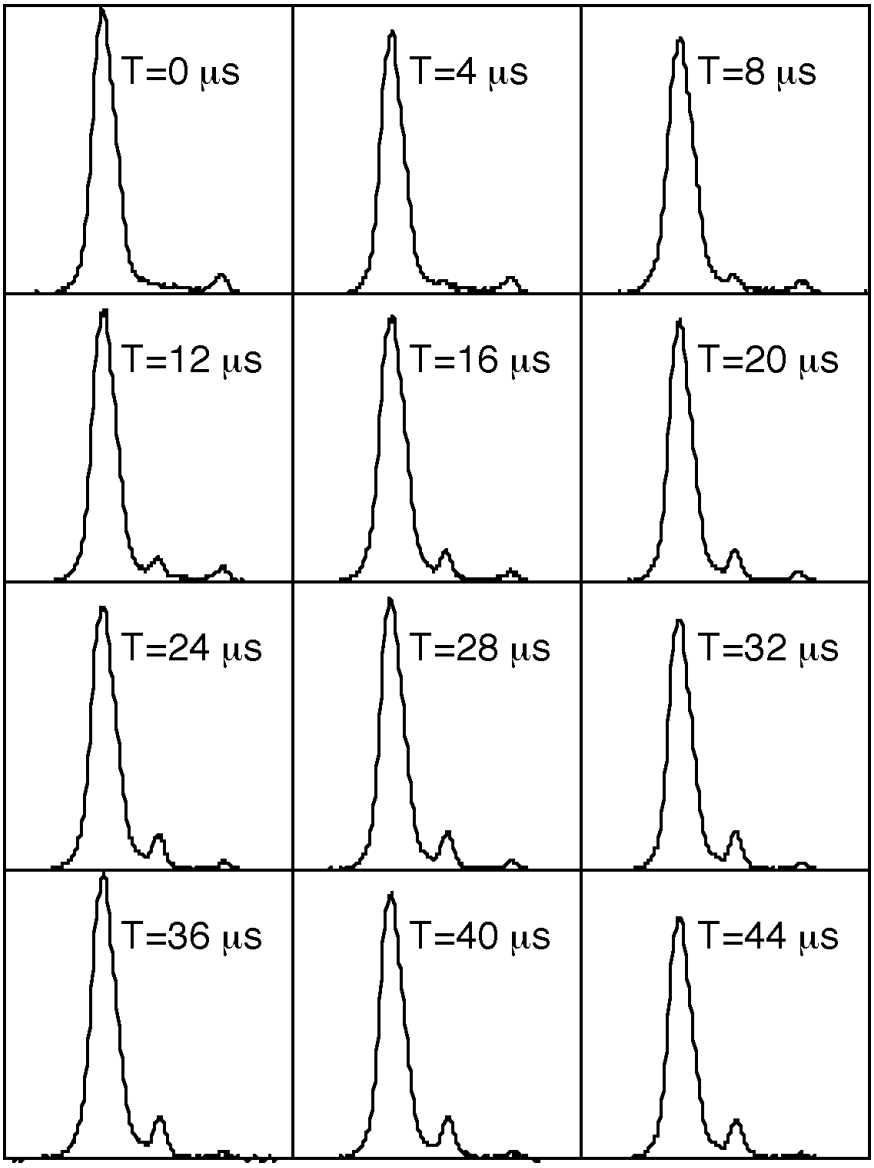

Figure 4.12: The panel shows the evolution of the curves as the loss time is varied. The parameters for this case are $V_0/h = 58 \pm 25\%$ kHz, a_{fast}=5000 m/s^2, a_{slow}=1500 m/s^2.

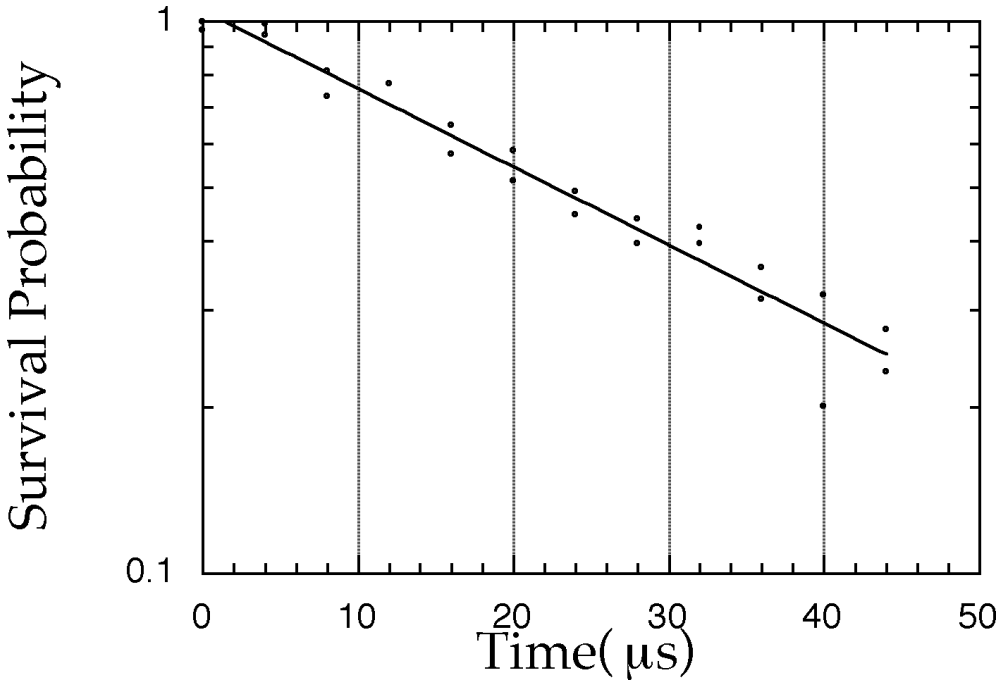

Figure 4.13: The survival probability for the previous page ($V_0/h = 58 \pm 25\%$ kHz, a_{fast}=5000 m/s^2, a_{slow}=1500 m/s^2). The solid line is fit to an exponential and for this case gives 30.7 μs.

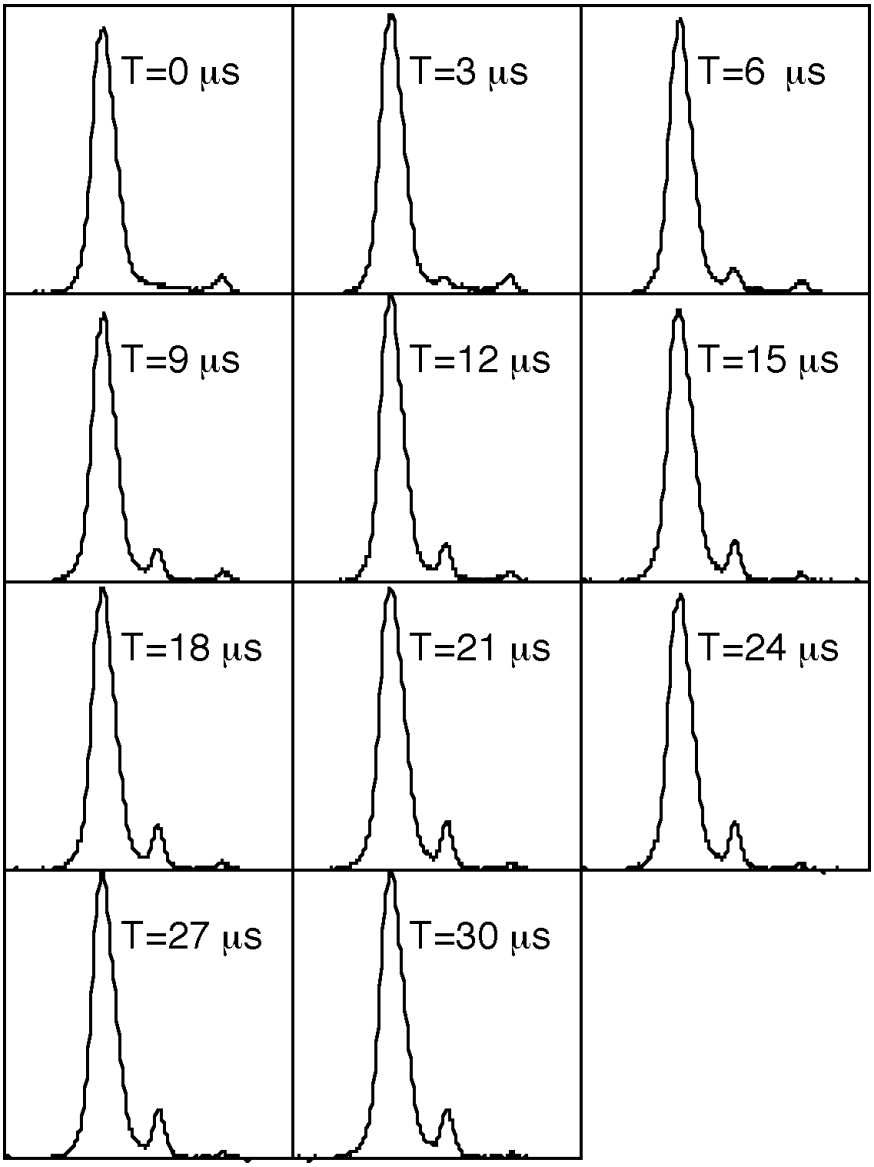

Figure 4.14: The panel shows the evolution of the curves as the loss time is varied. The parameters for this case are $V_0/h = 58 \pm 25\%$ kHz, a_{fast}=7000 m/s^2, a_{slow}=1500 m/s^2.

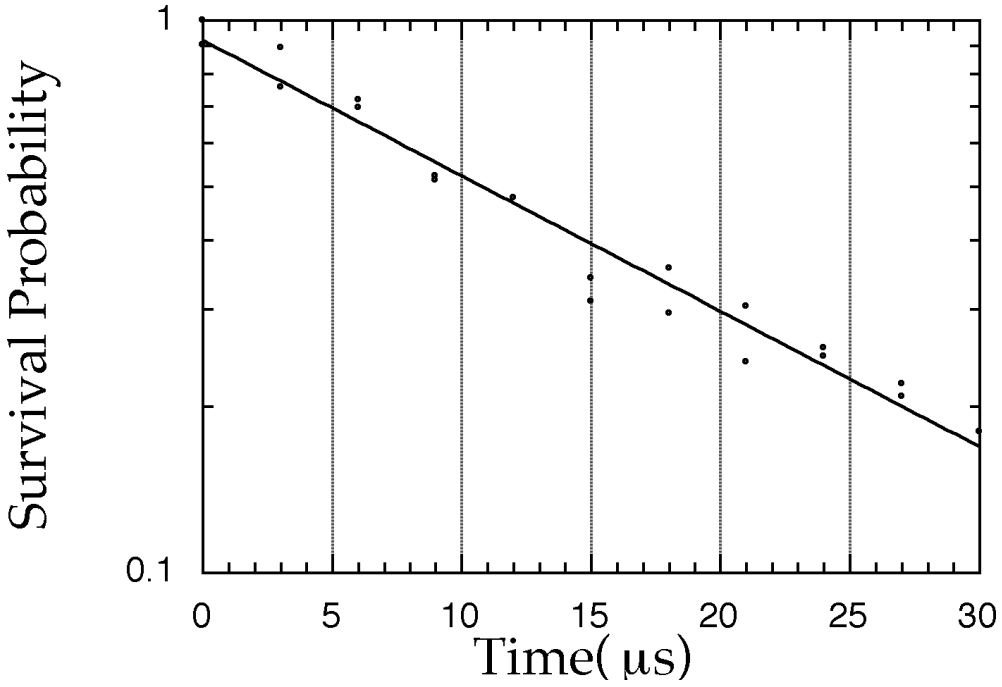

Figure 4.15: The survival probability for the previous page ($V_0/h = 58 \pm 25\%$ kHz, a_{fast}=7000 m/s^2, a_{slow}=1500 m/s^2). The solid line is fit to an exponential and for this case gives 17.7 μs.

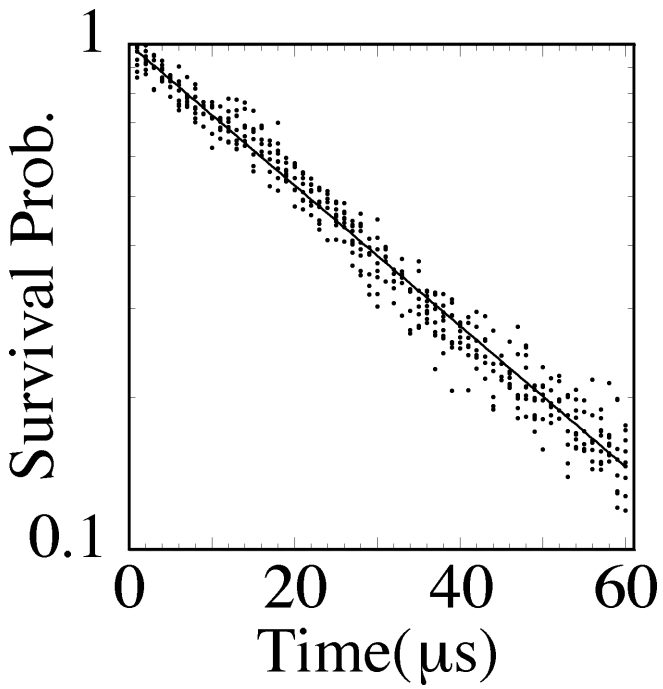

Figure 4.16: Example of experimentally measured survival probability for a_{slow}=1200 m/s^2, a_{fast}=4500 m/s^2, and V_0/h=50.8 kHz as a function of the duration of the fast acceleration. The solid line is an exponential fit to the data.

bar is small compared to the error bars which would result from our measurement of power. However, it is not possible to include error bars due to power uncertainty in the measured value of Γ unless we include some theoretical analysis with tunneling rates. The only experimental error bar we can put on the measurement is the uncertainty in the tunnel rates determined by the curve fit, and the error bar on acceleration. Therefore, it is more useful to compare our results with Landau-Zener tunneling theory and quantum mechanical simulations and either use the well depth as a fit parameter or bracket the results with theory curves at well depths determined by the experimental uncertainty in well depth.

4.3 Tunneling Experiment Procedure

To collect good tunneling data, it is essential to characterize the standing wave (Section 3.3.2) as accurately as possible and second, to obtain a high number of atoms in a simple acceleration. To accomplish this, we first obtained as symmetric and cold of atomic sample in the MOT as possible. The sample's temperature is minimized by a combination of adjusting sideband levels, proper alignment of trapping/cooling laser beams to minimize fringing effects, and correct detuning from resonance. All three of these parameters must be adjusted at the beginning of each day of running to produce the most uniform and coldest sample. The symmetry of the MOT sample is adjusted by making momentum measurements. As the atoms expand out spatially during the free drift potion of the experiment, if there is any non-uniformity in the magnetic fields or slight misalignment of the cooling beams, the pattern will not be spherically symmetric. Figure 4.17 shows a two dimensional CCD im-

age where both the launched atom peak and the initial atomic peak expand symmetrically. The fast acceleration time for this case is zero so there are only two peaks since there is no tunneling. In general, the quality of the accelerated peak was sensitive to the quality of the free expansion.

After the MOT sample was optimized, we next would align the interaction beam onto the atoms. This was described earlier in Section 3.3.2. The interaction beam was usually coarse adjusted at high well depth to optimize the number of atoms accelerated. Later, we reduced the well depth close to the experimental parameters for the run and adjusted the beams to produce the largest and most symmetric drag peak determined from the two dimensional images. When everything was optimized, we could easily accelerate almost 10% of the atoms in the MOT. Figure 4.18 is a two dimensional image of the results following a run which included tunneling with T_{loss} of 95 μs, V_0= 70 kHz, and a fast acceleration of 5000 m/s^2. The atoms which have tunneled are lined up with the ones which have survived. When not properly aligned, these atoms would sometimes spray out in various directions. For good tunneling results, it was necessary to obtain pictures like this one.

Once the interaction beams were aligned properly, we measured all of its parameters including beam waist, power, wavelength, and acceleration from heterodyne measurements. Since most of the experiment was automated, the rest of the time involved monitoring the power, detuning and making sure the MOT beams did not unlock from the absorption line as the computers acquired the data.

Figure 4.17: A typical two dimensional CCD image of the fluorescence from atoms taken after the free drift portion of the experiment where the loss time was zero. The fluorescence is proportional to the number of atoms. The large peak on the left represents atoms which were not accelerated and the small peak on the right represents atoms which were accelerated. With optimal alignment and acceleration we could accelerate almost 10% of the atoms. It was important to obtain symmetric pictures like this one for good tunneling data.

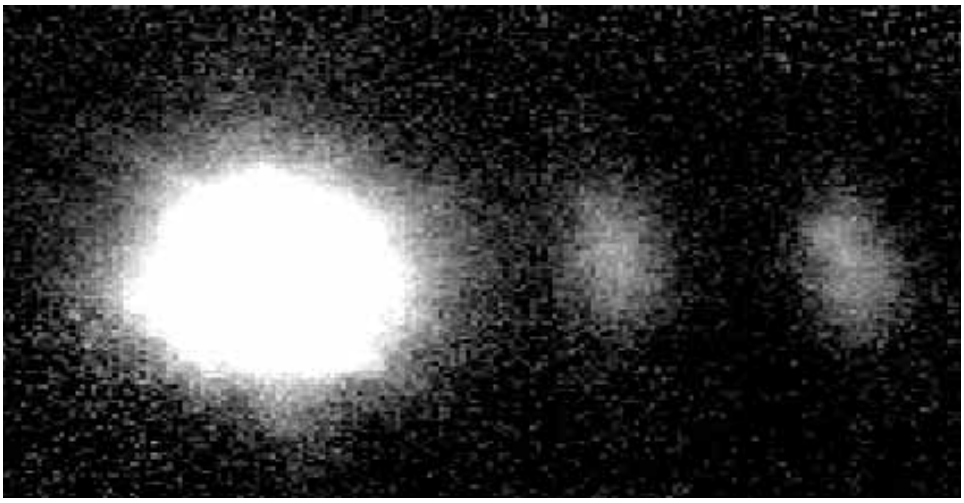

Figure 4.18: A typical two dimensional CCD image of the fluorescence from atoms taken after the free drift portion of the experiment where the loss time was non-zero. The fluorescence is proportional to the number of atoms. The large peak on the left represents atoms which were not accelerated. The small peak on the far right represents atoms that were accelerated and did not tunnel to the continuum and the small middle peak are the atoms which tunneled from the wells.

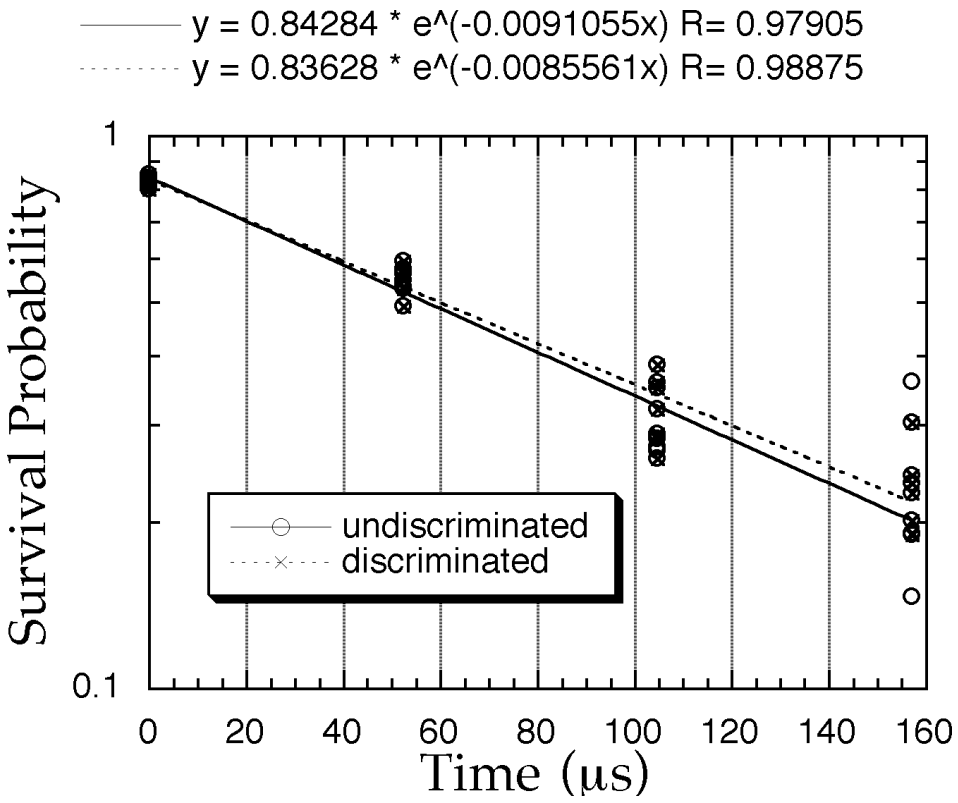

Figure 4.19: Plot shows the effect of power discrimination on the tunnel rates. Once we established that the curves were exponentials, we took data with just four points. Plot also shows the curve fits for discriminated and undiscriminated data. The determined decay rate is slightly different for each case.

4.4 Comparison with Theory

We compared our results of tunneling rates with the Landau-Zener tunneling theory as well as with quantum simulations. Figures 4.20, 4.21 and 4.22 show the experimental results for the tunneling rate versus acceleration with the quantum simulation results and the Landau-Zener curves. In Figure 4.20 the well depth is V_0/h= 92 kHz but has an absolute uncertainty of ± 25%. The well depth for Figure 4.21 is V_0/h=72 kHz but has a much better uncertainty of ± 10%. The reason for the improvement in uncertainty is due to a much more careful calibration of laser power and spot size for the second run. For Figure 4.20 we used the well depth as a fit parameter for the quantum simulations and for Figure 4.21 we bracketed the experimental results between two quantum simulations. Figure 4.22 is a run for slightly lower well depth. Here, the quantum simulations are for V_0/h= 54 kHz, V_0/h= 60 kHz and the experimentally determined well depth is V_0/h= 66 kHz with an error bar of ±25%. This curve also shows the small error bars resulting from the fitting to the exponential but does not include an error bar derived from power measurement. These figures certainly show a quantitative agreement of tunnel rates with theoretical predictions varying both the well depth and the acceleration.

From Equation 2.43 it is seen that the tunneling rate is exponentially dependent on the band gap. The band gap is monotonically related to the well depth in this regime so that the end result is a particularly high sensitivity of tunneling rate to well depth. Given the high sensitivity of tunneling rate to the well depth, the agreement with *an ideal simulation* over the range of accelerations is quite good, and further confirms the observation of tunneling. This is the primary evidence that the observed loss is due to quantum tunneling.

All these plots of loss rate versus acceleration (Figures 4.20, 4.21, 4.22) show clearly an experimental deviation from Landau-Zener theory at intermediate values of acceleration. The deviations are in the form of oscillations as a function of the acceleration. These oscillations also occur in the quantum simulations. This deviation is due to a fundamental difference between the experimental system and the Landau-Zener model. The Landau-Zener model assumes that the inter-band transition occurs only at the band gap (point of closest approach between the bands), however, in the present system the band curvature is not large, and transitions are no longer limited to the gap but can occur at different points along the band. A theoretical analysis of this problem shows that in a single Bloch period there are contributions to the tunneling probability at points of both nearest and farthest approach between the bands, where their curvature is zero [25, 26]. Contributions from other points along the band cancel out. This leads to interference effects in the tunneling probability which depend on the Bloch period. The period of the oscillation is proportional to acceleration while the amplitude of the oscillation is inversely proportional to acceleration. At smaller values of the acceleration, deviations about the Landau-Zener prediction are considerably larger. This is physically reasonable because coherent effects become dominant when tunneling is suppressed. The extreme case is the coherent regime of Bloch oscillations and Wannier-Stark ladders where tunneling from the trapped state plays no role. The interplay between coherent and irreversible effects has been studied theoretically and observed, for example, in atomic physics experiments [27, 28]. The present experiment, however, allowed a detailed study of these effects in a much simpler setting, and with no adjustable parameters for comparison.

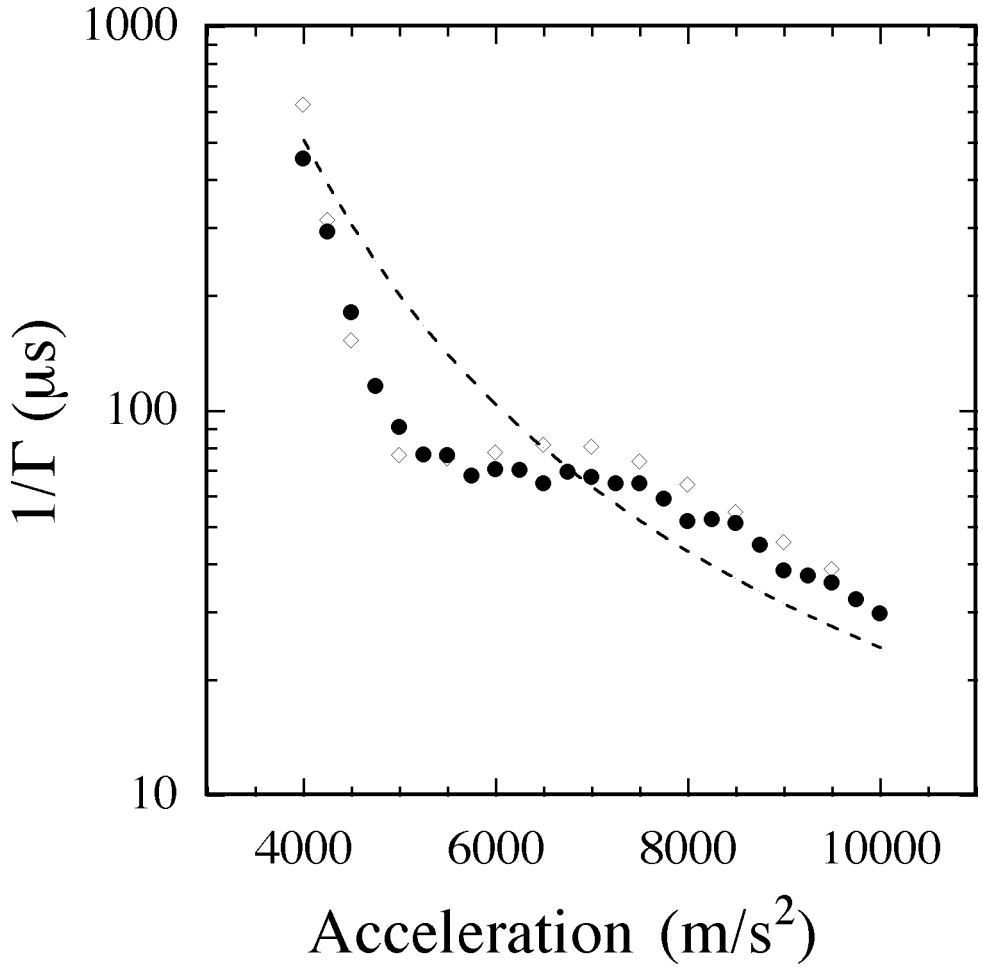

Figure 4.20: Tunneling rate as a function of acceleration. The experimental data are marked by sold dots. The uncertainty in the exponential fits to determine Γ are typically $\pm 2\%$, and the uncertainty in the acceleration for the the range shown is $\pm 50\ m/s^2$. The dashed lines are predictions of Landau-Zener theory. The well depth used in the quantum simulation (empty diamonds) and in the Landau-Zener theory was V_0/h= 72 kHz as a fit parameter to the data. The experimentally determined well depth for this run was V_0/h= 92 kHz but had an absolute uncertainty of $\pm 25\%$.

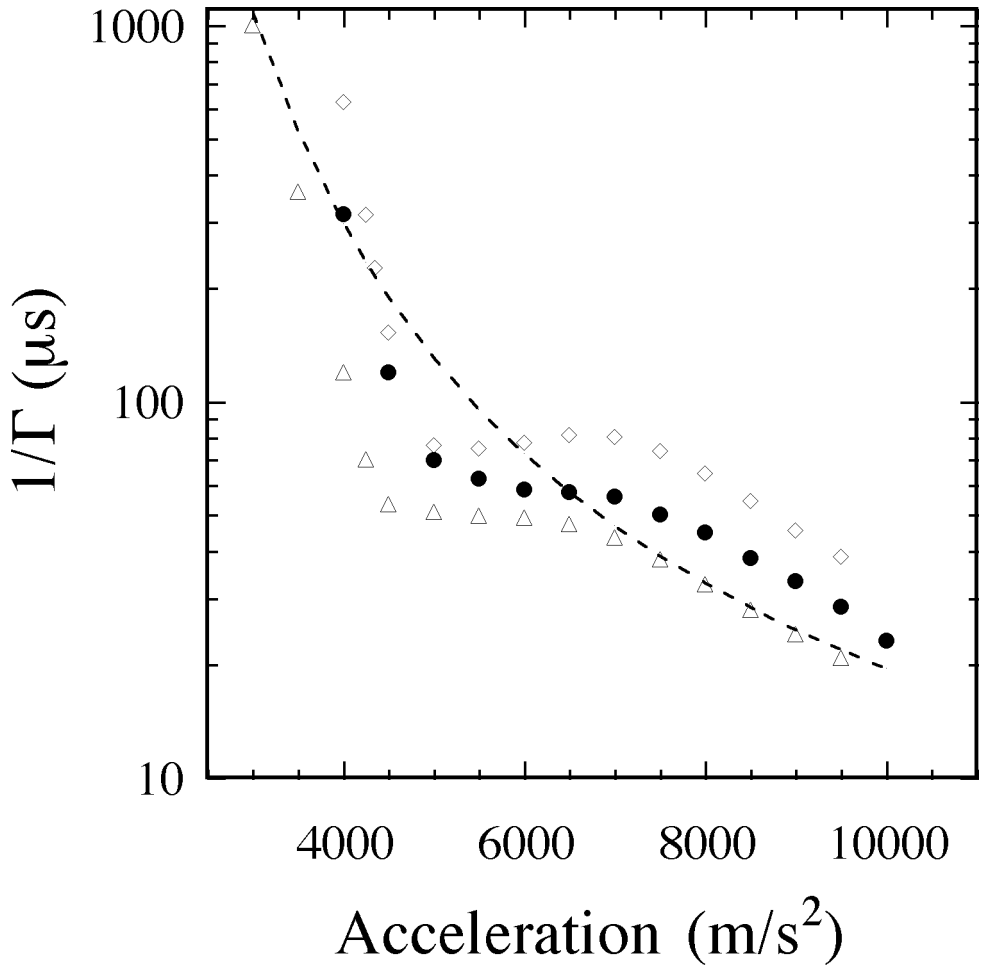

Figure 4.21: Tunneling rate as a function of acceleration. The experimental data are marked by sold dots. The uncertainty in the exponential fits to determine Γ are typically $\pm 2\%$, and the uncertainty in the acceleration for the the range shown is $\pm$ 50 m/s^2. The dashed lines are predictions of Landau-Zener theory. The experimental well depth was V_0/h= 72 kHz with an uncertainty of $\pm 10\%$. The data are bracketed between quantum simulations for well depths V_0/h= 60 kHz (empty triangles) and V_0/h= 72 kHz (empty diamonds).

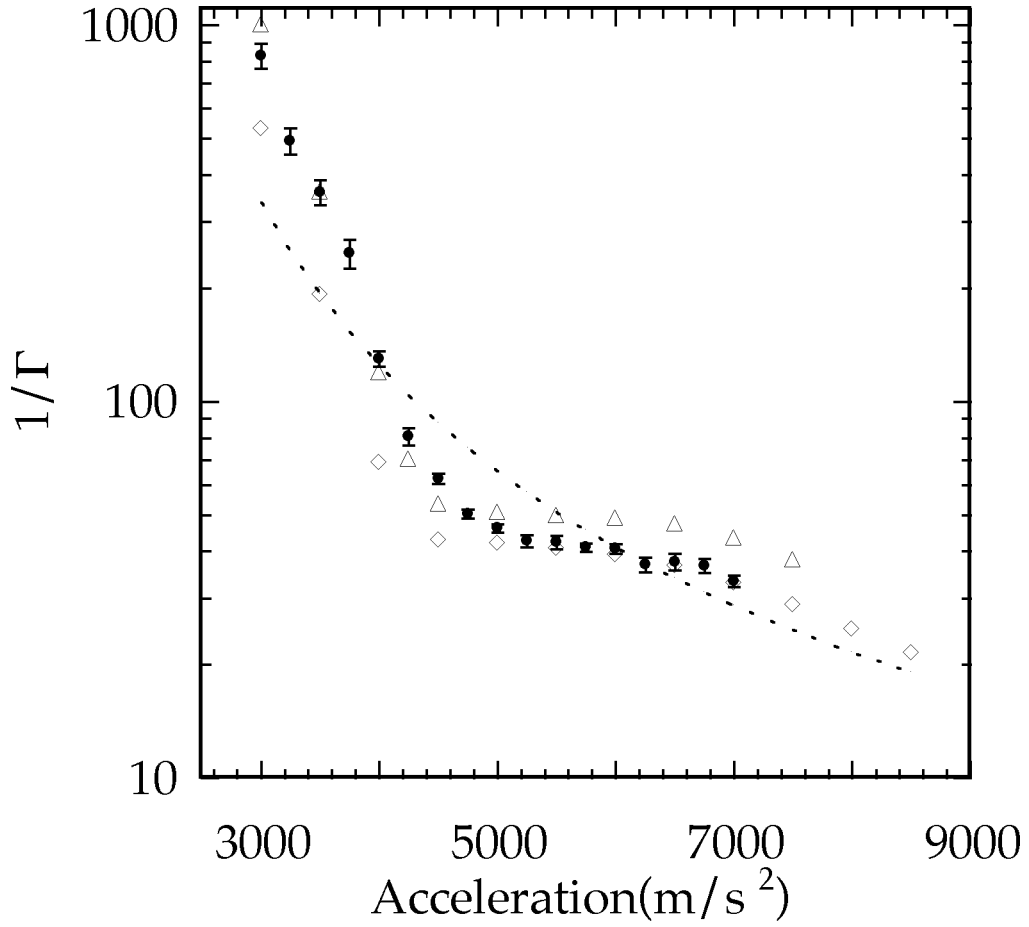

Figure 4.22: Tunneling rate as a function of acceleration. The experimental data are marked by sold dots. The uncertainty in the exponential fits to determine Γ are typically $\pm 2\%$, and the uncertainty in the acceleration for the the range shown is $\pm$ 50 m/s^2. The well depths used in the quantum simulations was V_0/h= 54 kHz (empty diamonds) and V_0/h= 60 kHz (empty triangles). The Landau-Zener curve is also for V_0/h= 54 kHz. The experimentally determined well depth for this run was V_0/h= 66 kHz but had an absolute uncertainty of $\pm 25\%$.

4.5 Other Factors Leading to Loss Rate from Wells

There are several other mechanisms which could conceivably contribute to a loss in atoms. Several possibilities include amplitude and phase noise of the optical potential, switching effects occurring during the time when the acceleration changes abruptly, and spontaneous scattering. All of these turned out to be negligible in this experiment.

We studied the amplitude and phase noise through the photodiode signals and optical heterodyne measurements respectively. The jitter in phase was far below that required to observe any loss of atoms as in the previous study of Wannier-Stark ladders [2]. In the Wannier-Stark case, depletion of the trapped atoms could only be induced by adding a much larger level of phase noise. The amplitude noise was eliminated by monitoring laser powers on the digital storage scope and rejecting traces with amplitudes $\pm 3\%$ outside a target value (usually the average power for the entire set of curves).

Fast switching between different accelerations has high frequency components that could possibly drive atoms out of the wells. We checked this by varying the switching times and did not observe any effect. The switching times were varied by programming the arbitrary waveform generator with different waveforms. An experimentally measured heterodyne with a non-zero switching time is shown in Figure 4.23. In this case the three accelerations are pieced together with portions of $a(t) \propto \sin^2(t/T_{switch})$ giving a $v(t') \propto \cos(\pi t'/T_{switch})$ where t' is referenced to the start of the switching portions of the curve. Specifically, the first acceleration is a slow one from t=0 to T_1 where $v(t) = a_s t$. The next piece is from t=T_1 to $T_1 + T_s$ where $v(t') = V_1 + \frac{a_f + a_s}{2} t' - \frac{T_s}{\pi} \frac{a_f - a_s}{2} \sin(\frac{\pi t'}{T_s})$ where t' is referenced from T_1 and represents the variable switch portion.

The next section is the fast acceleration for a duration T_{loss} where $v(t') = V_{offset} + a_f t'$ where t' is referenced from $T_1 + T_s$. Another variable switching section follows with $v(t') = V_2 + \frac{a_f+a_s}{2}t' - \frac{T_s}{\pi}\frac{a_s-a_f}{2}\sin(\frac{\pi t'}{T_s})$. The final section is another slow acceleration with $v(t') = V_3 + a_s t'$ where t' is referenced from $T_1+2T_s+T_{tun}$. The PC calculated these values from input parameters T_s, T_{loss}, a_{fast}, a_{slow}, V_{final}, V_{offset} and programmed the arbitrary waveform generator with the resulting curve.

As the value of T_{switch} is raised, the switching time is increased such that the change in acceleration can approach an adiabatic limit when compared to the Bloch frequency. One would expect that a non-adiabatic (fast) change in acceleration would result in a mapping of the wave function in the basis set of the slow acceleration's Hamiltonian to the basis set of the fast acceleration's Hamiltonian. This kind of interaction can drive atoms between the two bands. However, experimentally the results of a tunneling experiment with a T_{switch} of 40 μs and a T_{switch} of 0 μs provided the same decay rate if all other parameters (T_{loss}, a_{fast}, a_{slow}, V_{final}, V_{offset}) were consistent in both runs. More theoretical work needs to be completed on switching, especially related to the predicted short-time behavior (see Section 4.7.3). If the switching time becomes larger than 60μs we did see an effect which could be explained. At this point, the change in acceleration is so slow that the atom effectively is swept through different accelerations, each one with its own tunneling rate. This would then mimic a loss time which was effectively longer than the targeted value with a higher loss rate from the wells.

Spontaneous emission is another process which could drive atoms out of the wells and could have several elements. The first is that a spontaneous event

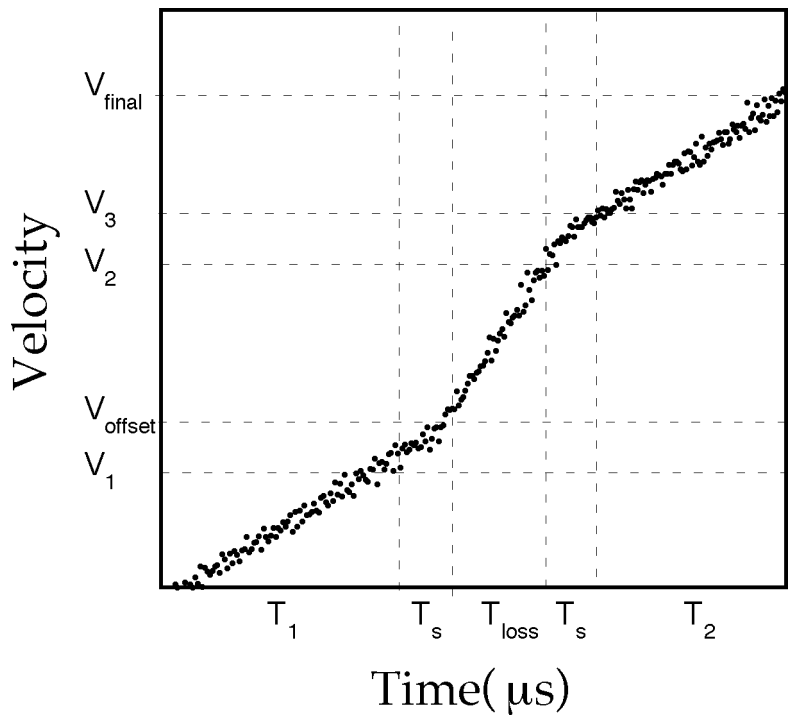

Figure 4.23: Figure shows experimentally measured heterodyne of waveform created with non-zero T_{switch} pieced between the constant acceleration parts.

can change the atoms velocity in the standing wave's direction by as much as two recoils or an energy change of 100 kHz. Since the well depth is only about 70 kHz it is quite easy for an atom's energy to be raised above the well depth and be transferred to higher bands. One other problem with the recoil aspect of spontaneous emission is that it now turns a one-dimensional problem into a three-dimensional one. The atom can get a momentum kick in any of the other two dimensions perpendicular to the standing wave and be launched out of the interaction region of the standing wave and even out of the binning view. Another effect arising from spontaneous emission is that during the process, the atom must be transferred to the excited state for a period of time on the order of the atomic lifetime. From the dipole approximation it can be shown that at this point, the nodes of the standing wave become anti-nodes. This is a similar process as in Sisyphus cooling [13], but in the case of accelerating nodes, when the atom returns to the ground state, it could have acquired a velocity with respect to the accelerating nodes such that it is no longer in the lowest band.

Since the standing wave is far detuned, the probability of spontaneous emission can be minimized. This probability is given by [14]

$$N = \frac{\Omega_{eff}\delta_L\gamma\Delta T_{\text{int}}}{4\left[(2\delta_L)^2+\gamma^2\right]} \tag{4.1}$$

where

$$\Omega_{eff} = \frac{8V_0}{\hbar} \tag{4.2}$$

For large detuning this gives

$$\begin{aligned} N &= \frac{\hbar\Omega_{eff}}{8}\frac{\Delta T_{\text{int}}\gamma}{2\hbar\delta_L} \\ &= \frac{Vo}{h}\left[\frac{\frac{\gamma}{2\pi}}{\frac{\delta_L}{2\pi}}\right]\pi\Delta T_{\text{int}} \end{aligned} \tag{4.3}$$

If we use the parameters for the run with V_0/h=70 kHz and $\delta_L/2\pi$=23 GHz we obtain a spontaneous emission rate of 10%/ms. Over the time scale which tunneling occurs (10-100s of μs) the probability of a spontaneous emission event is negligible.

4.6 Tunneling from Higher Bands

When the well depth gets large, other bands can be within the energy of the wells (See Figure 4.24). This condition opens up the possibility of atoms in a second band being trapped and accelerated along with the atoms in the lowest band. Starting from very low well depths, we observed a decline in the loss rate with increasing well depth until above a certain point where the loss rate became significant again. An example of this is shown in Figure 3.9 as noted before. The parameters for this curve are for conditions where the tunneling rate from the lowest band should be negligible, however, we still observed loss. This loss is is tunneling from the second band to the continuum and not tunneling from the lowest band to the second band. Adding to this effect is that atoms in the lowest band may make transitions to the second band and subsequently tunnel to the continuum from this band. This tunneling process now becomes very complicated.

4.7 Conclusion and Future Work

4.7.1 Conclusion

We have measured the tunneling rates for inter-band atomic center of mass transitions in an optical lattice with ultra-cold sodium atoms. This represents the first measurement of tunneling in the center of mass motion for atoms. The

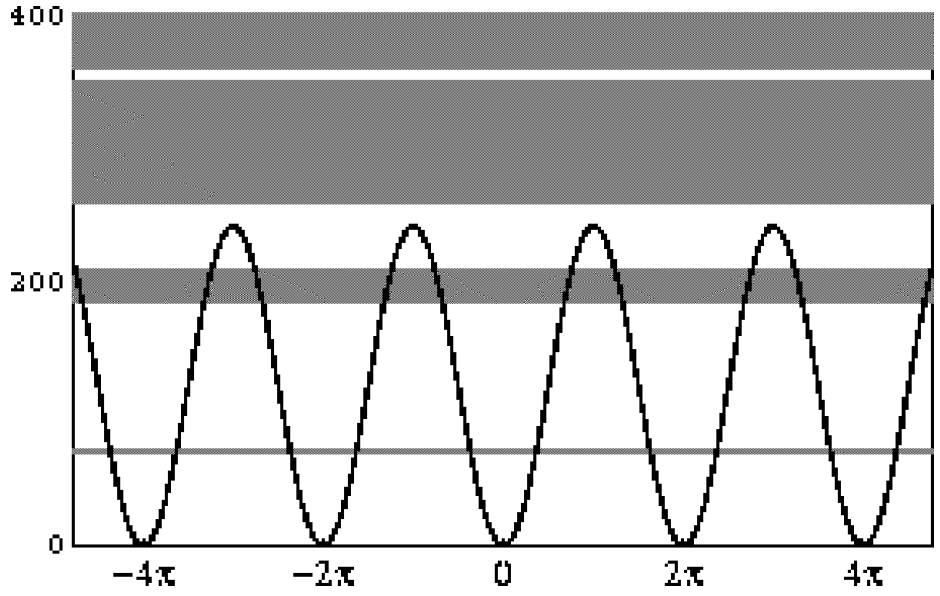

Figure 4.24: Figure shows band structure where tunneling between higher bands can occur when the well depth is larger. The well depth here is $V_0/\mathrm{h} =$ 120 kHz.

experimentally measured decay rates results agree well with Landau-Zener predictions and quantum simulations. Both the quantum simulations and experimental results show deviations from Landau-Zener adiabatic transition theory for an avoided crossing. This deviation is due to interference effects. Future extensions to this work include possibly the study of resonant tunneling, short-time non-exponential effects, and application of the accelerator for an atomic interferometer.

4.7.2 Enhanced Resonant Tunneling

Although we discuss the accelerating wells in terms of band structure, Bloch states are not exact eigenstates when a potential is applied which breaks the symmetry of the problem. In the case of an acceleration, the bands will break up into localized states in individual wells. When the tilt of the potential is such that the lowest level in one well is in resonance with the second level (or any other level) in an adjacent well (see Figure 4.25), the tunneling rate should have a resonant enhancement. The phenomena of enhanced tunneling is well known and observed in resonant tunneling diodes and transistors (See for example [20]). In the case of these devices, the wells are created by a double quantum well structure and tunneling of electrons occurs through the two barriers. When the energy level of the bound state in the well aligns with the energy of the incident electrons, an enhancement in current through the two barriers occurs. In the case of the standing wave of light, the enhancement of tunneling would manifest itself in an increased spatial spread over the standing wave as the atoms tunnel through the wells. After the interaction, the spatial extent of the atoms would be measured with different potential tilts (acceler-

ations) and at the resonant points the atomic spread should increase as the atoms tunnel through many wells.

4.7.3 Non-exponential Decay

An interesting aspect of decay processes is that for short times, there must be some deviation from an exponential [9, 10]. Consider an unstable system prepared in an initial state at time zero and we plot the probability of being in the excited state versus time. We also assume that the Hamiltonian is bounded by states from below. We wish to calculate

$$P(t) = |A(t)|^2 \tag{4.4}$$

using

$$A(t) = \langle \Psi | e^{-iHt/\hbar} | \Psi \rangle \tag{4.5}$$

which is the probability of being in the excited state Ψ. When we expand out the exponential for small t we get

$$P(t) = 1 - \frac{t^2}{\hbar^2} \langle | \Psi (H - \bar{E})^2 | \Psi \rangle + O(t^4) \tag{4.6}$$

where $\bar{E}$ is given by$\langle \Psi | H | \Psi \rangle$ Thus, one can see that for short times the decay time constant is not constant as in pure exponential decay, but varies as t. There may be other short-time effects such as oscillations as well. If we look at Figure 2.8 for the theoretical autocorrelation function we may see an indication of these short time effects.

Non-exponential short-time decay has been predicted for a long time but not experimentally verified. The reason for this is because the time in which short time effects occur is given by the inverse of the energy spacing between

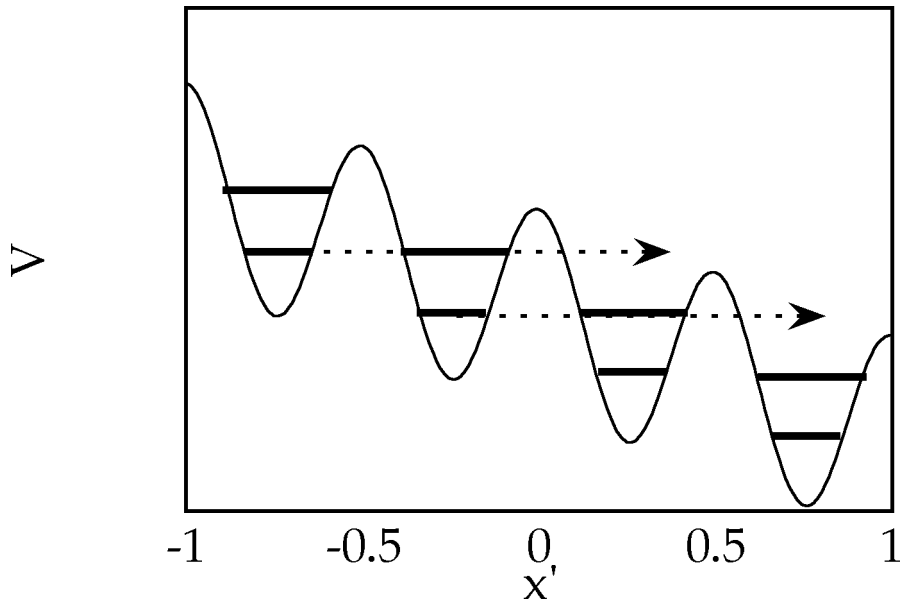

Figure 4.25: Figure shows schematically the potential where the possibility of resonant tunneling could occur.

the unstable state and the ground state. In many nuclear or optical transitions this time could be a short as 10^{-15} to 10^{-18} sec! To make this time longer, it is important to consider unstable systems which have smaller energy spacings. Unfortunately, in most systems the decay rate and the time which short time effects occur both decrease with increasing energy between states. This usually means that systems with measurable short time effects will have a decay rate which is too long to measure. In our tunneling system however these two rates are partially decoupled. The decay rate is dependent upon the energy spacing between bands (given mostly by the well depth) and on the acceleration. The short-time effects are determined only by the energy spacing. Therefore, we should be able to find a regime to maximize the short time behavior while keeping the decay time reasonable short. This is an area of future theoretical and experimental investigation.

4.7.4 Atomic Interferometer

One application for the accelerator described here is for a cold atomic beam used in an atom interferometer. The atom interferometer is a device similar to an optical interferometer except the interfering waves are atomic wave functions instead of electromagnetic fields. Like optical interferometers, the fringe visibility in atomic interferometers is limited by the coherence of the source. The important parameters for the source beam are $\delta v/v$ (velocity spread), brightness, and beam divergence. We have shown experimentally that the atomic accelerator described in this work can accelerate atoms without heating (increasing $\delta v/v$) the sample if the well depth is not large compared to the initial energies of the atoms. In our experiments here we accelerated some of the

atoms in a MOT, but it is also possible to use sub-recoil cooled atoms instead. Sub-recoil velocities can be obtained by stimulated Raman cooling and recently the realization of a Bose condensate offers another possibility [24]. To match the acceleration to a sub-recoil source we must lengthen the period of the standing wave and lower the well depth further. These changes will lower the zero point energy of each well. For minimal heating, the spread in momentum of the lowest state in each well must be lower than the spread in momentum for the initial state of the particle. Thus, lowering the zero point energy will decrease the heating. Lengthening the distance between wells will also decrease the tunneling probability, increasing the number of atoms that will accelerate. These modifications to the present system would allow the possibility of using sub-recoil samples for interferometry. An atomic interferometer using these techniques is our next major research project.

Appendices

Appendix A

Program to Calculate Heterodyne Frequency

```
#include  <stdio.h>
#include "/u2/cyrus/C/curveHandling.h"



/*************************************************************************/
/***** Finds the number of curves in a KestrelSpec file    *************/
/*************************************************************************/
int findNumCurves(char *fName, int *Nc)

     /***** Count the number of tabs on a line to determine the *****/
     /***** number of curves in the data file.                  *****/

{
  int nTabs;
  char ch = 0;
  int fileError = 0;
  FILE *fp, *fopen();


  fileError = ( (fp=fopen(fName,"r")) == NULL );
  if (fileError)
    /* file error! */;

  else {
    rewind(fp);

    for (nTabs=0; ((ch!=EOF) && (ch!='\n')); nTabs+=(ch=='\t') ) {
      ch=getc(fp);
      /*printf("%c", (ch=='\n') ? 'N' : ch); */
    }
    *Nc = nTabs+1;

    fileError = (fclose(fp) == EOF);
  }

  return fileError;
}


/*************************************************************************/
/***** Reads a 1D array from a file with several columns.       *****/
/*************************************************************************/

int readOneRealArrayFrom2DFile(char *fName, real f[],
```

```
int c, int NumColumns, int N)

     /***** Read real f[1..N] from the c'th column of fName,   *****/
     /***** padding at the end with zeroes.     *****/

{
  int count, x=1;
  real ff;
  int fileError;
  FILE *fp, *fopen();


  fileError = ( (fp=fopen(fName,"r")) == NULL );
  if (fileError)
    /*fclose(fp)*/;

  else {
    rewind(fp);

    count= 0;
    while ( ( EOF != fscanf(fp, "%f", &ff) )  &&  x<=N ) {
      count++;
      if (count==c ) {
f[x]=ff;
/*printf("%d\t%f\n", x, f[x]);*/
x++;
      }
      if (count==NumColumns) count=0;
    }

    while ( x<=N ) {
      f[x] = 0.0;
      /*printf("%d*\t%f\n", x, f[x]);*/
      x++;
    }

    fileError = (fclose(fp) == EOF);

  }

  return fileError;
}


/************************************************************************/
/***** Reads a 2D array from a 2D file.       ******************/
/************************************************************************/

int read2DRealArrayFromFile (char *fName, real distribution[][ARRAY_SIZE+1],
      int Nc, int Np)

     /*****    *****/
     /*****    *****/

{
  int c=1, p=1;
  int fileError = 0;
  FILE *fp, *fopen();


  fileError = ( (fp=fopen(fName,"r")) == NULL );
```

```
  if (fileError)
    /* file error! */;

  else {
    rewind(fp);

    while (    ( EOF != fscanf(fp, "%f", &distribution[c][p]) )
   && (p<=Np) ) {
      /*printf("%d\t%d\t%f\n", c, p, distribution[c][p]);*/
      c++;
      if (c > Nc) {
c=1;
p++;
      }
    }

    while ( p<=Np ) {
      distribution[c][p] = 0.0;
      /*printf("*%d\t%d\t%f\n", c, p, distribution[c][p]);*/
      c++;
      if (c > Nc) {
c=1;
p++;
      }
    }

    fileError = (fclose(fp) == EOF);

  }

  return fileError;
}


/*************************************************************************/
/***** Writes a 2D array to a 2D file ************************/
/*************************************************************************/

int write2DRealArrayToIntegerFile (char *fName,
    real distribution[][ARRAY_SIZE+1],
    int Nc, int Np)

     /***** Write real distribution[1..N]  as int to fName. *****/

{
  char *separator = ",";
  int c,p;
  int fileError;
  FILE *fp, *fopen();

  fileError = ( (fp=fopen(fName,"w")) == NULL );
  if (fileError)
    /* file error! */;

  else {
    for (p=1; p<=Np; p++){
      for (c=1; c<=(Nc-1); c++)
fprintf(fp, "%d%s", (int) distribution[c ][p ], separator);
      fprintf (fp, "%d%s", (int) distribution[Nc][p ], "\n"     );
    }
    fileError = (fclose(fp));
```

```
  }

  return fileError;
}


#include  <stdio.h>
#include        "curveHandling.h"


/*************************************************************************/
/***** Reads an array from a file ************************/
/*************************************************************************/

int readFloatArrayFromFile(char *fName, float distribution[], int N)

     /***** Read float distribution[1..N] from fName, padding at *****/
     /***** the end with zeroes.                                  *****/

{
  int x=1;
  int fileError;
  FILE *fp, *fopen();


  fileError = ( (fp=fopen(fName,"r")) == NULL );
  if (fileError)
    /*fclose(fp)*/;

  else {
    rewind(fp);

    while ( ( EOF != fscanf(fp, "%f", &distribution[x]) )  &&  x<=N ) {
      /*printf("%d\t%f\n", x, distribution[x]);*/
      x++;
    }

    while ( x<=N ) {
      distribution[x] = 0.0;
      /*printf("%d*\t%f\n", x, distribution[x]);*/
      x++;
    }

    fileError = (fclose(fp) == EOF);

  }

  return fileError;
}


/*************************************************************************/
/***** Writes an array to a file         ****************************/
/*************************************************************************/

int writeFloatArrayToIntegerFile(char *fName, float distribution[], int N)

     /***** Write float distribution[1..N]  as int to fName.     *****/

{
  int x;
```

```
  int fileError;
  FILE *fp, *fopen();

  fileError = ( (fp=fopen(fName,"w")) == NULL );

  if (!fileError) {
    for (x=1; x<=N; x++)
      fprintf(fp, "%d\n", (int) distribution[x]);

    fileError = (fclose(fp) == EOF);
  }

  return fileError;
}
/*************************************************************************/
/***** Writes an array to a file    ***********************************/
/*************************************************************************/

int writeFloatArrayToFloatFile(char *fName, float distribution[], int N)

     /***** Write float distribution[1..N]  as float to fName.   *****/
{
  int x;
  int fileError;
  FILE *fp, *fopen();

  fileError = ( (fp=fopen(fName,"w")) == NULL );

  if (!fileError) {
    for (x=1; x<=N; x++)
      fprintf(fp, "%f\n", distribution[x]);

    fileError = (fclose(fp) == EOF);
  }

  return fileError;
}


/*************************************************************************/
/***** Writes two arrays to a file ************************/
/*************************************************************************/


int writeFloatTwoArraysToIntegerFile(char *fName, float distributionA[],
     float distributionB[], int N)

     /***** Write float distribution[1..N]  as int to fName.     *****/

{
  int x;
  int fileError;
  FILE *fp, *fopen();

  fileError = ( (fp=fopen(fName,"w")) == NULL );

  if (!fileError) {
    for (x=1; x<=N; x++)
      fprintf(fp, "%d\t%d\n", (int) distributionA[x], (int) distributionB[x]);

    fileError = (fclose(fp) == EOF);
```

```
  }

  return fileError;
}


/*************************************************************************/
/*************************************************************************/
/***** Writes two arrays to a file ************************/
/*************************************************************************/


int writeFloatTwoArraysToFloatFile(char *fName, float distributionA[],
   float distributionB[], int N)

     /***** Write float distribution[1..N]  as int to fName.    *****/

{
  int x;
  int fileError;
  FILE *fp, *fopen();

  fileError = ( (fp=fopen(fName,"w")) == NULL );

  if (!fileError) {
    for (x=1; x<=N; x++)
      fprintf(fp, "%f\t%f\n", distributionA[x], distributionB[x]);

    fileError = (fclose(fp) == EOF);
  }

  return fileError;
}



#define   ARRAY_SIZE          32002
#define   PI                  acos(-1.)
#define   real                float

int findNumCurves(char *fName, int *Nc);

int readOneRealArrayFrom2DFile   (char *fName, real f[], int c, int Nc, int N);
int writeRealArrayToIntegerFile     (char *fName, real f[], int N);
int writeRealArrayToRealFile        (char *fName, real f[], int N);
int writeRealTwoArraysToIntegerFile (char *fName, real f[],real g[], int N);
int writeRealTwoArraysToRealFile    (char *fName, real f[],real g[], int N);

void getMoments  (real distribution[], int N,
  real *normPtr, real *meanPtr, real *stdDevPtr);
void findMinRegion(real f[], int startIndex, int endIndex, int regionSize,
                   real *minimum, int *minimumIndex);
void findMaxRegion(real f[], int startIndex, int endIndex, int regionSize,
                   real *maximum, int *maximumIndex);
int analyzeSquarePulse (real y[], int numPts,
                        real *yBaseline, real *yMax, real *yMin,
                        int *fwhmIndex1, int *fwhmIndex2);
void subtractBaseline(real distribution[], int N, real baseline);
int getWfmInfo         (real y[], int numPts, real xStep, int ptOffset,
                        real *yBaseline, real *yMax, real *yMin, real *xFWHM);

void twofft (real data1[], real data2[], real fft1[], real fft2[], long int N);
```

```
void four1  (real data[], long int N, int isign);
void realft (real data[], long int N, int isign);


#include <stdio.h>
#include <math.h>
#include        "/u2/cyrus/C/curveHandling.h"


/*************************************************************************/

void getMoments(real distribution[], int N,
                real *norm, real *mean, real *stdDev)

   /***    Find the norm, mean, and standard deviation of  ***/
   /***    the distribution function distribution[1..N]    ***/


{
int i;
real x;
real total0, total1, total2;

total0 = total1 = total2 = 0.;
for (i=1;i<=N;i++) {
  x= (real) i;
  total0 +=         distribution[i];
  total1 +=     x * distribution[i];
  total2 += x * x * distribution[i];
}
*norm   = total0;
*mean   = total1/(*norm);
*stdDev = sqrt(total2/(*norm) - (*mean)*(*mean));

}

/*************************************************************************/

void findBaseline(real distribution[], int N, real *baseline)


{
int group_beginning, j;
real avg, min_avg;
int groupSize=10;                       /* number of neighboring         */
                                        /* points to consider in a group */

group_beginning =1;
for (j=group_beginning, min_avg=0.; j<=group_beginning+groupSize-1; j++)
min_avg += distribution[j];
min_avg /= groupSize;

for (group_beginning =1; group_beginning <= (N+1-groupSize); group_beginning++) {
for (j=group_beginning, avg=0.; j<=group_beginning+groupSize-1; j++)
avg += distribution[j];
avg /= groupSize;
if (min_avg > avg) min_avg=avg;
}

*baseline = min_avg;

}
```

```
/*************************************************************************/

void subtractBaseline(real distribution[], int N, real baseline)


{
int j;

for (j=1; j<=N; j++)
distribution[j] -=baseline;
}



/*************************************************************************/

/*   THIS ROUTINE NEEDS DEBUGGING

void findBaselinePoint(real distribution[], int N, real *baseline, int *Px)


{
int group_beginning, j, x;
real avg, min_avg;
int groupSize=10;                       /* number of neighboring         * /
                                        /* points to consider in a group * /

group_beginning =1;
for (j=group_beginning, min_avg=0.; j<=group_beginning+groupSize-1; j++)
min_avg += distribution[j];
min_avg /= groupSize;

for (group_beginning =1; group_beginning <= (N+1-groupSize); group_beginning++) {
for (j=group_beginning, avg=0.; j<=group_beginning+groupSize-1; j++)
avg += distribution[j];
avg /= groupSize;
if (min_avg > avg) {
min_avg=avg;
x = group_beginning + groupSize/2;
}
}

*Px = x;
*baseline = min_avg;

}

void findPeakPoint(real distribution[], int N, real *peak, int *Px)
{
int i,x ;
real baseline;

for (i=1; i<= N;  i++) distribution[i] *= (-1);
findBaselinePoint(distribution, N, baseline, x)

*Px = x;
*peak = -1*baseline;
}

/*************************************************************************/
```

```
/*************************************************************************/


#include <stdio.h>
#include <math.h>

#include        "curveHandling.h"


/*************************************************************************/

int homodyneCount (real y[], int numPts, real tStep,
   real *yBottom, real *yTop, FILE *fp);

/*************************************************************************/

void main(int argc, char *argv[])

{

real y[ARRAY_SIZE];                          /* Inputs  */
int  numPts=ARRAY_SIZE;
real tStep = .4/50.;       /*us*/

real yBottom, yTop;                          /* Outputs */
int err;

char inFileName[100], outFileName[100], *fileRoot;
FILE *inFile, *outFile;
int i;

if (argc != 2) {
  printf("\nYou need to indicate a root filename!\n");
  exit (1);
}
fileRoot = argv[1];
sprintf(inFileName, "data/%s.dat", fileRoot);
sprintf(outFileName,"data/%s.frq", fileRoot);

                             printf ("\n\nReading \"%s\" .....\n",inFileName);

inFile = fopen (inFileName, "r");
outFile= fopen (outFileName, "w");

err=readOneRealArrayFrom2DFile(inFileName, y,
                           2, 2, 32000);
if (err) {
  printf("\nError reading \"%s\".  \n", inFileName);
  exit (1);
}

                             printf ("Writing \"%s\" .....\n",outFileName);

err= homodyneCount (&y[1], numPts, tStep,
    &yBottom, &yTop, outFile);

if (err) {
  printf("\nError writing \"%s\".  \n", outFileName);
  exit (1);
```

```
}
                              printf ("Closing files .....\n");

fclose(outFile);
fclose(inFile);

                              printf("\n\nDone.\n");
                              printf(" top=  %f  \n bot=  %f  \n",
            yTop, yBottom);
                              printf("\n err= %d\n", err);

}

/*************************************************************************/

int homodyneCount (real y[], int numPts, real tStep,
   real *yBottom, real *yTop, FILE *fp)

       /* Assumes y[0..numPts-1] is a square pulse with a small sinusoid */
       /* added onto the flattop.  tStep is the temporal spacing between */
       /* elements.  This routine returns the bottom and top values of   */
       /* the sinusoid, and writes information on the sinusoid periods   */
       /* to the file fp.                                                */

{

#define RegionSize 11                          /* number of points to      */
                                               /* average when looking for */
                                               /* the max and min vals     */
int err=0;
int i;
real t, f, newCross, oldCross, yMid;

int iDummy1, iDummy2;

/*
real rDummy;

err=analyzeSquarePulse (y, numPts,
yBottom, yTop, &rDummy, &iDummy1, &iDummy2);
*/

findMinRegion(y, 0, numPts-1, RegionSize, yBottom, &iDummy1);
findMaxRegion(y, 0, numPts-1, RegionSize, yTop,    &iDummy1);

yMid = (*yBottom + *yTop )/2.;

i=0;  oldCross= i * tStep;

for (i=0+1; i<numPts; i++) {
  if ( (y[i-1] <yMid) && (y[i]>=yMid) ) {
    newCross= i*tStep -  tStep*(y[i] - yMid )/ (y[i]-y[i-1]);
    t=(newCross+oldCross)/2.;
    f= 1./(newCross-oldCross);
    fprintf(fp,"%f \t %f \n", t, f);
    oldCross=newCross;
  }

}
return err;
```

```
}

/*****************************************************************************/
```

Appendix B

Program to Calculate Drag Ratio

```
#include  <stdio.h>
#include "/u2/cyrus/C/curveHandling.h"



/*************************************************************************/
/***** Finds the number of curves in a KestrelSpec file    *************/
/*************************************************************************/
int findNumCurves(char *fName, int *Nc)

     /***** Count the number of tabs on a line to determine the *****/
     /***** number of curves in the data file.                  *****/

{
  int nTabs;
  char ch = 0;
  int fileError = 0;
  FILE *fp, *fopen();


  fileError = ( (fp=fopen(fName,"r")) == NULL );
  if (fileError)
    /* file error! */;

  else {
    rewind(fp);

    for (nTabs=0; ((ch!=EOF) && (ch!='\n')); nTabs+=(ch=='\t') ) {
      ch=getc(fp);
      /*printf("%c", (ch=='\n') ? 'N' : ch); */
    }
    *Nc = nTabs+1;

    fileError = (fclose(fp) == EOF);
  }

  return fileError;
}


/*************************************************************************/
/***** Reads a 1D array from a file with several columns.       *****/
/*************************************************************************/

int readOneRealArrayFrom2DFile(char *fName, real f[],
```

```
int c, int NumColumns, int N)

     /***** Read real f[1..N] from the c'th column of fName,   *****/
     /***** padding at the end with zeroes.     *****/

{
  int count, x=1;
  real ff;
  int fileError;
  FILE *fp, *fopen();


  fileError = ( (fp=fopen(fName,"r")) == NULL );
  if (fileError)
    /*fclose(fp)*/;

  else {
    rewind(fp);

    count= 0;
    while ( ( EOF != fscanf(fp, "%f", &ff) )  &&  x<=N ) {
      count++;
      if (count==c ) {
f[x]=ff;
/*printf("%d\t%f\n", x, f[x]);*/
x++;
      }
      if (count==NumColumns) count=0;
    }

    while ( x<=N ) {
      f[x] = 0.0;
      /*printf("%d*\t%f\n", x, f[x]);*/
      x++;
    }

    fileError = (fclose(fp) == EOF);

  }

  return fileError;
}


/************************************************************************/
/***** Reads a 2D array from a 2D file.       ******************/
/************************************************************************/

int read2DRealArrayFromFile (char *fName, real distribution[][ARRAY_SIZE+1],
      int Nc, int Np)

     /*****    *****/
     /*****    *****/

{
  int c=1, p=1;
  int fileError = 0;
  FILE *fp, *fopen();


  fileError = ( (fp=fopen(fName,"r")) == NULL );
```

```
  if (fileError)
    /* file error! */;

  else {
    rewind(fp);

    while (    ( EOF != fscanf(fp, "%f", &distribution[c][p]) )
   && (p<=Np) ) {
      /*printf("%d\t%d\t%f\n", c, p, distribution[c][p]);*/
      c++;
      if (c > Nc) {
c=1;
p++;
      }
    }

    while ( p<=Np ) {
      distribution[c][p] = 0.0;
      /*printf("*%d\t%d\t%f\n", c, p, distribution[c][p]);*/
      c++;
      if (c > Nc) {
c=1;
p++;
      }
    }

    fileError = (fclose(fp) == EOF);

  }

  return fileError;
}


/*************************************************************************/
/***** Writes a 2D array to a 2D file ************************/
/*************************************************************************/

int write2DRealArrayToIntegerFile (char *fName,
    real distribution[][ARRAY_SIZE+1],
    int Nc, int Np)

     /***** Write real distribution[1..N]  as int to fName. *****/

{
  char *separator = ",";
  int c,p;
  int fileError;
  FILE *fp, *fopen();

  fileError = ( (fp=fopen(fName,"w")) == NULL );
  if (fileError)
    /* file error! */;

  else {
    for (p=1; p<=Np; p++){
      for (c=1; c<=(Nc-1); c++)
fprintf(fp, "%d%s", (int) distribution[c ][p ], separator);
      fprintf (fp, "%d%s", (int) distribution[Nc][p ], "\n"     );
    }
    fileError = (fclose(fp));
```

```
  }

  return fileError;
}


#include <stdio.h>
#include <math.h>
#include        "/u2/cyrus/C/curveHandling.h"


/*************************************************************************/

void getMoments(real distribution[], int N,
                real *norm, real *mean, real *stdDev)

   /***    Find the norm, mean, and standard deviation of  ***/
   /***    the distribution function distribution[1..N]    ***/


{
int i;
real x;
real total0, total1, total2;

total0 = total1 = total2 = 0.;
for (i=1;i<=N;i++) {
  x= (real) i;
  total0 +=         distribution[i];
  total1 +=     x * distribution[i];
  total2 += x * x * distribution[i];
}
*norm   = total0;
*mean   = total1/(*norm);
*stdDev = sqrt(total2/(*norm) - (*mean)*(*mean));

}

/*************************************************************************/

void findBaseline(real distribution[], int N, real *baseline)


{
int group_beginning, j;
real avg, min_avg;
int groupSize=10;                       /* number of neighboring         */
                                        /* points to consider in a group */

group_beginning =1;
for (j=group_beginning, min_avg=0.; j<=group_beginning+groupSize-1; j++)
min_avg += distribution[j];
min_avg /= groupSize;

for (group_beginning =1; group_beginning <= (N+1-groupSize); group_beginning++) {
for (j=group_beginning, avg=0.; j<=group_beginning+groupSize-1; j++)
avg += distribution[j];
avg /= groupSize;
if (min_avg > avg) min_avg=avg;
}
```

```
*baseline = min_avg;

}

/*************************************************************************/

void subtractBaseline(real distribution[], int N, real baseline)


{
int j;

for (j=1; j<=N; j++)
distribution[j] -=baseline;
}



/*************************************************************************/

/*   THIS ROUTINE NEEDS DEBUGGING

void findBaselinePoint(real distribution[], int N, real *baseline, int *Px)


{
int group_beginning, j, x;
real avg, min_avg;
int groupSize=10;                       /* number of neighboring         * /
                                        /* points to consider in a group * /

group_beginning =1;
for (j=group_beginning, min_avg=0.; j<=group_beginning+groupSize-1; j++)
min_avg += distribution[j];
min_avg /= groupSize;

for (group_beginning =1; group_beginning <= (N+1-groupSize); group_beginning++) {
for (j=group_beginning, avg=0.; j<=group_beginning+groupSize-1; j++)
avg += distribution[j];
avg /= groupSize;
if (min_avg > avg) {
min_avg=avg;
x = group_beginning + groupSize/2;
}
}

*Px = x;
*baseline = min_avg;

}

void findPeakPoint(real distribution[], int N, real *peak, int *Px)
{
int i,x ;
real baseline;

for (i=1; i<= N;  i++) distribution[i] *= (-1);
findBaselinePoint(distribution, N, baseline, x)

*Px = x;
*peak = -1*baseline;
```

```
}

/*************************************************************************/


/*************************************************************************/



#include <stdio.h>
#include <math.h>
#include        "/u2/cyrus/C/curveHandling.h"


#define fnIn  "lz.f.dat"
#define fnOut "not used"

#define T_Max    60
#define T_Step    1
#define Repeats   6
#define NumSets    (T_Max/T_Step)
#define NumPts     (NumSets*Repeats)

/*
int readOneRealArrayFrom2DFile   (char *fName, real f[], int c, int Nc, int N);
int findNumCurves(char *fName, int *Nc);
*/

void main()

{
  int numColumns;         /* Better be 2!  */
  int ptNum, setNum;
  int err;
  real x[NumPts+1], y[NumPts+1];                                    /* inputs */
  real x1[NumSets+1], y0[NumSets+1], y1[NumSets+1], y2[NumSets+1]; /*outputs */



                    /*  IO  */

  findNumCurves(fnIn, &numColumns);
  printf("Number of columns in \"%s\":  %d\n", fnIn, numColumns);
  printf("error=%d\n", numColumns-2);
  err=readOneRealArrayFrom2DFile (fnIn, x, 1, 2, NumPts);
  printf("error=%d\n", err);
  err=readOneRealArrayFrom2DFile (fnIn, y, 2, 2, NumPts);
  printf("error=%d\n", err);


                    /* calc stats  */

  for (setNum=1; setNum<=NumSets; setNum++) {
    x1[setNum]=y0[setNum]=y1[setNum]=y2[setNum]=0.;
    for (ptNum= (setNum-1)*Repeats+1; ptNum<=setNum*Repeats; ptNum++) {
      printf("%d \t %f \t %f \n",ptNum, x[ptNum], y[ptNum]);
      x1[setNum]=x[ptNum];
      if (y[ptNum]>=0) {
y0[setNum]+=1;
y1[setNum]+=y[ptNum];
y2[setNum]+=y[ptNum]*y[ptNum];
      }
```

```
    }
    y1[setNum] /= y0[setNum];
    y2[setNum] /= y0[setNum];
  }

  for (setNum=1; setNum<=NumSets; setNum++) {
    /*printf("%f \t %f \t %f \t %f \n",
   x1[setNum], y0[setNum], y1[setNum],
           sqrt(y2[setNum]-y1[setNum]*y1[setNum]) );
    */
    printf("%f \t %f \t %f \n",
   x1[setNum], y1[setNum],
           sqrt(y2[setNum]-y1[setNum]*y1[setNum]) );

  }

}


#include <stdio.h>
#include <math.h>
#define fnRoot  "st2"
#define recoil .02946   /* m/s^2  */

#define screenLeft  100
#define screenRight 360

#define numCurves  241
#define aFastStart 4500.
#define aFastStep  3000.
#define vOffset    35.
#define vFinal     75.
#define ttFracStart 0.
#define ttFracStep  0.20
#define numTTs      24
#define numShortTTs 21
#define shortStep    (1.e-6)  /*sec*/
#define numReps     5


#define screenOffset (screenLeft-1)
#define numPts (screenRight-screenLeft-1)


/*********************************************************************/
  void getRegions (int c, float *oL,  float *oR,
                          float *a1L, float *a1R,
                          float *a2L, float *a2R  )
{
int cCount;

*oL=115-screenOffset;
*oR=135-screenOffset;
*a1L=148-screenOffset;
*a2R=330-screenOffset;


if      (c<=105)  {*a1R=277-screenOffset; *a2L=*a1R+1;}
else if (c<=110)  {*a1R=281-screenOffset; *a2L=*a1R+1;}
else if (c<=115)  {*a1R=282-screenOffset; *a2L=*a1R+1;}
else if (c<=120)  {*a1R=283-screenOffset; *a2L=*a1R+1;}
```

```
else if (c<=225)  {*a1R=277-screenOffset; *a2L=*a1R+1;}
else if (c<=230)  {*a1R=281-screenOffset; *a2L=*a1R+1;}
else if (c<=235)  {*a1R=282-screenOffset; *a2L=*a1R+1;}
else if (c<=241)  {*a1R=283-screenOffset; *a2L=*a1R+1;}

/*  FOR st1
if      (c<=105)  {*a1R=281-screenOffset; *a2L=*a1R+1;}
else if (c<=110)  {*a1R=281-screenOffset; *a2L=*a1R+1;}
else if (c<=115)  {*a1R=287-screenOffset; *a2L=*a1R+1;}
else if (c<=120)  {*a1R=292-screenOffset; *a2L=*a1R+1;}

else if (c<=225)  {*a1R=281-screenOffset; *a2L=*a1R+1;}
else if (c<=230)  {*a1R=281-screenOffset; *a2L=*a1R+1;}
else if (c<=235)  {*a1R=287-screenOffset; *a2L=*a1R+1;}
else if (c<=241)  {*a1R=292-screenOffset; *a2L=*a1R+1;}
*/
}

/*********************************************************************/

void main()


{
  int c;
  int  repCount, ttCount, accCount, numAccs;
  float aFast, ttFrac, tunTime;

/*  float sum1, sum2, mean, sd;  */
  float z[numCurves+1][numPts+1];
  float ratios[numCurves+1];
  float offset,offset1,offset2, area1, area2, max1, max2;
  float offsetL, offsetR, area1L, area1R, area2L, area2R;
  void getRegions (int c, float *oL,  float *oR,
                          float *a1L, float *a1R,
                          float *a2L, float *a2R  );
  void readz(float z[][numPts+1], char *fn);
  float findBaseline (float curve[], int start, int stop);
  float findArea     (float curve[], int start, int stop);
  float findMax      (float curve[], int start, int stop);
  void subtract      (float curve[], float offset);

  char *fnIn[50], *fnOut[50];

  sprintf(fnIn, "%s.txt", fnRoot);
  sprintf(fnOut, "%s.kg", fnRoot);
  readz(z, fnIn);

  aFast=aFastStart;
  ttCount =1;  ttFrac=ttFracStart;
  repCount=1;
  accCount=1;  aFast =aFastStart;

  for (c=1; c<=numCurves; c++)  {

    getRegions (c, &offsetL,  &offsetR, &area1L, &area1R, &area2L, &area2R);
    offset = findBaseline(z[c], offsetL, offsetR);
    subtract(z[c], offset);
    area1 = findArea(z[c], area1L, area1R);
    area2 = findArea(z[c], area2L, area2R);
    max1  = findMax (z[c], area1L, area1R);
```

```
    max2  = findMax (z[c], area2L, area2R);
    ratios[c] = area2/(area1+area2);

    tunTime=(vFinal-vOffset)*recoil/aFast * ttFrac;
/*
    printf("%f \t %f \t %f \t %i\n", aFast, tunTime*1.e6, ratios[c], c);
*/

    repCount++;
    if (repCount>numReps) {
      repCount=1;
      ttCount++;  ttFrac+=ttFracStep;
      if (ttCount>numTTs) {
ttCount=1;  ttFrac=ttFracStart;
accCount++;  aFast+=aFastStep;
      }
    }
    numAccs=accCount;

  }

  writeRatios(fnOut, ratios, numAccs);

} /*main*/
/*********************************************************************/

writeRatios(char *fnOut[], float ratios[], int numAccs)

{
  FILE *fp;
  int c;
  int  repCount, ttCount, accCount;
  float aFast, ttFrac, tunTime;
  float sum1, sum2, mean, sd;

  fp = fopen(fnOut, "w");

  for (accCount=1, aFast=aFastStart;
       accCount<=numAccs;
       accCount++, aFast +=aFastStep)  {

    fprintf(fp,"tunnel time (us) [%7.0f m/s^2]\tdrag ratio [%7.0f m/s^2]\t",
    aFast, aFast);

  } /* accCount */
  fprintf(fp, "\n");

  ttFrac=ttFracStart;
  for (ttCount = 1;
       ttCount<=numTTs;
       ttCount++) {
    for (repCount=1 ; repCount <= numReps; repCount ++)  {
      for (accCount=1, aFast=aFastStart;
   accCount<=numAccs;
   accCount++, aFast +=aFastStep)  {

if (ttCount>numShortTTs){
  ttFrac = ttFracStart + ttFracStep*(ttCount-numShortTTs);
  tunTime=(vFinal-vOffset)*recoil/aFast * ttFrac;
}
else
```

```
  tunTime= (ttCount-1)*shortStep;

c=repCount
  + numReps * ((ttCount-1)
       + numTTs * (accCount-1));

if (c<=numCurves)
  fprintf(fp, "%f \t %f \t", tunTime*1.e6, ratios[c]);

      } /* accCount */
      fprintf(fp, "\n");
    }   /* repCount */
  }     /* ttCount  */

/*  for (c=numReps; c<=numCurves; c+=numReps) {
    sum1=sum2=0;
    for (cc=0; cc<numReps; cc++){
      sum1+=ratios[c-cc];
      sum2+=ratios[c-cc]*ratios[c-cc];
    }
    mean=sum1/numReps;
    sd  =sqrt(sum2/numReps-sum1*sum1/repeats/numReps);
    printf("%f \t %f \t %f \n", freqStep*( (c-1)/numReps)+freqStart,
                        mean, sd);
  }
*/

  fclose(fp);

}

/*********************************************************************/

float findBaseline (float curve[], int start, int stop)

{
  int j;
  float base=0.0;

  for (j=start; j<=stop; j++)
    base+=curve[j];
  base /=(stop-start+1);

  return base;
}


/*********************************************************************/

float findArea     (float curve[], int start, int stop)

{
  int j;
  float area=0.0;

  for (j=start; j<=stop; j++)
    area+=curve[j];
  return area;
}
```

```
/*************************************************************************/

float findMax     (float curve[], int start, int stop)

{
  int j;
  float max=0.0;

  for (j=start; j<=stop; j++)
    max+=curve[j];
  return max;
}


/*************************************************************************/

void subtract(float zz[], float offset)

{
  int j;

  for (j=1; j<numPts; j++)
    zz[j] -= offset;

}

/*************************************************************************/

void readz(float z[][numPts+1], char *fn)

{
  int ix, iy;
  FILE *fp;

  fp =fopen(fn,"r");
  for   (iy=1; iy<=numPts; iy++)
    for (ix=1; ix<=numCurves; ix++)
      fscanf (fp,"%f", &z[ix][iy]);
  fclose(fp);
}


/*************************************************************************/



. .
```

Bibliography

[1] Atomic loss from far-detuned optical lattice has been studied also, however even here tunneling is obscured by other losses. B.P. Anderson et al, Phys. Rev. A **53**, R3727 (1996).

[2] S.R. Wilkinson, C.F. Bharucha, K.W. Madison, Qian Niu, and M.G. Raizen, Phys. Rev. Lett. **76**, 4512 (1996).

[3] F. L. Moore, J. C. Robinson, C. Bharucha, P. E. Williams, and M. G. Raizen, Phys. Rev. Lett. **73**, 2974 (1994).

[4] J. C. Robinson, C. Bharucha, F. L. Moore, R. Jahnke, G. A. Georgakis, Q. Niu, M. G. Raizen, and Bala Sundaram, Phys. Rev. Lett. **74**, 3963 (1995).

[5] J. C. Robinson, C. F. Bharucha, K.W. Madison, F. L. Moore, Bala Sundaram, S. R. Wilkinson, and M. G. Raizen, Phys. Rev. Lett. **76**, 3304 (1996).

[6] F. L. Moore, J. C. Robinson, C. F. Bharucha, Bala Sundaram, and M. G. Raizen, Phys. Rev. Lett. **75**, 4598 (1995).

[7] Maxime Ben Dahan, Ekkehard Peik, Jakob Reichel, Yvan Castin, Christophe Salomon, Phys. Rev. Lett. **76**, 4508 (1996).

[8] Laser cooling and trapping is reviewed by Steven Chu in Science **253**, 861 (1991).

[9] L.Fonda, G.C. Ghirardi, and A. Rimini, Rep. Prog. Phys. **41**, 587 (1978).

[10] K. Grotz and H.V. Klapdor, Phys. Rev. C **30**, 2098 (1984).

[11] L.A. Khalfin, Soviet Physics JETP **6**, 1053 (1958).

[12] E. Mertzbacher, *Quantum Mechanics*, Wiley and Sons (1970).

[13] C. Cohen-Tannoudji, J Dupont-roc, and Gilbert Grynberg, *Atom-Photon Interactions* (John Wiley and Sons, Inc., 1992).

[14] R. Graham, M. Schlautmann, and P. Zoller, Phys. Rev. A **45**, R19 (1992).

[15] P. Meystre, and M. Sargent III, *Elements of Quantum Optics*, Springer-Verlag (1991).

[16] N.W. Aschcroft and N.D. Mermin, *Solid State Physics* (Sauners College, 1976).

[17] Qian Niu, Xiao-Geng Zhao, G. A. Georgakis and M.G. Raizen, Phys. Rev. Lett. **44**, 3455 (1996).

[18] For a recent review, see E.E. Mendez and Gerald Bastard, Phys. Today **46**, No. 6, 34 (1993).

[19] G. Zener, Proc. Roy. Soc. **A137**, 696; Y. Gefen, E. Ben-Jacob and A. O. Caldeira, Phys. Rev. **B36**, 2770 (1987).

[20] For a recent review, see Federico Capasso and Cupriyo Datta, Phys. Today **43**, No. 2, 74 (1990).

[21] Martin Fischer, Master's Thesis, The University of Texas at Austin, 1993.

[22] John Robinson, Ph.D Thesis, The University of Texas at Austin, 1995.

[23] W. L. Wiese, M. W. Smith, and B. M. Miles, *Atomic Transition Probabilites*, v. 2, National Standard Reference Data Service, National Bureau of Standards (1969).

[24] M. H. Anderson, J. R. Ensher, M. R. Matthews, C. E. Wieman, and E. A. Cornell, Science **269**, 198 (1995).

[25] S. Dyrting and Bala Sundaram, in preparation.

[26] C.F. Bharucha, K.W. Madison, P.R. Morrow, S.R. Wilkinson, Bala Sundaram, and M.G. Raizen, submitted to Phys. Rev. Lett.

[27] J.E. Avron, Phys. Rev. Lett. **37**, 1568 (1976); Ann. Phys. (N.Y.) **143**, 33 (1982).

[28] L. Sirko, S.Yoakum, A. Haffmans, and P.M. Koch, Phys. Rev. A **47**, R782 (1993).

Vita

Patrick Russell Morrow was born on February 18, 1969 to Patricia and Robert Morrow in Lincoln, Nebraska. After graduating as Valedictorian from Lincoln Southeast High School in Lincoln, Patrick earned a Bachelor's of Science degree in Electrical Engineering and a Bachelor's of Arts in Physics at Rice University in the Spring of 1991. In the Fall of 1991 he began graduate work in physics at The University of Texas at Austin. In the Spring of 1992 he joined Professor Mark G. Raizen's laboratory to work on quantum optics experiments with trapped atoms.

Permanent address: 1618-A West 6th St.
Austin, Texas 78703

This dissertation was typeset with LaTeX[‡] by the author.

[‡]LaTeX is a document preparation system developed by Leslie Lamport as a special version of Donald Knuth's TeX Program.